REVIEW

of the

TRICAL COMMUNICATION LABORATORY

PPON TELEGRAPH AND TELEPHONE PUBLIC CORPORATION

Former Reports of the Electrical Communication Laboratory
Nippon Telegraph and Telephone Public Corporation
from Vol.1, No.1, Sept. 1953 to Vol. 7, No. 12, Dec. 1959

洋図

VOLUME 8
NUMBERS 11-12

November-December
1960

Published Bimonthly by

HE ELECTRICAL COMMUNICATION LABORATORY
NIPPON TELEGRAPH AND TELEPHONE PUBLIC CORPORATION
1551, Kitizyôzi, Musasino-si, Tôkyô, Japan

Review of the Electrical Communication Laboratory

EDITORIAL COMMITTEE

Susumu OKAMURA *Chairman*

Tadasu FUKAMI	Giichi ITO	Hideo KAWASAKI
Yukio NAKAMURA	Tatsuya SHIMBORI	Takuzo SHINDO
Toyotaro SHIRAMATSU	Takakichi UZAWA	Ginsaku YASAKI
Koji MAEDA	Nobukazu NIIZEKI	Osamu TUKIZI

EDITORIAL STAFF

Susumu HIRANO *Editor*

Tutomu SAITO *Assistant Editor*

Masao HIROSE 〃

The Review of the Electrical Communication Laboratory is published six times a year (bimonthly) by the Electrical Communication Laboratory, Nippon Telegraph and Telephone Public Corporation, 1551, Kitizyôzi, Musasino-si, Tôkyô, Japan. Telephone: Tôkyô (391) 2261 and 2271.

All rights of republication, including translation into foreign languages, are reserved by the Electrical Communication Laboratory, NTT.

Subscriptions are accepted at ¥ 1,200 per year. Single copy ¥ 300 each. Foreign postage is ¥ 300 per year or ¥ 50 per copy. Remittance should be made in check payable to the Electrical Communication Laboratory and sent to the Director.

Printed by Aoyama Printing Co., Tokyo, Japan

R E V I E W
of the
ELECTRICAL COMMUNICATION LABORATORY

NIPPON TELEGRAPH AND TELEPHONE PUBLIC CORPORATION

Volume 8, Numbers 11-12 November-December 1960

U.D.C. 534.13 : 539.4
621.365.923.34

Stress and Deformation in Conical Vibrating Plate*

***Kazuo IKEGAYA*†**

Distributions of stress and deformation in a conical thin shell with axial applied force are obtained analytically, and the stress and deformation are found to be concentrated on the inner and outer edges of the shell. The axial stiffness of a conical plate is extremely large compared with that of a flat plate; therefore, forming by press working has proven to be a very useful method of producing diaphragms which vibrate as a rigid piston. The relations between stress, axial stiffness, and slope of a conical shell are also considered in this paper.

1. Introduction

As mentioned in a previous paper,(1) it is thought that the axial stiffness of the conical part of telephone transmitter and receiver diaphragms is large enough for diaphragm to vibrate as a rigid piston within the desired frequency range.

But the magnitude of the stiffness depends on the slope of the conical shell; and the resonant frequency of the bending vibration of the conical shell, which may determine the upper limit of useful frequency range of the diaphragm, depends on the magnitude of the stiffness. And especially to prevent creeping of telephone receiver diaphragms, it is desirable that the static stress and strain produced by the magnetic force should not be concentrated on one any part of the conical shell; and furthermore the magnitude of the static stress and strain should be as small as possible.

Therefore, the internal stress and strain of the conical part of diaphragms produced by static axial force have been considered, the stress on a conical thin shell has been analyzed statically, and the distributions of bending moments and normal components of displacements which may be the most important factors for a conical diaphragm were obtained. The relations between these magnitudes and the slope of the conical shell were considered, and its axial stiffness was also investigated.

2. Fundamental Equations and Their Solutions

Theoretical studies on the thin shell have already been carried out by many authors.(2)-(6) In this paper, the results for the axial symmetric case were applied to the conical thin shell.

---

* MS in Japanese received by the Electrical Communication Laboratory on 27 April, 1960. Originally published in the *Kenkyû Zituyôka Hôkoku* (*Electrical Communication Laboratory Technical Journal*), N.T.T., Vol. 9, No. 6, June pp. 681–689, 1960.

† Station Apparatus Research Section.

As in the papers by the authors referred to above, we shall use the following notation for the element of the conical shell shown in Fig. 1:

T_l = meridian membrane force per unit length of shell section
N_l = shearing force in plane perpendicular to meridian plane per unit length of shell section
M_l = bending moment in meridian plane per unit length of parallel circle
w = normal component of displacement
l = distance along cone element, measured from vertex
α = angle between axis of rotation and an element of cone
h = thickness of shell
E = Young's modulus
ν = Poisson's ratio.

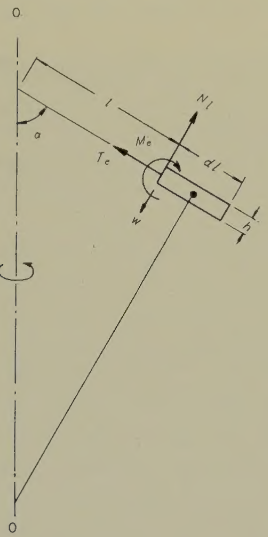

Fig. 1—Element of conical shell.

In general the vertical angle 2α of the conical diaphragm is nearly 180°, therefore in studying fatigue, creeping, and axial stiffness, it is sufficient to take into consideration only the bending moment M_l as stress and the normal component w as displacement. Accordingly the attention is payed to M_l and w as stress and strain throughout this paper.

According to the references(2)-(5) it is known that the following equations hold:

$$T_l l = -N_l l \tan\alpha + C\tan\alpha, \tag{1}$$

$$M_l = -\frac{Eh}{12(1-\nu^2)}\left(\frac{d^2w}{dl^2} + \frac{\nu}{l}\frac{dw}{dl}\right), \tag{2}$$

$$\frac{dw}{dl} = \frac{\tan^2\alpha}{Eh}\left(l\frac{d^2U}{dl^2} + \frac{dU}{dl} - \frac{U}{l} + \frac{C}{l}\right), \tag{3}$$

where C is a constant which is determined by the conditions of the external force, and

$$U \equiv N_l l. \tag{4}$$

Putting

$$x \equiv 2\lambda\sqrt{l} \tag{5}$$

and

$$\lambda^4 \equiv \frac{12(1-\nu^2)}{h^2\tan^2\alpha}, \tag{6}$$

the function U satisfies the following ordinary differential equation of the fourth order.

$$\frac{d^4U}{dx^4} + \frac{2}{x}\frac{d^3U}{dx^3} - \frac{9}{x^2}\frac{d^2U}{dx^2} + \frac{9}{x^3}\frac{dU}{dx} + U = 0. \tag{7}$$

The general solution of Eq. (7) is:

$$\begin{aligned} U \equiv N_l l = {} & A_1\left(+\operatorname{ber} x - \frac{2}{x}\operatorname{bei}' x\right) \\ & + A_2\left(-\operatorname{bei} x - \frac{2}{x}\operatorname{ber}' x\right) \\ & + A_3\left(-\operatorname{kei} x - \frac{2}{x}\operatorname{ker}' x\right) \\ & + A_4\left(-\operatorname{ker} x + \frac{2}{x}\operatorname{kei}' x\right), \end{aligned} \tag{8}$$

where A_1, A_2, A_3, and A_4 are coefficients determined by the boundary conditions, and

$$\operatorname{ber} x \pm j\operatorname{bei} x = J_0(xj\sqrt{\pm j}) = I_0(x\sqrt{\pm j})$$

$$\ker x \pm j\,\mathrm{kei}\,x = K_0(x\sqrt{\pm j})$$

$$\mathrm{ber}'\,x = \frac{d}{dx}\mathrm{ber}\,x \qquad \text{etc.}$$

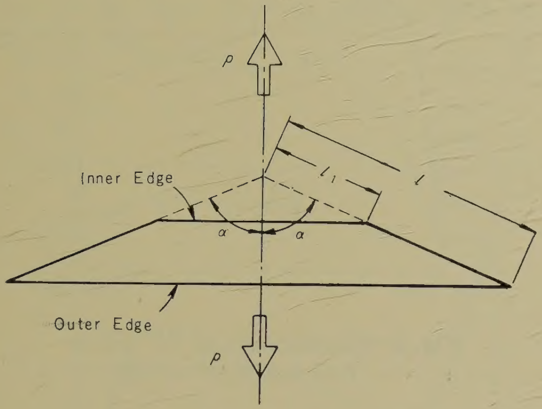

Fig. 2—Conical shell.

3. Bending Moment and Displacement

The coefficients A's in the general solution U may be determined by the boundary conditions as follows: Assume the conical shell is as shown in Fig. 2, the distances from the vertex to the inner and outer edges are l_1 and l_2, and axial forces p are applied on these edges; while the slope at the edges is maintained stable by clamping the edges. Then the boundary conditions are

$$N_l l = \frac{p}{2\pi} \qquad \text{at } l=l_1 \text{ and } l_2, \tag{9}$$

$$\frac{dw}{dl} = 0 \qquad \text{at } l=l_1 \text{ and } l_2, \tag{10}$$

and

$$T_l l = \frac{p}{2\pi}\cot\alpha \quad \text{at } l=l_1 \text{ and } l_2; \tag{11}$$

therefore using Eq. (1), it follows that

$$C = \frac{p}{2\pi}\operatorname{cosec}^2\alpha. \tag{12}$$

Substituting Eq. (8) into Eq. (3),

$$\begin{aligned}\frac{dw}{dl} = \frac{\lambda^2\tan^2\alpha}{Eh}\Big[&A_1\Big(-\mathrm{bei}\,x - \frac{2}{x}\,\mathrm{ber}'\,x\Big)\\ &+A_2\Big(-\mathrm{ber}\,x + \frac{2}{x}\,\mathrm{bei}'\,x\Big)\\ &+A_3\Big(-\ker x + \frac{2}{x}\,\mathrm{kei}'\,x\Big)\\ &+A_4\Big(+\mathrm{kei}\,x + \frac{2}{x}\,\ker' x\Big) + \frac{4}{x^2}C\Big].\end{aligned} \tag{13}$$

Using the results that Eqs. (8) and (13) satisfy the boundary conditions Eqs. (9), (10), and (12), the coefficients A's can be determined, hence we have

$$\begin{aligned}M_l = A_1&\Big[+\frac{2}{x}\,\mathrm{bei}'\,x + \frac{4}{x^2}(1-\nu)\Big(-\mathrm{bei}\,x - \frac{2}{x}\,\mathrm{ber}'\,x\Big)\Big]\\ +A_2&\Big[+\frac{2}{x}\,\mathrm{ber}'\,x - \frac{4}{x^2}(1-\nu)\Big(+\mathrm{ber}\,x - \frac{2}{x}\,\mathrm{bei}'\,x\Big)\Big]\\ +A_3&\Big[+\frac{2}{x}\,\ker' x - \frac{4}{x^2}(1-\nu)\Big(-\ker x - \frac{2}{x}\,\mathrm{kei}'\,x\Big)\Big]\\ +A_4&\Big[-\frac{2}{x}\,\mathrm{kei}'\,x - \frac{4}{x^2}(1-\nu)\Big(-\mathrm{kei}\,x - \frac{2}{x}\,\ker' x\Big)\Big] + \frac{16}{x^4}\,\frac{1-\nu}{\sin^2\alpha}\,\frac{p}{2\pi},\end{aligned} \tag{14}$$

and integrating Eq. (13) and eliminating its integration constant, we have

$$w=\frac{\tan^2\alpha}{2Eh}\Big[(A_1+x\,\mathrm{ber}'\,x-2\mathrm{ber}\,x)$$
$$+A_2(-x\,\mathrm{bei}'\,x+2\mathrm{bei}\,x)$$
$$+A_3(-x\,\mathrm{kei}'\,x+2\mathrm{kei}\,x)$$
$$+A_4(-x\,\mathrm{ker}'\,x+2\mathrm{ker}\,x)+\frac{2p}{\pi}\,\frac{\log x}{\sin^2\alpha}\Big]. \tag{15}$$

Putting $w_1 \equiv w)_{l=l_1}$, and $w_2 \equiv w)_{l=l_1}$, the stiffness for the axially applied force shown in Fig. 2 may be considered nearly equal to $p/(w_2-w_1)$. This is easily obtained from Eq. (15).

4. Numerical Examples

In this section numerical examples are given for the telephone diaphragms made of 0.06 mm thick duralumin which are shown in Fig. 3.

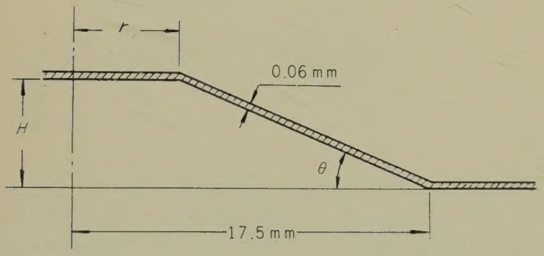

Fig. 3—Conical vibrating plate.

In Fig. 4 and Fig. 5 the distributions of the bending moment M_l and the normal component of displacement w along the cone meridians are shown for $r=7.5$ mm., $H=3$ mm and for $r=2.5$ mm., $H=3$ mm. respectively.

From these curves it may be seen that the bending moment M_l concentrates on both inner and outer edges, and at the same time its magnitude is very small at the middle part. This tendency is evident especially for the long meridian of cone l_2-l_1 as shown in Fig. 5. For comparison the curve of M_l for the short meridian ($r=10$ mm., $H=3$ mm.) is also given in Fig. 6. The reversals of bending moments shown in these curves are caused by clamping the edges. The bending moment at the inner edge is larger than at the outer edge; therefore it is desireable to

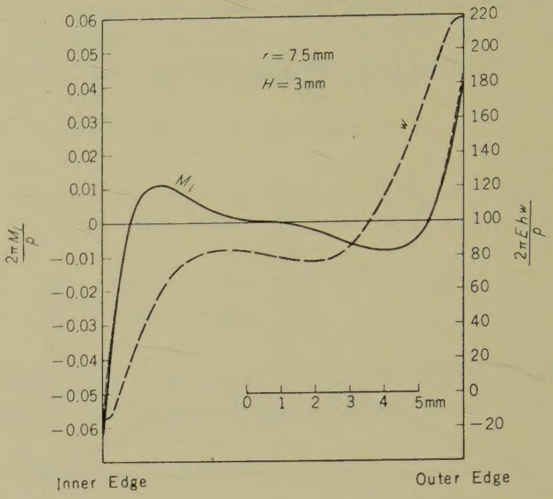

Fig. 4—Distributions of M_l and w ($r=7.5$ mm, $H=3$ mm).

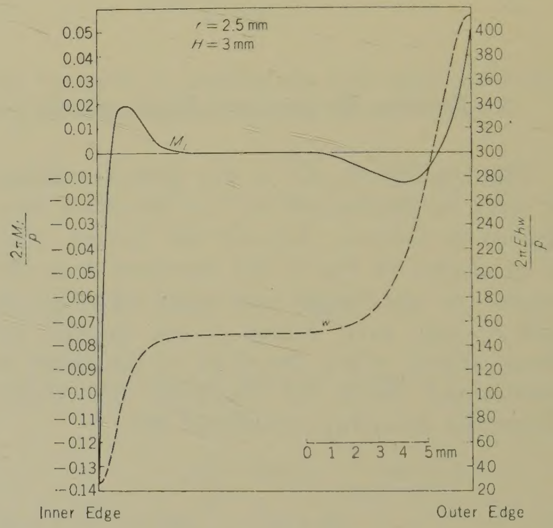

Fig. 5—Distributions of M_l and w ($r=2.5$ mm, $H=3$ mm).

consider the magnitude of the bending moment at the inner edge in discussing the magnitude of the stress in a cone. These considerations on the distribution of the bending moment are true also for the normal component of displacement, but it may be seen that the strain at the inner edge is smaller than at the outer edge.

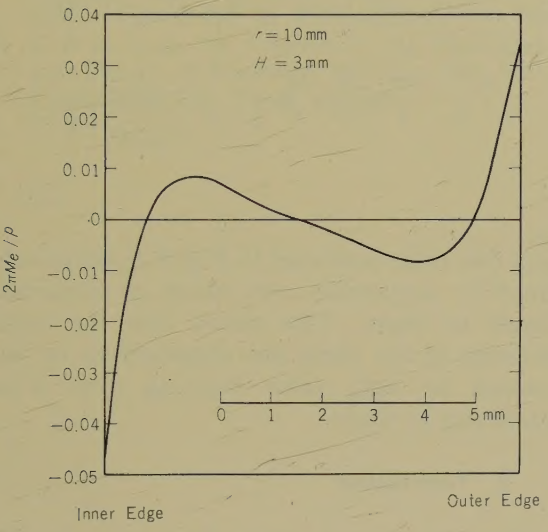

Fig. 6—Distribution of M_l ($r=10$ mm, $H=3$ mm).

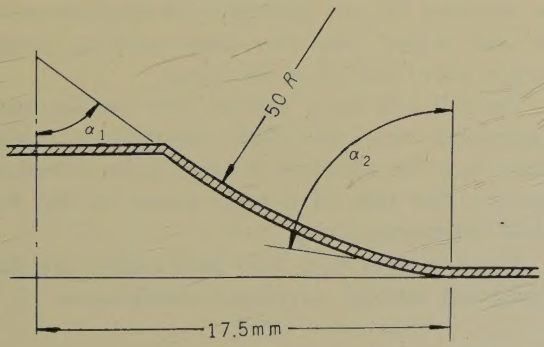

Fig. 7—Conical vibrating plate with bent meridian.

Next, the effect of the bent meridian shown in Fig. 7 has been investigated. It has been assumed that the radius of curvature of the meridian (taken as 50 mm here) is much larger than the other dimensions or that the meridian is almost straight. Then assuming that the same differential equation, Eq. (7), also holds in this case, and putting the angles $2\alpha_1$ and $2\alpha_2$ as in Fig. (7) ($2\alpha=\alpha_1+\alpha_2$), then the boundary conditions for such a shell reduce to

$$\left.\begin{aligned} N_l l &= \frac{p}{2\pi}\,\frac{\sin\alpha_1}{\sin\alpha} \qquad l=l_1 \\ &= \frac{p}{2\pi}\,\frac{\sin\alpha_2}{\sin\alpha} \qquad l=l_2, \end{aligned}\right\} \quad (16)$$

and

$$\left.\begin{aligned} T_l l &= \frac{p}{2\pi}\,\frac{\cos\alpha_1}{\cos\alpha} \qquad l=l_1 \\ &= \frac{p}{2\pi}\,\frac{\cos\alpha_2}{\cos a} \qquad l=l_2, \end{aligned}\right\} \quad (17)$$

instead of Eqs. (9) and (11) respectively. Therefore using boundary conditions (16) and (17),

$$c=\frac{p}{2\pi}\,\frac{\cos(\alpha-\alpha_1)}{\sin^2\alpha}=\frac{p}{2\pi}\,\frac{\cos(\alpha_2-\alpha)}{\sin^2\alpha}, \quad (18)$$

and another boundary condition (10), the coefficients A's and therefore the bending moment M_l can be obtained.

The dotted line along the full line labelled M_l in Fig. 4 indicates the distribution of the bending moment in this case ($r=7.5$ mm, $H=3$ mm, radius of the curvature of meridian $=50$ mm), which shows a slight decrease at the inner edge and for slight increase at the outer edge.

There is another point of view in the investigation of these numerical results. In Fig. 3 holding the height H constant and varying the inner radius r (or angle of slope θ) the bending moments at both edges and the axial stiffness behave as shown in Fig. 8. From these results it is noticed that the moment at the outer edge varies slightly but

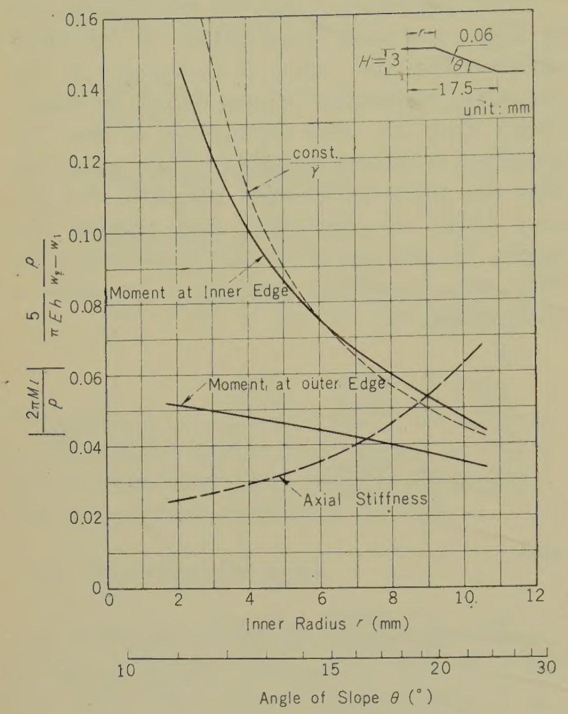

Fig. 8—Bending moments and axial stiffness vs. inner radius of conical shell.

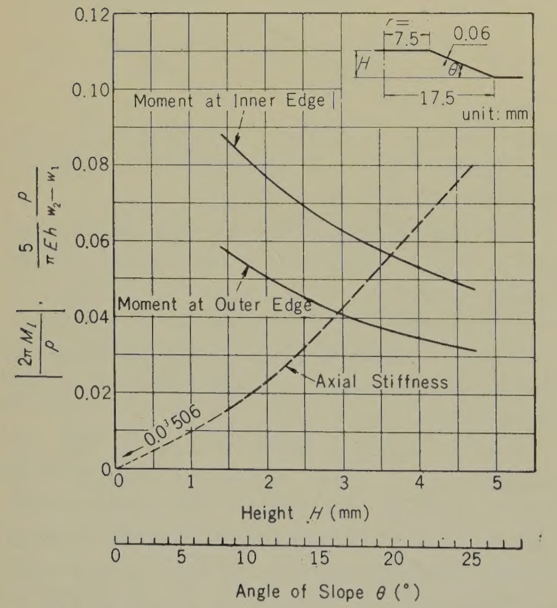

Fig. 9—Bending moments and axial stiffness vs. height of conical shell.

that of the inner edge increases greatly with the slope becomes gentle, and the rate of increase is smaller than that of the inverse of inner radius $1/r$.

Then let us vary the height and slope of conical shell holding the inner radius constant. The bending moments at the edges and the axial stiffness for $r=7.5$ mm are shown in Fig. 9. In this case, the bending moments increase slightly but the axial stiffness decreases with the slope becoming to be gentle. For zero height shell or flat plate(7)(8)(9)

$$\frac{p}{w_2-w_1}=\frac{4\pi}{3}\frac{E}{1-\sigma^2}\frac{h^3}{a^2}\frac{1}{1-\mu^2-\frac{4\mu^2}{1-\mu^2}(\log\mu)^2}, \tag{19}$$

and this value indicated in Fig. 9 is extremely small in comparison with those of moderate height or slope. This shows that the axial stiffness of flat plate can considerably be increased by only press working even if its curvature is slight.

5. Conclusion

Distribution of bending moment and displacement in conical thin shell applied the external axial force has been investigated analytically and numerically, and these magnitudes are found to clearly concentrate on the inner and outer edges of the shell. The axial stiffness is obtained by the difference of displacements at both edges, and its magnitude is much larger than that of a flat plate.

Then it has been proved the well-known experience that the slight swelling out the plate may be effective in keeping its vibration pattern like that of a rigid piston in the desired frequency range.

These results may also give useful data for designing conical telephone diaphragms.

Acknowledgments

The author wishes to express his appreciation to Doctors Toshio Hayasaka, Giichi Ito, and Kenro Masuzawa for many useful sug-

gestions concerning the problems, and for criticism and advice throughout the progress of this work.

References

(1) K. Ikegaya and M. Murakami: Some investigations on the Conical Vibrating Plates for telephone, *Rev. Electr. Comm. Labor.*, NTT, Japan

(2) E. Meißner: Das Elastizitäts-problem für dünne Schalen von Ringflächen- Kugel- oder Kegelform, *Phys. Zeits.*, **14,** 8, s. 343, 1913.

(3) A. E. H. Love: A Treatise on the Mathematical Theory of Elasticity, 4th ed., p. 590, 1927, Cambridge Univ. Press, London.

(4) S. Timoshenko: Theory of Plates and Shells, p. 354, 1940, McGraw-Hill Book Co., New York·

(5) G. L. Meriam: Stress and Displacements in a Rotating Shell, *Journ. Appl. Mech.*, **10,** 2, p. A-53, 1943.

(6) N. J. Hoff: Thin Circular Conical Shells under Arbitrary Loads, *Journ. Appl. Mech.*, **22,** 4, p. 557, 1955.

(7) G. Ito: The Specific Responses of Carbon Transmitters in Low Frequencies, *Journ. Inst. Electr. Comm. Engr. Japan*, **39,** 3, p. 187, 1956.

(8) T. Hayasaka: Acoustic Engineering, p. 397, 1957, The Nikkan-Kogyo Press.

(9) R. J. Roark: Formulas for Stress and Strain, 3rd ed., p. 200, 1954, McGraw-Hill Book Co., New York.

* * * *

REVIEW OF THE ELECTRICAL COMMUNICATION LABORATORY
VOLUME 8, NUMBERS 11-12, NOVEMBER-DECEMBER, 1960

U.D.C. 534.13 : 621.395.6

Some Investigations on the Conical Vibrating Plates for Telephone*

***Kazuo IKEGAYA*†** and ***Masayuki MURAKAMI*†**

For the purpose of understanding the properties of conical telephone diaphragms, larger conical vibrating plates for experiments were made and their characteristic constants were measured. From these results the "Frequency constant" and "Stiffness constant" have been defined as very useful constants for the design of vibrating plates. Their values were determined experimentally. Then by observations of modes of vibration, it has been concluded that the radial corrugations on the conical vibrating plates are unneccessary.

In the next place, the vibrating plates for new telephone transmitter and receiver have been investigated and the effectiveness of the frequency constant and the stiffness constant above mentioned have been verified. And it has been known that the method of fixing the magnetic armature into the vibrating plate for receiver has influence upon its modes of vibration or area factor, then a most useful method has been newly proposed for fixing the armature.

1. Introduction

Metallic diaphragms pressed conically are used in telephone transmitters and receivers. Because of this process of press working it is thought that the central part of a diaphragm acts mechanically as a rigid additive mass and acoustically as a sound radiator in contact with the medium. But in designing a conical diaphragm it is necessary to determine the fundamental resonant frequency of the vibrating system which consists of a rigid additive mass and a flat ring plate.

In this paper, some investigations on the conical diaphragms of the No. 4 type telephone are described, and to facilitate more reasonable design procedures the "Frequency constant" and the "Stiffness constant" which will be very useful have been defined. Aluminum conical vibrating plates twice the size of the actual transmitter and receiver diaphragms used in the No. 4 type telephone were produced for convenience in measuring modes of vibration.

The vibrating-displacement frequency response and the frequency constant were both measured in a vacuum using the double-size vibrating plates. Also, the stiffness constants of the flat ring plate have been determined experimentally. These constants have been compared with the constants of the diaphragms actually used in telephones.

By observing the modes of vibration of the experimental vibrating plates, we determined that radial corrugations on the conical section give no beneficial effects; furthermore, a new useful method of fixing the magnetic armature to the diaphragm of the new telephone receiver was developed.

2. Frequency Constant

As mentioned above, to enable easier and more accurate measurements to be made, double-size conical vibrating plates were fabricated and their properties were investigated. Fig. 1 illustrates these double-size vibrating plates. The plates are made of 0.1 mm thick aluminum, and thirty different types with various values of D, d and H, were prepared. Moreover for comparison, several additional plates of the same dimensions but with seven radial corrugations were fabricated. The excitation was electromagnetic to a small permendur disk which was pasted on the center of each plate as a magnetic armature.

---

* MS in Japanese received by the Electrical Communication Laboratory on 6 April, 1959. Originally published in the *Kenkyû Zituyôka Hôkoku* (*Electrical Communication Laboratory Technical Journal*), N.T.T., Vol. 9, No. 5, May pp. 431-443, 1960.

† Station Apparatus Research Section.

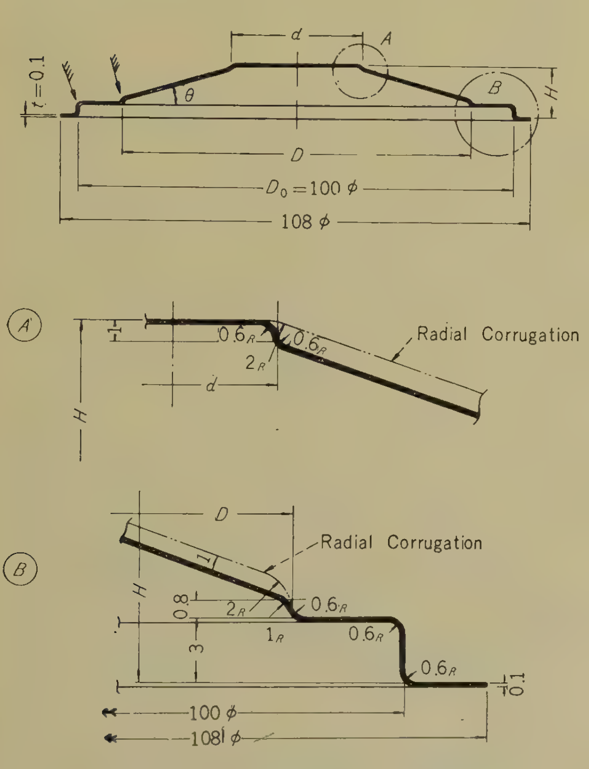

Fig. 1—Experimental vibrating plate.

The measurements of the vibrating-displacement frequency response of the double-size plates were all made in vacuum because elimination of the effects of the radiation impedance to the acoustic medium was desired.

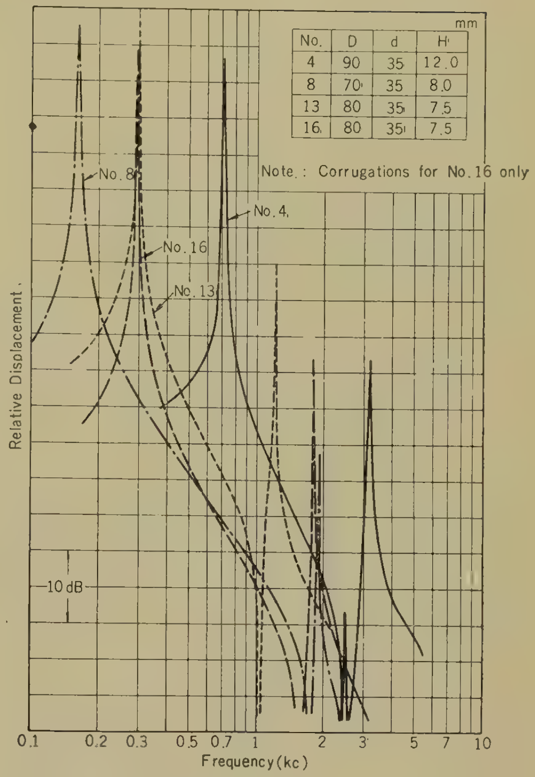

Fig. 2—Displacement frequency responses of experimental vibrating plates.

Fig. 2 shows the typical displacement frequency response at the center of the vibrating plates. Next, the effective mass and the fundamental resonant frequency of these plates were obtained by the additive-mass method. It goes without saying that in this case the magnetic gap between the exciting pole and the armature was extended enough to eliminate the influence of the negative stiffness in the gap. As the added mass a small brass disk was pasted on the center of the plate. From these measurements it was shown that the reciprocal square of the fundamental resonant frequency is directly proportional to the additive mass within the region where the weight of the added mass does not exceed several times the weight of the vibrating plate. In other words, the modes of vibration of the plate are not transformed even if an added mass of several times that of the plate is added to it. Therefore it follows that the fundamental resonant frequency even when an added mass is used can be easily calculated. Fig. 3 shows an example of these data.

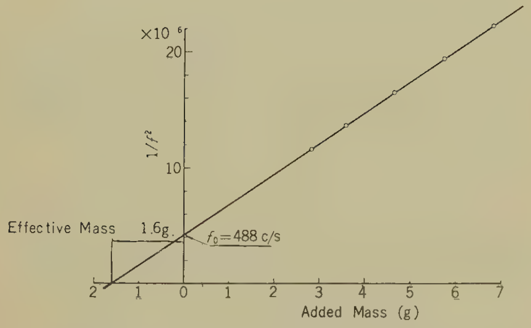

Fig. 3—Determination of effective mass by additive mass method.

From these results we may realize a conical vibrating plate with any desired resonant frequency. In general, for a clamped circular plate of radius a and thickness t, the natural frequencies are

$$f_{mn}=\frac{\alpha^2{}_{mn}}{4\pi a^2}\frac{t\sqrt{E}}{\sqrt{3\rho(1-\sigma^2)}}, \tag{1}$$

where

f_{mn} : natural frequency of (m, n) mode
α_{mn} : eigenvalue of (m, n) mode
E : Young's modulus
ρ : density
σ : Poisson's ratio

It would be very convenient if the same expression could be applied to the fundamental resonant frequency of the conical vibrating plate under consideration. For this reason, it is assumed the fundamental resonant frequency can be expressed by⁽¹⁾

$$f_0=\frac{\bar{\alpha}_0\, t}{D_0^2}\sqrt{\frac{E}{\rho(1-\sigma^2)}} \tag{2}$$

which is similar to Eq. (1). Then from this equation it is possible to design a conical vibrating plate with the desired fundamental resonant frequency by a value of the constant α determined experimentally. The authors call this non-dimensional constant $\bar{\alpha}_0$ the "Frequency constant" of a conical vibrating plate. The results which were obtained with every vibrating plate show that the fundamental resonant frequency f_0 of a vibrating plate is dependent not upon the diameter d of the central part of the vibrating plate or its height H, but upon the inner diameter D of the vibrating ring. The relation between the Frequency constant $\bar{\alpha}_0$ and the ratio of the inner and outer diameters of the ring, $\mu=\mathrm{D}/\mathrm{D}_0$, is given in Fig. 4, in which the dotted lines indicate the 90% confidence zone. It is shown that the values of this constant for the double-size vibrating plates agrees with the values for the diaphragm of telephone receivers and transmitters.

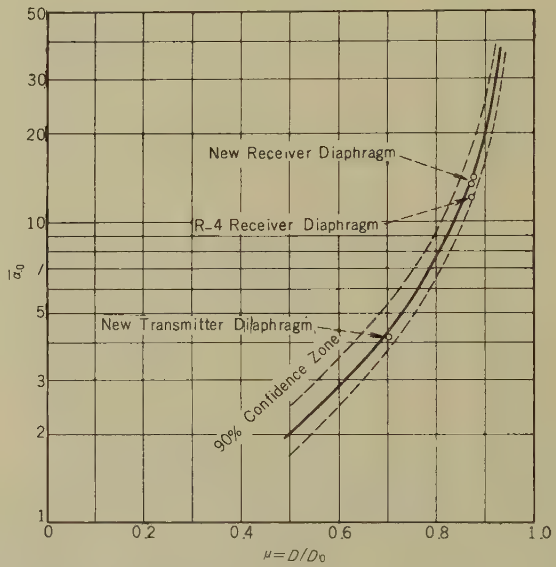

Fig. 4—Frequency constant of telephone diaphragms.

3. Stiffness Constant

In general a preformed vibrating plate is considered as a vibrating ring with a rigid part at its center (see Fig. 5). When the outer and inner diameter of the vibrating ring are 2a and 2b respectively, and its thickness t, the axial static stiffness of this system is given by⁽²⁾⁽³⁾⁽⁴⁾

$$s=\frac{4\pi}{3}\frac{E}{1-\sigma^2}\frac{t^3}{a^2}\frac{1}{1-\mu^2-\frac{4\mu^2}{1-\mu^2}(\log\mu)^2}, \tag{3}$$

where

$\mu \equiv b/a$
E : Young's modulus
σ : Poisson's ratio.

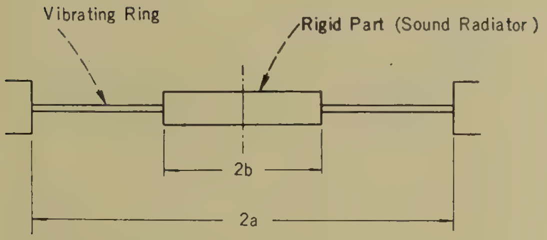

Fig. 5—Model of preformed vibrating plate.

On the other hand, we may obtain the effective stiffness s_0 of a vibrating plate from Fig 3, and, assuming that s_0 is expressed by

$$s_0=\bar{\beta}_0 \frac{E}{1-\sigma^2}\frac{t^3}{D_0^2} \tag{4}$$

similarly to Eq. (3). The authors called this non-dimensional constant $\bar{\beta}_0$ the "Stiffness constant" of a conical vibrating plate, whose value depends not uqon d and H but on D, and therefore on μ. The relation between $\bar{\beta}_0$ and μ is given in Fig. 6, where the dotted lines indicate the 90 % confidence zone. The values corresponding to $\bar{\beta}_0$ in Eq. (3) are

$$\left.\begin{aligned}&\frac{16\pi}{3}\frac{1}{1-\mu^2-\dfrac{4\mu^2}{1-\mu^2}(\log\mu)^2}\\ &\quad =4\pi\frac{2-x}{x^3-\dfrac{1}{30}x^5-\dfrac{1}{30}x^6-\cdots\cdots}\\ &x\equiv 1-\mu=(a-b)/a,\end{aligned}\right\} \tag{5}$$

and these values are shown in the same figure. The difference between the experimental values of $\bar{\beta}_0$ and the calculated ones from Eq. (5) seems to be due to the pure statical investigation of Eq. (5) or to roundness of the shoulders indicated by the arrows in Fig. 1. It is also observed that values of the constants of the double-size experimental diaphragms agree well with the values of telephone transmitter and receiver diaphragms.

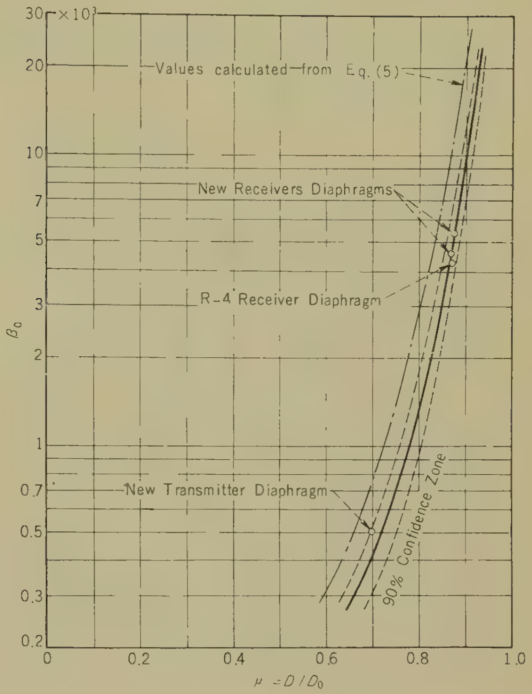

Fig. 6—Stiffness constant of telephone diaphragms.

4. Modes of Vibration

In order to conjecture the characteristics and especially the area factors of a preformed vibrating plate, observation of the modes of vibration of the plate is quite fast; furthermore this observation is necessary.

Figs. 7 and 8 show examples of the modes of vibration of vibrating plates at their fundamental resonant frequencies. The former is for a plate without corrugations and the latter for a plate with radial corrugations on the conical parts, but both of the figures are quite alike and show that the conical part of a plate vibrates almost as a rigid piston. Figs. 9 and 10 also show examples of two plates with and without radial corrugations at the second resonant frequency. These modes seem to be identical, similar to the case of Figs. 7 and 8.

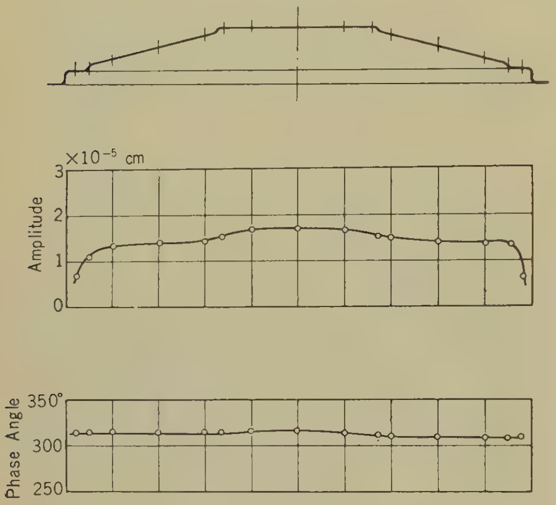

Fig. 7—Modes of vibration of experimental vibrating plate (D=90, d=35, H=12.0, without radial corrugations).

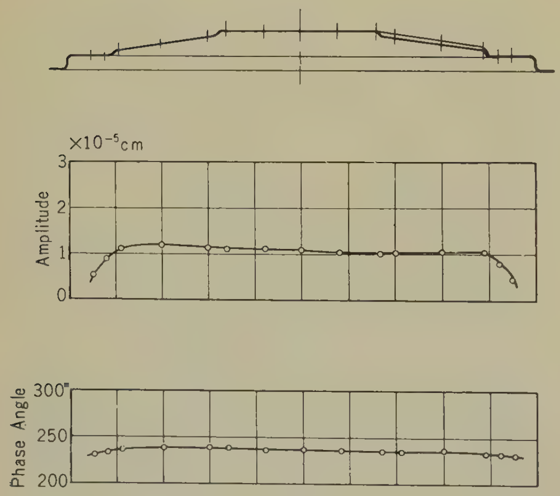

Fig. 8—Modes of vibration of experimental vibrating plates (D=80, d=35, H=9.0, with radial corrugations).

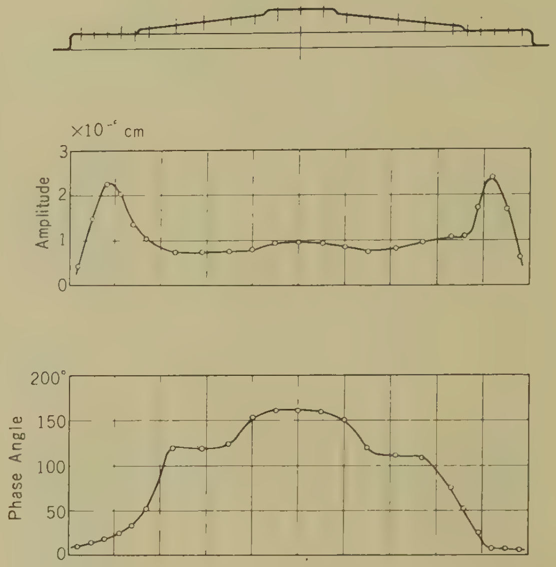

Fig. 9—Modes of vibration of experimental vibrating plate (D=70, d=15, H=8.0, without radial corrugations).

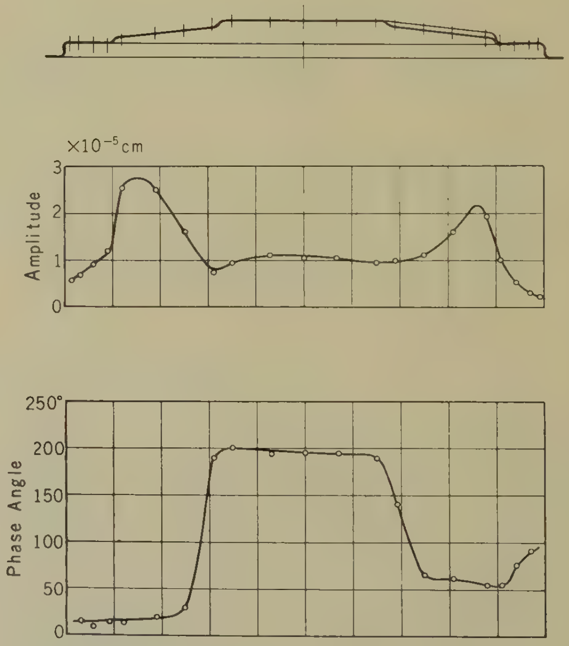

Fig. 10—Modes of vibration of experimental vibrating plate (D=80, d=35, H=7.5, with radial corrugations).

Table 1

DIAPHGRAGMS FOR NEW TELEPHONE RECEIVERS AND THEIR CONSTANS

Ⓐ

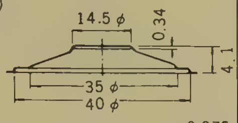

$t = 0.075$

No.	f_0'	m_0	s_0	K
1	2128	0.73	1.29×10^8	0.72
2	2086	0.68	1.17×10^8	0.79
3	2185	0.69	1.30×10^8	0.56

f_0: mean measured value 3498
calculated value 3700

Ⓑ

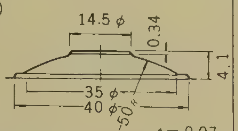

$t = 0.07$

No.	f_0'	m_0	s_0	K
1	1710	0.66	0.761×10^8	0.64
2	1707	0.69	0.693×10^8	0.75
3	1726	0.67	0.787×10^8	0.67

f_0: mean measured value 2925
calculated value 3454

Ⓒ

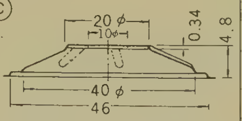

With ring armature $t = 0.075$

No.	f_0'	m_0	s_0	K
1	1564	1.03	0.994×10^8	0.72
2	1554	1.03	0.991×10^8	0.74
3	1555	1.04	0.992×10^8	0.73

f_0: mean measured value 2512
calculated value 2701

Ⓒ' Same dimensions as type Ⓒ

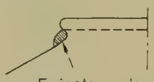

Epicote resin applied

No.	f_0'	m_0	s_0	K
4	1495	1.08	0.952×10^8	0.77
5	1522	1.06	0.968×10^8	0.77
6	1560	1.06	1.07×10^8	0.78

Ⓓ

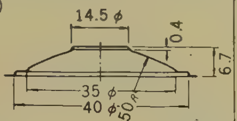

$t = 0.07$

No.	f_0'	m_0	s_0	K
1	1872	0.72	0.995×10^8	0.71
2	1789	0.73	0.921×10^8	0.72
3	1878	0.76	1.06×10^8	0.71

f_0: mean measured value 3386
calculated value 3454

Ⓓ' Same dimensions as type Ⓓ

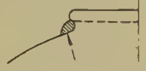

Epicote resin applied

No.	f_0'	m_0	s_0	K
4	1867	0.82	1.13×10^8	0.79
5	1819	0.80	1.04×10^8	0.80

Ⓔ

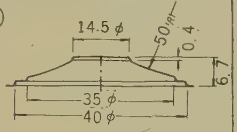

$t = 0.07$

No.	f_0'	m_0	s_0	K
1	1868	0.81	1.11×10^8	0.75
2	1904	0.72	1.03×10^8	0.77
3	1853	0.86	1.16×10^8	0.81

f_0: mean measured value 3169
calculated value 3454

Ⓔ' Same dimensions as type Ⓔ

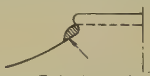

Epicote resin applied

No.	f_0'	m_0	s_0	K
4	1897	0.82	1.16×10^8	0.79
5	1862	0.82	1.12×10^8	0.80

Notes. f_0': fundamental resonant frequency (∾), f_0: fundamental resonant frequency of plate only (∾), t: thickness (mm), m_0: effective mass (g), s_0: effective stiffness (dyn/cm), K: area factor.

From these results we could not perceive any effect of radial corrugations on the conical part of vibrating plate. So it can be concluded that so far as the slope of conical part of vibrating plate is within this limit bending vibration will be prevented.

5. Diaphragms for the New Telephone Receiver

On the basis of the above investigations five duralumin diaphragms for the new telephone receiver, which are illustrated in Table 1, have been made. In this table the measured values of fundamental frequency, effective mass, effective stiffness, area factors, and the value of f_0 calculated from the frequency constant $\bar{\alpha}_0$ are also given.

5.1. Vibrating Displacement and Sound Pressure

Examples of vibrating displacement at the center of these diaphragms in vacuum and sound pressure in a 7.7 c.c. coupler are shown in Figs. 11 and 12. These two curves are similar to each other, so we may expect that the diaphragms under test are useful for the new telephone receiver whose desired frequency range is upper limit about 4000 cycles per second.

5.2. Modes of Vibration at the Fundamental Resonant Frequency

As the modes of vibration of a diaphragm have an effect upon its effective area; namely, on the sensitivity of the receiver, we have observed the modes of vibration at fundamental resonant frequency in order to obtain the data to judge its quality. In Figs. 13 to 17 examples of modes of vibration are shown, and it can be seen that these modes are dependent upon the existance of radial corrugations on the conical part of the diaphragm. For diaphragms without corrugations (Figs. 13(a), 16 and 17) the displacement at the circumference of the flat central part or at the part fixing the armature is remarkable, and for plates with corrugations (Figs. 13(b),

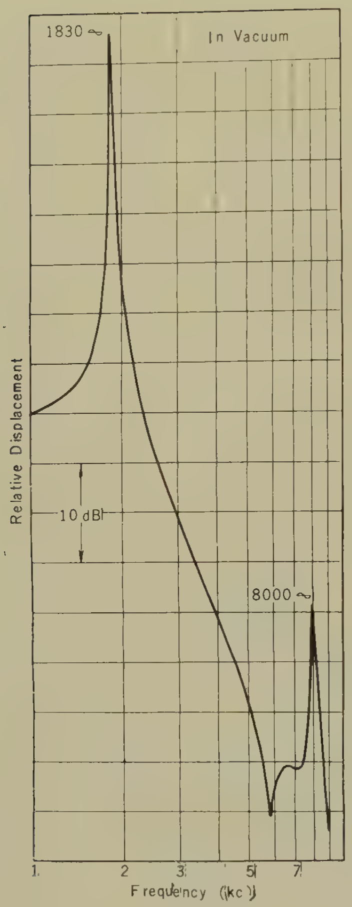

Fig. 11—Vibrating displacement at the center of new telephone receiver diaphragm (Type Ⓔ).

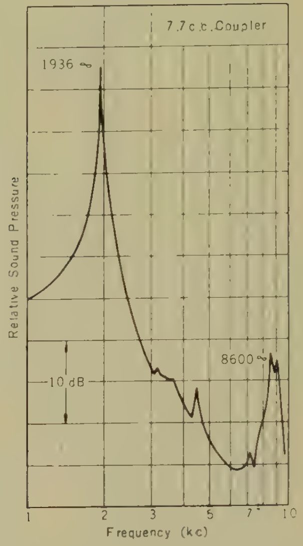

Fig. 12—Sound pressure produced by new telephone receiver diaphragm (Type Ⓔ).

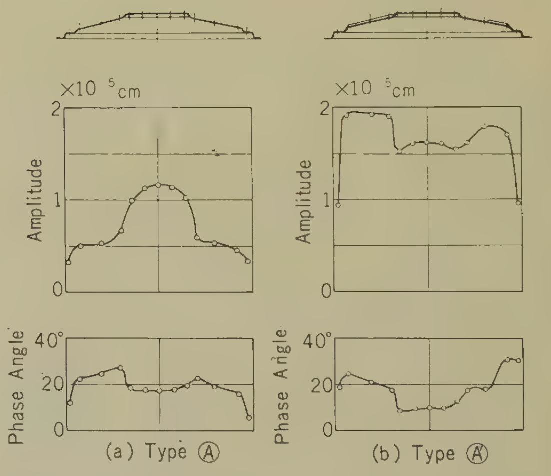

Without Radial Corrugation With Radial Corrugations

Fig. 13—Modes of vibration of new telephone receiver diaphragms.

14 and 15) the magnetic armature is fixed extremely rigidly by the corrugating process increasing the stiffness sufficiently to prevent deformation. From these investigations we see that if we can fix the armature without decrease of stiffness, the modes of vibration will be much improved, and therefore increase in the area factor and improvement of the sensitivity of the telephone receiver may be expected. But it must be noticed that the radial corrugations were found to be useless in the former investigations on the experimental vibrating plates. This is because in the former case the magnetic armatures were pasted on these plates, and so no decrease of stiffness was caused by the process of fixing the armature. Accordingly the modes of vibration were ideal. On the other hand, the process of fixing the armature to the diaphragm of a telephone receiver causes a de-

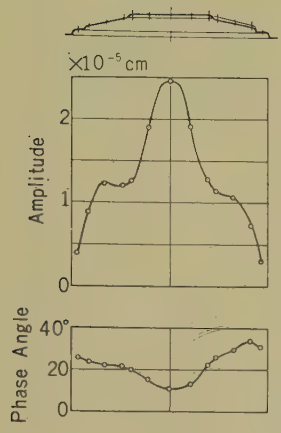

Fig. 14

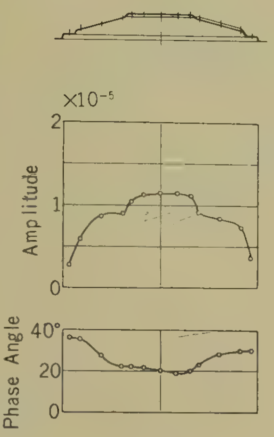

Fig. 15

Fig. 14—Modes of vibration of new telephone receiver diaphragm (Type ©, with ring armature and radial corrugations).

Fig. 15—Modes of vibration of R-4 receiver diaphragm (with radial corrugations).

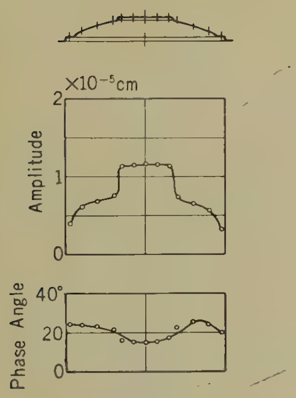

Fig. 15

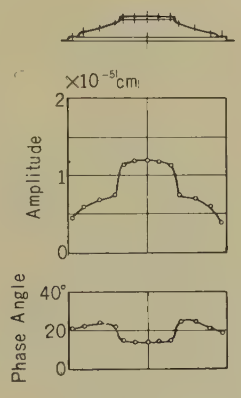

Fig. 16

Fig. 16—Modes of vibration of new telephone receiver diaphragm (Type Ⓓ).

Fig. 17—Modes of vibration of new telephone receiver diaphragm (Type Ⓔ).

crease of stiffness, but this decrease may be prevented by the use of corrugations. That is to say the contribution of corrugating the conical part of the diaphragm is not to stiffen it but to prevent a decrease of stiffness.

5.3. Method of Attaching the Armature

As mentioned above, the deformation of the circumference of the flat central part of telephone receiver diaphragm without radial corrugations is extremely large. Therefore in order to recheck this deformation, it was necessary to stiffen the deformed part by some suitable way and then to observe the modes of vibration. In the experiments this part was stiffened by applying Epicote resin. The fundamental resonant frequency, effective mass, effective stiffness and area factor of vibrating plates with resin are given in Table 1. Example of the modes of vibrations measured for these plates with resin, at the fundamental resonant frequency, are also shown in Figs. 18 and 19. As the constants and the modes of vibration can be varied and the area factor raised by applying resin, a suitable method of fixing the armature by which no decrease of stiffness is caused must be obtained. Fig. 20 shows a new method of fixing the armature which resembles the method of attaching caps to beer bottles.

The experimental data of the constants of telephone receiver diaphragms for which the

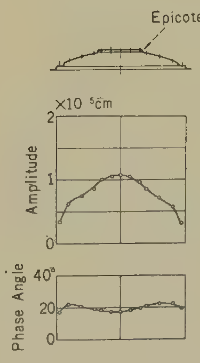

Fig. 18

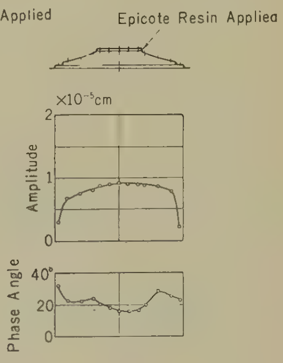

Fig. 19

Fig. 18—Modes of vibration of new telephone receiver diaphragm (Type Ⓓ′, Epicote resin applied, see Fig. 16).

Fig. 19—Modes of vibration of new telephone receiver diaphragm (Type Ⓔ′, Epicote resin applied, see Fig. 17).

Table 2

CONSTANTS OF DIAPHRAGMS FOR TELEPHONE RECEIVER WITH NEW METHOD OF FIXING THE ARMATURE

No.	t	f_0'	m_0	s_0	K
1	0. 063	1625	0. 77	0.802×10^8	80. 9
2	0. 061	1521	0. 77	0.702×10^8	79. 5
3	0. 065	1745	0. 79	0.949×10^8	80. 9
4	0. 063	1615	0. 79	0.813×10^8	80. 2
5	0. 061	1546	0. 75	0.707×10^8	79. 1

Notes.
f_0': fundamental resonant frequency (~),
t: thickness (mm),
m_0: effective mass (g),
s_0 : effective stiffness (dyn/cm),
K : area factor.

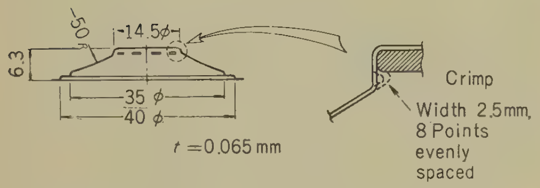

Fig. 20—Diaphragm for new telephone receiver with new method of fixiug the armature.

new method of a fixing the armature was adopted are given in Table 2, and it may be seen that this new method is as effective in increasing the area factor as the application of resin is. This method is adopted in the new telephone receiver.

5.4. Creeping

For the electromagnetic receiver the creeping of the material of the diaphragm caused by magnetic attraction is a serious problem because it is required that there be no static variation of the air gap length. From this reason the magnitude of creeping of the diaphragm (see Fig. 20) for the new telephone receiver to which the new method of fixing the armature applied was measured. The applied load was 1 kg weight at three points, but the magnitude of creeping was saturated at under one micron so it can be concluded that the creeping in this case is negligible (see Fig. 21).

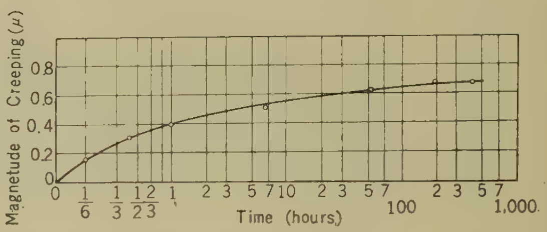

Fig. 21—Magnitude of creeping of the diaphragm for the new telephone receiver with new method of fixing the armature.

Table 3

DIAPHRAGMS FOR NEW TELEPHONE TRANSMITTERS AND THEIR CONSTANTS

Ⓐ 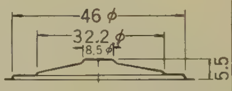 $t = 0.052$	Ⓑ 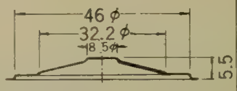 With Corrugations $t = 0.051$
$f_0 = 745$ $m_0 = 0.195$ $s_0 = 4.32 \times 10^6$ $K = 71.9$	$f_0 = 697$ $m_0 = 0.196$ $s_0 = 3.77 \times 10^6$ $K = 7.18$
Ⓒ 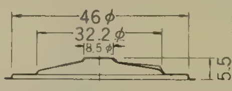 With Corrugations $t = 0.051$	Ⓓ 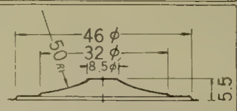 $t = 0.062$
$f_0 = 743$ $m_0 = 0.188$ $s_0 = 4.10 \times 10^6$ $K = 70.5$	$f_0 = 890$ $m_0 = 0.226$ $s_0 = 7.08 \times 10^6$ $K = 71.9$

Notes.
f_0: fundamental resonant frequency of diaphragm only (~),
t: thickness (mm),
m_0: effective mass (g),
s_0 : effective stiffness (dyne/cm),
K: area factor.

6. Diaphragm for Telephone Transmitter

Four duralumin diaphragms for the new telephone transmitter, which are shown in Table 3, have been made. In this table the mean values of the fundamental resonant frequency, effective mass, effective stiffness, and area factor are given for groups of three to five plates.

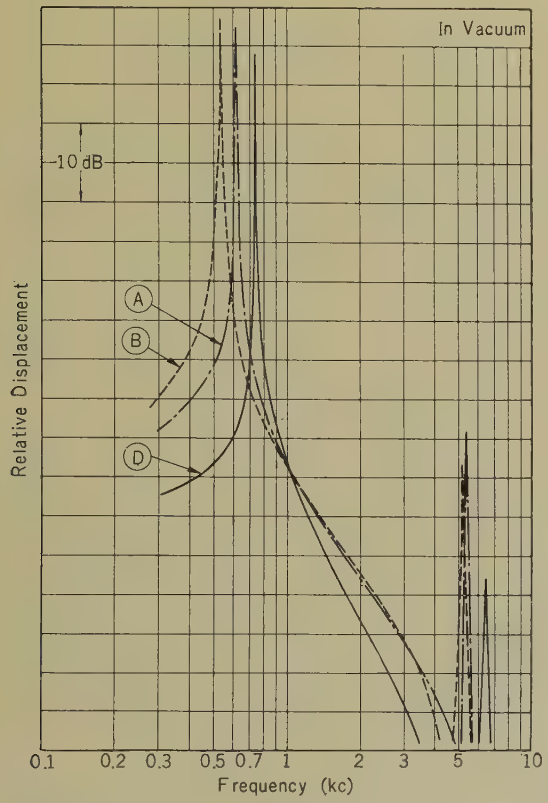

Fig. 22—Vibrating displacement at the centers of diaphragms for new telephone transmitters.

6.1. Vibrating Displacement

An example of the vibrating displacement at the center of these diaphragms by electromagnetic excitation in vacuum are shown in Fig. 22, and from this result we may expect that the diaphragms under test are useful for the new telephone transmitter desired frequency range upper limit is about 4000 cycles per second.

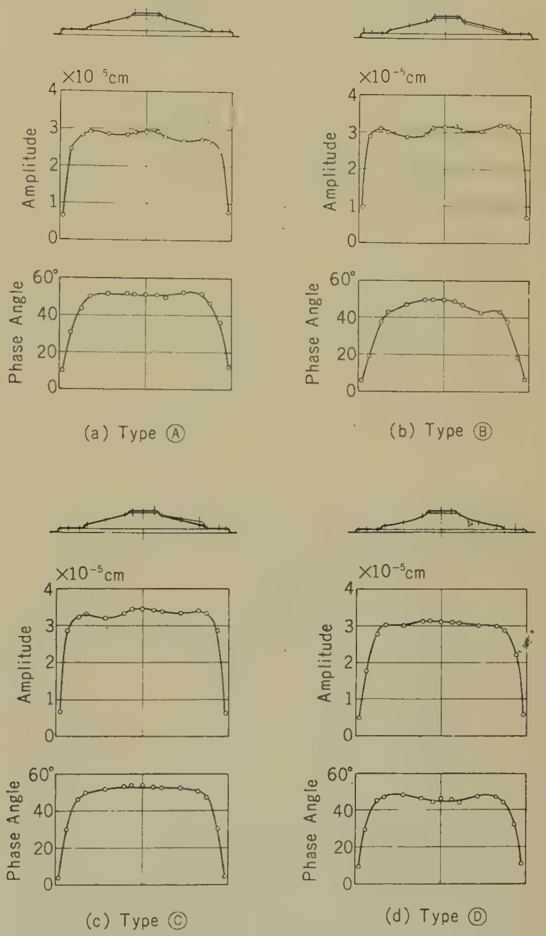

(a) Type Ⓐ (b) Type Ⓑ

(c) Type Ⓒ (d) Type Ⓓ

Fig. 23—Modes of vibrations of new telephone transmitters diaphragms.

6.2. Modes of Vibration at the Fundamental Resonant Frequency

Some examples of modes of vibration are shown in Fig. 23. In this case the ratio of the inner and outer diameters μ is very small as compared with the ratio μ of the receiver diaphragms (see Table 3), and consequently the conical part of the diaphragm acts almost as a rigid piston and its bending vibration is produced only at the flat ring part. The modes of vibration of a diaphragm with an electrode of 0.08 g weight is shown in Fig. 24, and those for a diaphragm with the electrode and the carbon granule in Fig. 25. They were excited by the standard receiver RM-303 through a small coupler.

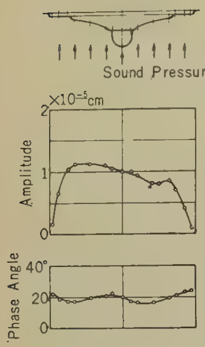

Fig. 24

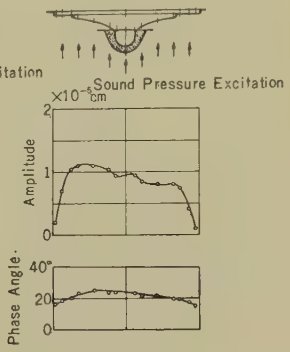

Fig. 25

Fig. 24—Modes of vibration of new telephone transmitter diaphragm with movable electrode (Type Ⓓ).

Fig. 25—Modes of vibration of new telephone transmitter diaphragm with movable electrode and carbon granules (Type Ⓓ).

7. Conclusion

In order to better understand the properties of conical diaphragms for telephone transmitters and receivers, some experimental double-size conical vibrating plates have been made, and their fundamental resonant frequency, effective mass, effective stiffness, etc. have been measured. From these results the "Frequency constant" and the "Stiffness constant" which are very useful for the design of telephone diaphragms have been defined, and their values were experimentally determined. Then by observing the modes of vibration it has been concluded that radial corrugations on the conical diaphragm are unnecessary.

Next investigations on diaphragms for telephone transmitters and receivers have been conducted and as a result the effectiveness of the frequency constant and the stiffness constant have been verified. And it is shown that the method of fixing the magnetic armature to the telephone receiver diaphragms has an influence upon the modes of vibration and area factors, and an extremely good method of a fixing the armature has been proposed and its effectiveness has also been confirmed.

Of course there are many other important problems concerning telephone transmitter and receiver diaphragms other than the problems discussed above; namely the second resonant frequency and the modes of vibration at its frequency, etc. Moreover, there are many unascertained aspects about the press working; the minimum amount of working and their order to obtain the required accuracy, the magnitude of stroke of one press working, the design of press die, etc., and these questions call for further investigations.

Acknowledgment

The authors wish to express their appreciation to Doctors Toshio Hayasaka, Giichi Ito, and Kenro Masuzawa for many useful suggestions and valuable advice throughout the progress of this work. They also wish to acknowledge the help of Mr. Kaoru Nishiguchi and Mr. Kenzo Ogawa in making both the experimental vibrating plates and the telephone diaphragms.

References

(1) T. Hayasaka: Theory of Acoustic Vibration, p. 114, 1948, Corona Co.
(2) G. Ito: The Specific Responses of Carbon Transmitters in Low Frequencies, *Jour. Inst. Elect. Comm. Engrs .Japan*, Vol. 39, No. 3, p. 187, 1956.
(3) T. Hayasaka: Acoustic Enginerrting, p. 397, 1957, Nikkan-Kogyo Press.
(4) R. J. Roark: Formulas for Stress and Strain, p. 209, 1954, McGraw-Hill.

* * * *

REVIEW OF THE ELECTRICAL COMMUNICATION LABORATORY
VOLUME 8, NUMBERS 11-12, NOVEMBER-DECEMBER, 1960

U.D.C. 534.78 : 465.6] : 621.391

On Fundamental Qualities of Vowel Sounds in Speech Communication*

(Part 2)

Continued from p. 425.

Yoshiyuki OCHIAI† and ***Teruo FUKUMURA***†

3. Study of Auditory Confusion

When the response mode of the listeners based upon the "identification" method of signal-quality judgment is adopted as our principal method of quality measurement, the most intensive interest of our studies is focused upon the relation of correspondence between an ensemble of timbre-signals as stimuli and an ensemble of timbre-qualities as responses, that is, on the problem of the "auditory confusion." For example, if we want to understand more concretely the quality characteristics of BED so far explained, we must come to the points to be decided: Under a particular band-cutting distortion, what is the degree of confusion of a particular voice signal with which this signal corresponds to quality responses? Also, how does this type of confusion correspond to the pattern deformation due to this distortion? This does not mean a one-sided study of the listener's response based only upon "correct" judgement as found in the past tranditional articulation studies, but takes into consideration also the minute characteristics appearing in the "incorrect" judgment. We can thus attain novel and clear interpretations of the "quality" itself and even the "distortion." The term "quality modification" which has been used corresponding to the pattern deformation stems from the special study of the auditory confusion presented here.

3.1. Confusion in the Distortionless Condition

When clarifying the quality phenomena from the viewpoint of correspondence between a deformed signal pattern and the listener's quality response, there are some problems about the fact that signal and quality do not show one-to-one correspondence even under the distortionless condition, where no physical distortion exists. Although the present study is aimed at a quality study of speech under physical distortion, this subjective quality study in the distortionless condition will be considered as the basis of our study, because it is thought to indicate directly the concrete mechanism of quality formation. The quality to be dealt with first is voice quality.

3.1.1. Confusion Matrix and Voice Quality Configuration

The confusion matrix is obtained by tabulating the frequency of correspondence observed in each combination of signal and quality. Table 2 shows the confusion matrix for BED of experiment No. 6. The capital letters vertically aligned on the left side of the confusion matrix are signal symbols showing kinds of voice at the sending point. The lower-case letters horizontally aligned in the under part are quality symbols showing

---

* MS in Japanese received by the Electrical Communcation Laboratory, Aug. 18, 1960. Originally published in the *Kenkyû Zituyôka Hôkoku* (*Electrical Communication Laboratory Technical Journal*), N.T.T., Vol. 9, No. 12, pp. 1469–1549, 1960.

† Nagoya University.

Table 2

VOCAL QUARITY CONFUSION MATRIX IN THE ALL-PASS CONDITION (EXPERIMENT NO. 6)

All-pass Condition					
	t	s′	m′	h	Σ
T	362	116	16	6	500
S′	84	322	92	2	500
M′	21	72	355	52	500
H	4	19	13	464	500
Σ	471	529	476	524	2000

Notes:
Capital letters = Transmitting signals.
Lower-case letters = Receiving qualities.
Blocks with heavy outline show definite subgroups.
Blocks with dotted outline show somewhat ambiguous subgroups.
el = elision.
Voices = All male voices.

listeners’ response at the receiving point. The figure in cells shows the aggregate of frequency of correspondence between signals and qualities for four listeners. It is seen from the confusion matrix that there are some trends in confusion occurrence and further that any two voices which are adjacent to each other in such arrangement are mutually related most closely. This arrangement of voices is called “voice-quality configuration.” It can be shown that the voice ensemble adopted here is further divided into 3 subgroups as indicated by the smaller blocks in the table. When we examine the arbitrary combination of any two voices, it is possible to consider the “reciprocity” of confusion. For example, as seen from the figures in the table, the trend of confusion from “T” to “s′”, is more marked than that from “S′” to “t”, and in such a case the confusion is said to be nonreciprocal. For a combination of “S′” and “M′”, on the other hand, there is fairly similar frequency of correspondence, between “S′”→“m′” and “M′”→“s′”, and it may be said that the reciprocity holds to a certain extent. On the contrary, lack of reciprocity between “M′” and “H” is most marked. From the fact that the reciprocity does not hold in some combinations, it follows that there seems to be a certain kind of bias in judgment of listeners regarding criteria of the differentiation of two voices of similar voice quality. How such a bias is established can not be immediately answered, but it may be inferred that the reason for the lack of reciprocity that seems to take place between “M′” and “H”, for example, is that a clue to quality judgment of “H” is better grasped than that of “M′”. In the case of “T” and “S′”, “T” is only similar to the quality of “s′”, while “S′” has qualities similar to both “t” and “m′”. It can then be explained that the confusion frequency of “S′” is shared by two different confusion-objects, thus resulting in nonreciprocal confusion. In any case, the manner of configuration by which voice qualities are arranged in the ensemble reveals, so to speak, some matter and substance regarding the listeners’ perception of voices and consequently this is intimately related to the listeners’ subjectivity. To begin with the discussion of reciprocity and lack of reciprocity in confusion so far described is just to stress how the idea of “direction” is indispensably important in the analysis of confusion phenomenon. For further details of fundamental interpretation of confusion, reference must be made to the Literature (38).

3.1.2. Relation between the Envelope Shape of the Vocal Pattern and Voice-Quality Arrangement

Now we pass into the comparative observation between voice-confusion in the distortionless condition and the vocal pattern of individual voices. [Experiment No. 6.]

Here analytical study was done by utilizing the sonagraph. Fig. 9 is obtained by averaging five vowel patterns in each voice given by the sonagraph, in which, however, characteristics of higher frequency emphasis of the

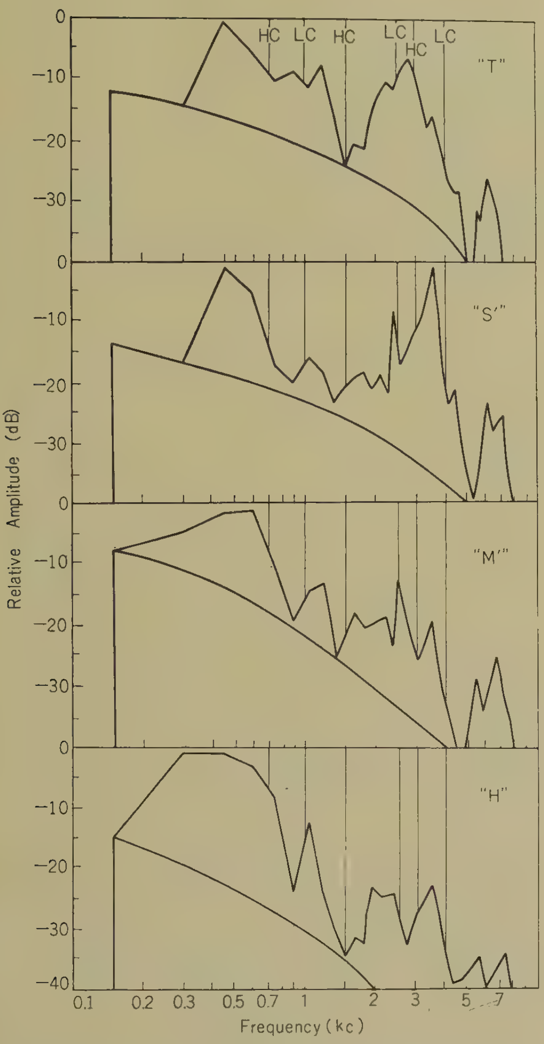

Fig. 9—Base envelopes found in each vocal-pattern (Experiment No. 6).

analizer are duly compensated for and adjusted to exactly flat characteristics.

The almost linearly decreasing curves are drawn as shown in the pattern figures, by tracing the basis of the principal glens of the pattern as one of the simple ways of characterizing the shape of these patterns. These curves thus obtained can not be said to correspond directly and immediately to some physical concrete substance. However, they may be considered as bearing upon some direct expression of vocal pattern characteristics which is governed at least by the vibration modes of the vocal cord and probably further by the resonance position and selectivity mode of an articulatory organ. Fig. 10 (A) shows an averaged pattern of each vocal pattern, and Fig. 10 (B) gives only the envelopes obtained after discarding all peak structures from each vocal pattern. We propose that these envelopes be designated the "base envelope."

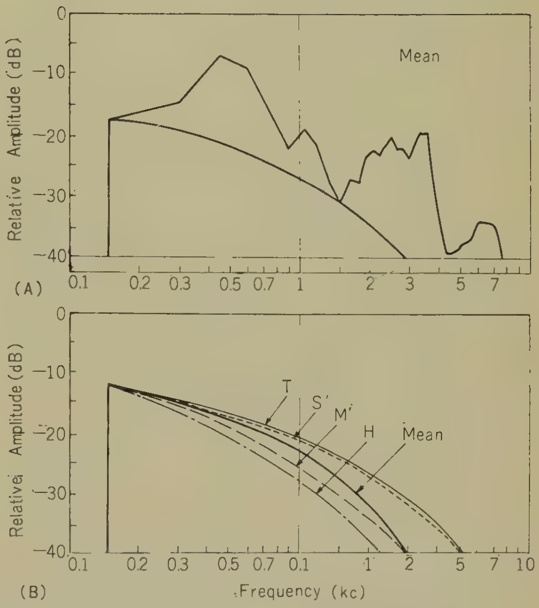

Fig. 10—Comparison of averaged form of vocal pattern and "base envelope" with regard to four individual voices.

When comparing each voice, it is well to notice that the slopes of the envelope curves run in the order of "T", "S′", "M′" and "H", and further that this order conforms to the voice-quality arrangement in the confusion matrix as already explained. From this fact it is assumed that the voice-quality classification has something to do with such a simple extraction of shape characteristics of vocal patterns. Careful observation naturally can be carried out by comparatively examining the shape of the envelopes of the four individual vocal patterns, instead of their base envelopes, and the shape of an averaged pattern of four voices. For example, the shapes of the patterns of "S′" and "M′" are very similar to the averaged one, while the other two, "T" and "H", particularly "H", are not similar to the averaged one. Joint consideration of this fact and the ambiguity of voice judgment observed in the confusion matrix yields the conclusion that the voices having the patterns similar to averaged one are most ambiguous in regard to voice-quality judgment. From this it follows immediately that when listeners try to classify voices in a given ensemble for memorizing them in their mind, the principal scheme of their voice-classification does not depend on a particularly localized frequency band of patterns, but relies possibly upon silhouette shapes outlined throughout the whole patterns. The extractive representation of pattern by base envelope as shown in Fig. 10 (B) is simple and effective, but can not be considered to furnish us sufficiently full information, although it is even of interest to note that rough arrangement of voice quality is possible very reasonably in this way.

[experiment No. 1]

The voice ensemble in this experiment consists of "F°" (male), "S°" (male), "C°" (child), "Y°" (female) and "H°" (female) voices. The confusion matrix in the all-pass reference condition is shown in Table 3.

Table 3

VOICE QUARITY CONFUSION MATRIX IN THE ALL-PASS CONDITION (EXPERIMENT NO. 1)

	f°	s°	y°	c°	h°	Σ
F°	352	31	6	8	3	400
S°	16	321	28	30	5	400
Y°	1	24	283	34	58	400
C°	1	11	47	320	21	400
H°	0	8	32	10	350	400
Σ	370	395	396	402	437	2000

F°=Male, S°=Male, Y=Female, H°=Female, C°=Child.

The voice-quality arrangement is shown in the order of "F°, S°, Y°, C° and H°". The vocal patterns of the individual voices and their averaged pattern are shown in the order of the voice quality arrangement in Fig. 11.

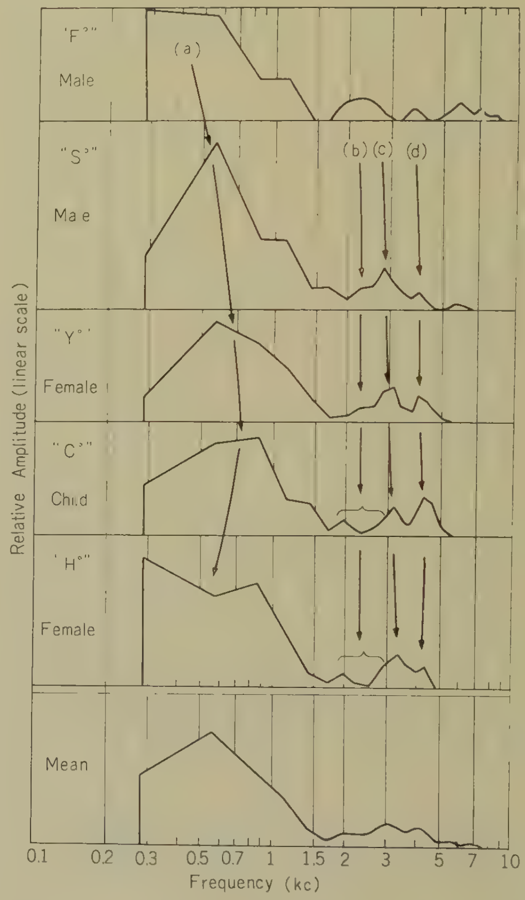

Fig. 11—Explanation of pattern arrangement corresponding to voice configuration (Experiment No. 1).

The experimental processes to obtain these patterns are carried out utilizing a frequency analyzer as explained in Chapter 1. The four full lines with arrows drawn through these pattern figures are:

(a) the line which is formed by the first formants of the five vowels and the second formants of "A" and "O" (sometimes with "U").

(b) the line which is formed by the second formants of vowels, "I" and "E".

(c) the line which is formed by the third formants of the five vowels.

(d) the line which is formed by the fourth formants of the five vowels.

The frequency position of these lines in the patterns becomes higher approximately according to the order of voice-quality arrangement, with the exception of voice "H°", where its frequency position of lower formant cannot be indicated so definitely as in the cases of other voices because of the complexity of the pattern shape. It has been found that the formant positions approximately coincide with the physical stature of the calling subjects and seem determinable by the size and volume of their articulatory organs. However, the position of the higher formants for example, the third (c) and the fourth (d) formant lines of "H°"'s voice are relatively high notwithstanding her comparatively large physique, and these data do not seem connected directly with the size of the articulatory organs.

In voices "C°" and "H°", pattern parts indicated by the (b) line are quite dispersed, revealing that the positions of the second formant of "I" and "E" are considerably apart from each other. This seems to be caused by the fact that the calling subjects have pronounced "E" with their mouths a little wider open than normal.

Now the relation between vocal-patterns and voice-quality arrangement will be examined for individual voices. Let us look at the outlined forms of pattern envelopes in Fig. 11. Several facts of importance can be seen: First, the form of the intermediate voice "Y°" in arrangement is very much like that of the averaged pattern; second; "C" and "S" are alike; third, the forms of the two voices "F°" and "H°" at both ends of the arrangement are the least alike. Similarity to the average pattern in these cases is noticed not only in the envelope forms as a whole, but also in the position of each formant as shown by lines (a), (b), (c), (d). These present relatively clear and intimate correspondence between the characteristics of the pattern form and modes of grouping in voice-quality configuration. As the vocal pattern, presently under observation, is too narrow by about 25 dB in component amplitude by the limitation of oscillographic recording, the details of the base envelopes can not be sufficiently obtained as before. Nevertheless, it is of interest, as showing a clue to the mechanims of vocal quality formation, that fairly clear correspondence has been found between positional relation of the pattern formants and voice-quality arrangement. Among various voice groups, the "Y°"–"H°" group does not apparently correspond to mutual disimilarity of these two patterns, but this seems to be due to complexity in the lower part of the "H°" pattern, because the "H°" pattern form in its lower part has a part of characteristic of "C°" as the smallest physique on one hand, and a part of characteristic of "F°" as the largest physique on the other hand. The strong fundamental component of "H°" results from the fact that the frequency is already situated in the part of the first formants of "I" and "U". Then it follows that in this case when pronouncing these vowels, the size of the throat cavity is as large as that of a male, while the reinforcement of the third harmonics may be attributed to the fact that when pronouncing other vowels the size of the cavity is that of a female or child. The voice whose vowel pattern changes from the region of a male voice to nearly that of a child according to the kind of vowel is peculiar. The relation between vocal patterns and confusion, in such a case, can not easily be explained. The separate article (39) may be referred to for the details of the characteristics of voice "H°".

〔Experiment No. 5〕

The confusion matrix is shown in Table 4. The voice qualities are arranged in the order of "K′", "M", "C′" and "S".

Subgrouping by sex, such as "K′"–"M" or "C′"–"S", is most conspicuously noticed, then follows grouping of "M"–"C′", which is rather nonreciprocal. The respective vocal

Table 4

VOICE QUALITY CONFUSION MATRIX IN THE ALL-PASS CONDITION EXPERIMENT NO. 5)

	k′	m	c′	s	Σ
K′	256	40	1	3	300
M	43	235	7	15	300
C′	6	32	222	37	300
S	2	6	57	235	300
Σ	310	313	287	260	1200

K′=Male, M=Male, C′=Female, S=Female.

patterns of individual voices and their averaged pattern are shown in the order of the voice-quality arrangement in Fig. 12. The frequency analyzer was the same one explained in Section 1.

From the observation of the outlined forms of pattern envelopes in this figure, it is easily seen, as in the preceding cases, that the patterns of voices "C′" and "M" having intermediate voice quality are most similar to an averaged pattern. The position and strength of formants in the upper part may be considered to correspond to the subdivision of the ensemble by sex into two groups, "K′"–"M" and "C′"–"S", as explained in Section 3. Although the grouping of "C′"–"M" can be explained by similarity of pattern forms, it is impossible to find any interpretation of the nonreciprocal trend of confusion of "C′" →"m" without further minute inspection of pattern shapes coming down to the details of individual vowels.

Runing through the data of the above three experiments, correspondence between the confusion under the distortionless condition and the relation of vocal pattern arrangement is sufficiently traced. It is recognized from voice-quality arrangement and vocal pattern representation that the listeners' classification of voice quality primarily depends upon the outlined shapes of pattern envelopes. To explain fully, in the cases where the ensemble consists only of male voices as in experiments No. 2 and 6, the listeners can classify voices only on the basis of the simpler shape of the base envelope in vocal patterns obtained by excluding peak structures from our observation. In experiments No. 1 and 5 where consciously the sex element was brought into the voice ensemble, the shapes of the base envelopes do not correspond simply to voice-quality arrangements. In such cases, however, the listener's ability

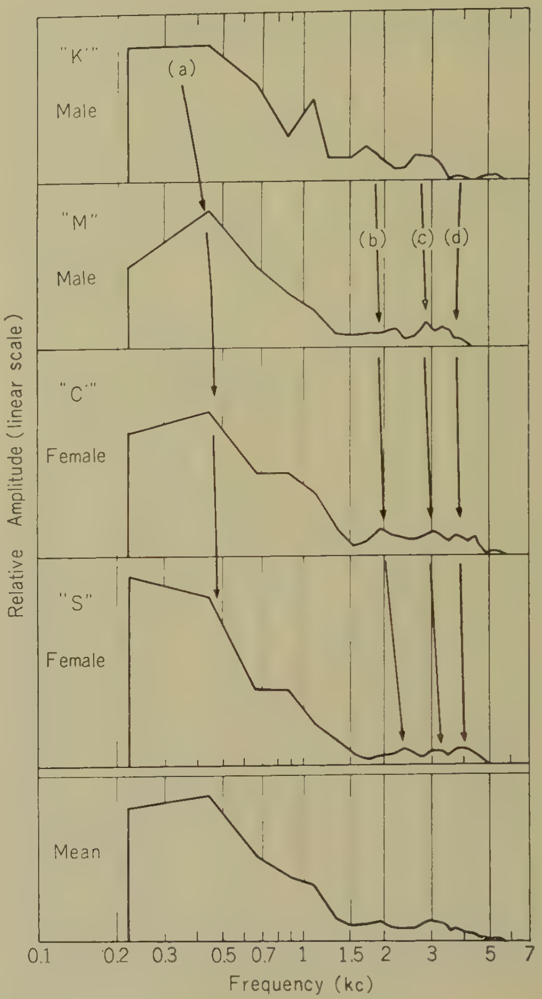

Fig. 12—Explanation of pattern arrangement corresponding to voice-quality arrangement (Experiment No. 5).

to discerne sex difference seems to depend primarily upon the position and strength of formants in the upper part, and then seem to depend upon the relative position of the peak structures localized in the frequency dimension, as a clue for more delicate quality difference.

3.2. General Treatment of Confusion Phenomena

The effort made in the preceding section, is to make clear the matter of voice-quality configuration and to trace the mechanism of voice-group classification, based exclussively upon the confusion matrices in various experiments. It is by this confusion study of voice ensemble that we aimed at deriving an interprtation of vocal pattern. However, it becomes exceedingly and evidently troublesome to examine the confusion in the most detailed phase, because the confusion matrix has the same number of degrees of freedom as the number of total cells found in its matrix. In the preceding section, as an aspect of confusion phenomena, the direction of confusion is pointed out, and the importance of direction for the analysis of confusion phenomena is stressed, citing the proposal of the concept of reciprocity of confusion. In dealing with confusion, other important concepts are the "amount of frequency" and the "equivocation" regarding correspondence between signals and qualities. In order to particularize the confusion matrix systematically and generally, further discussion may be made on these fundamental concepts as follows.

3.2.1. Principle of Confusion Analysis

1) Direction of confusion

The aim of the analysis of the confusion matrix is to clarify the mechanism of quality formation by tracing the relation between quality response and pattern forms of signals. Therefore our main interest regarding confusion matrix analysis in general distortion cases will naturally be focused on the following two questions: (1) To what matter of quality responses does the pattern of a particular signal deformed by a certain type of distortion correspond? In order words, how is a particular signal deformed by distortion connected with a set of responses of all qualities? (2) For a particular quality, to what content of quality response does a set of patterns of all signals deformed by certain distortion correspond. In other words, how is a set of signals deformed by distortion connected with a particular quality?

The former question (1) deals principally with quality modification of a signal by distortion and this problem is necessarily connected with the concept of "quality deterioration" or "quality destruction" by distortion. The latter question (2) treats exclusively quality modification of signals by distortion, thus turning out to a particular quality, and this problem is necessarily connected with the concept of "quality construction" or "quality formation" by distortion. Confusion considered from the former standpoint is called "outgoing confusion" which goes from a particular signal to an entire group of qualities. Confusion considered from the latter standpoint is called "incoming confusion" which comes to a particular quality from a group of signals. The concept of direction is thus introduced by distinguishing between outgoing and incoming confusions. These new concepts naturally stem from the essential consideration of the quality-theory based upon confusion analysis. Confusion should not be treated as a phenomenon where one signal is simply misheard as another. By considering signal patterns at the sending point and qualities at the receiving point, it becomes possible to study the mutual correspondences between them along two directions. The quality-theory orientated along this line can have its basis, in the interpretation of confusion phenomena.

2) Frequency of confusion occurrence and uncertainty of correspondence

When analizing the confusion matrix separately in two directions, not only uncertainty of correspondence between signals and qualities, but also frequency of confusion occurrence should be taken into consideration as far as we are dealing with an ensemble.

When, for instance, a certain distortion increases not only the uncertainty of correspondence; but also the frequency of occurrence of outgoing confusion from a particular signal, this distortion should be considered as "quality-destructively" acting on this particular signal. But on the other hand, when a certain distortion increases not only uncertainty of correspondence, but also the incoming confusion to a particular quality, this distortion can be said to be "quality-constructively" acting regarding this particular quality. Introducing the concept of confusion direction and then evaluating in each direction the occurring frequency of confusion as well as uncertainty of correspondence, it becomes possible for the first time to attain both generality and simplicity in confusion analysis.

3.2.2. Interpretation of Phonemic Confusion Phenomena from the Concept of Outgoing and Incoming Confusions

It is very important in quality theory to introduce the concept of the incoming confusion as well as outgoing confusion into the analysis of confusion phenomena. Confusion analysis in the past seems to have been limited mostly to what we call outgoing confusion. By the combined consideration of incoming and outgoing confusions, the problem of reciprocity can properly be evaluated. In addition the confusion phenomena can be treated in more generality than ever, and from these basic treatments, several new facts become available for the interpretation of quality phenomena. For example, the phonemic confusion in BED, the quality of which is characterized by concentration of quality density. The outgoing-confusion characteristics can fully account for the process of quality destruction, as the nature of the confusion on this direction may be considered to be strongly related to the eliminated part of the pattern of phoneme. On the other hand, the incoming confusion may be considered as directly bearing upon the residual quality, as it has much to do with the remaining part of the pattern. It is in this respect that the incoming confusion phenomena are full of interest. From these points of view, Fig. 13 is made to express the importance domain of each phonemic quality of five vowels. In the figure, phonemic quality characteristics in the ordinary sense are fully utilized, being combined with the data of phonemic confusion characteristics: namely, for each vowel, the percentage value of correct articulation and the ratio of incoming confusion to particular phonemes are used jointly in the same figure.

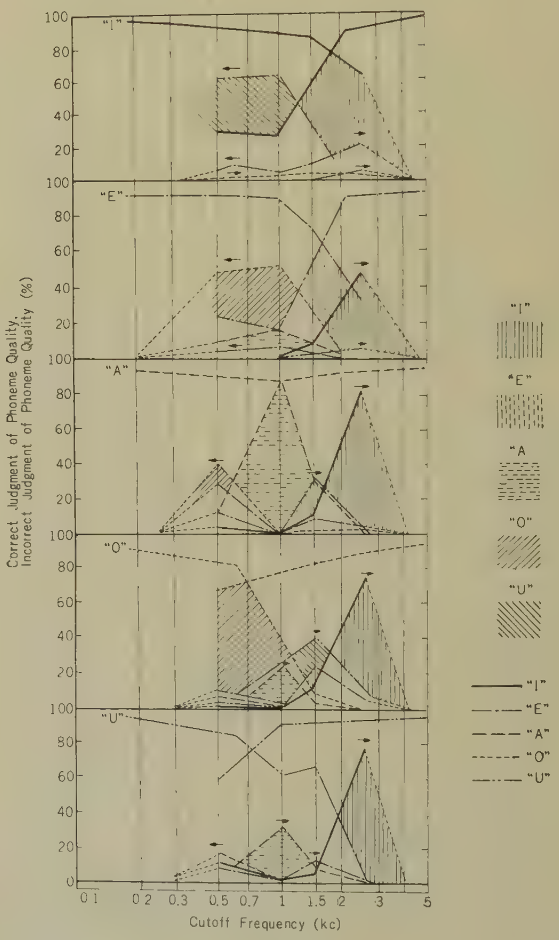

Fig. 13—Representation of quality distribution of 5 Japanese vowels by confusion characteristics and quality loss characteristics (Experiment 2).

Even from the results of this experiment, where the cutoff conditions were quite rough and could not cover the entire frequency range required, it is easily seen that an incoming confusion to a particular quality, is fairly stabilized regardless of the kind of source from which it originates, and further that the mode of incoming confusion appears very concentrated on the frequency scale. It will also be distinctly seen in this figure how the position of the quality-balancing point relates to the real position of quality accumulation.

The new concept of "negative importance" is duly discovered by taking the incoming confusion into consideration in addition to the outgoing confusion. Then the quality interpretation of the frequency band can be, from the viewpoint of quality distribution, expected to be more delicate and fine. The traditional thinking of importance as being only "positive", seems to stem from the point of view which is limited to outgoing confusion. Where a given frequency-band position corresponds to a quality accumulating point of a particular phoneme quality, the confusion incoming to this phoneme suddenly increases, because the position may be regarded as "positively" important for this phoneme. On the contrary, when some particular band region other than the one considered above corresponds to a very conspicuous quality accumulating point of some phoneme other than the phoneme considered, the outgoing confusion from this phoneme suddenly increases on that band region; this means that the position of this kind will prove itself not only unnecessary but even harmful to the phoneme in consideration. The concrete examples of the description will be found in Fig. 13. "Negative importance," or the concept of "nuisance," comes out in this way. The problem treated above is limited to the consideration of phonemic quality only. However, the really significant problem lies in the interaction between voice quality and phonemic quality. The transmission theory primarily aiming at one-sided transmission of intelligibility only and keeping the voice quality elements out of sight, necessarily leads us to an easy thought to regard voice elements as only "redundant" for phonemic elements. According to us, to do away with nuisance does not mean to save the frequency bands from an economical viewpoint, but to express positively the intelligibility. This consideration goes out of the sphere of faithful transmission based on the traditional idea of "fidelity" in communication.

3.2.3. Definition of Confusibility

In order to analyze confusion phenomena in two directions, and to represent occurring frequency and uncertainty of correspondence quantitatively, it is convenient to use the same measure of information amounts as used in information theory(37)(41)(42). The figures in the confusion matrix show occur-

Table 5

GENERALIZED REPRESENTATION OF MATRIX CONFUSION

(A)

	x_1	x_2	$\cdots x_i \cdots$	x_n	Σ
X_1	α_{11}	α_{12}	$\cdots\alpha_{1j}\cdots$	α_{1n}	$N_{1\cdot}$
X_2	α_{21}	α_{22}	$\cdots\alpha_{2j}\cdots$	α_{2n}	$N_{2\cdot}$
$\vdots$	$\vdots$	$\vdots$	$\vdots$	$\vdots$	$\vdots$
X_i	α_{i1}	α_{i2}	$\cdots\alpha_{ij}\cdots$	α_{in}	$N_{i\cdot}$
$\vdots$	$\vdots$	$\vdots$	$\vdots$	$\vdots$	$\vdots$
X_n	α_{n1}	α_{n2}	$\cdots\alpha_{nj}\cdots$	α_{nn}	$N_{n\cdot}$
Σ	$N_{\cdot 1}$	$N_{\cdot 2}$	$\cdots N_{\cdot j}\cdots$	$N_{\cdot n}$	N

(B)

quality / Signal	(X_i)
$p(X_i)$	$p(X_i, x_j)$

$$p(x_j X_i) = \frac{p(X_i, x_j)}{p(X_i)}$$

ring frequency, from which the statistical probability (ratio) can immediately be calculated.

If in the generalized confusion matrix in Table 5 (A), statistical probability concerning the correspondence between a particular signal X_i and a particular quality x_j is shown by $p(X_i, x_j)$, we obtain:

$$p(X_i, x_j) = \frac{\alpha_{ij}}{N}$$

Occurrence probabilities of this signal and this quality are respectively

$$p(X_i) = \frac{N_{i\cdot}}{N}, \quad p(x_j) = \frac{N_{\cdot j}}{N},$$

For conditional probability between signal X_i and quality x_j, we have

$$p(x_j X_i) = \frac{\alpha_{ij}}{N_{i\cdot}}, \quad p(X_i x_j) = \frac{\alpha_{ij}}{N_{\cdot j}},$$

from which is obtained the following relation:

$$p(X_i, x_j) = p(X_i) p(x_j|X_i) = p(x_j) p(X_i|x_j).$$

Therefore, as shown before in Table 5(B), frequency ratio in the matrix can be completely replaced by the statistical probability. Using the values thus transformed, the quantity to express the uncertainty of correspondence in the direction from a single to a quality group, that is the outgoing confusion will be:

$$C^{i\prime}_{\text{out}} = -\sum_j p(x|_j X_i) \log p(x_j|X_i)$$

which, further weighted by the probability of occurrence, leads to the expression:

$$C^{i}_{\text{out}} = -\sum_j p(x_j, X_i) \log p(x_j|X_i)$$

The *individual outgoing confusibility* is defined by this quantity in which are taken into account at the same time the uncertainty of correspondence and frequency of correspondence. In the same way, regarding the incoming confusion.

$$C^{j}_{\text{in}} = -\sum_i p(X_i, x_j) \log p(X_i|x_j)$$

is obtained for a quality x_j, and it defines the *individual incoming confusibility*. These quantities are measured in the unit of "bit" if the base of the logarithms is taken as 2. Of course, the sums of individual confusibilities of all signals and of all qualities are equal to "uncertainty" $H(x|X)$ and "equivocation" $H(X|x)$ respectively. The total sums, there denoted by C_{out} and C_{in}, are called *ensemble outgoing confusibility* and *ensemble incoming confusibility* and calculated by the following formulas:

$$C_{\text{out}} = \sum_i C^{i}_{\text{out}}, \quad C_{\text{in}} = \sum_j C^{j}_{\text{in}}.$$

Further, the information amount transmitted, R, is calculated from the confusion matrix in the following manner: i.e.,

$$R = H(X) - H(X\,x) = H(x) - H(x\,X)$$

$$= H(X) - C_{\text{in}} = H(x) - C_{\text{out}}.$$

To make the occurrence frequency of each signal equal and to avoid elision in perception, as has been done in our experiments, the following relation

$$H(X) \geqq H(x)$$

always exists. Thus, we have finally a relation

$$C_{\text{in}} \geqq C_{\text{out}}.$$

The individual confusibility defined above generally takes into account both the frequency and the dispersion of correspondence between signal and quality. Strictly speaking, however, further consideration concerning the occurrence mode of each signal is needed to combine the dispersion and the frequency of correspondence into a factor directly reflecting the quality effect of distortion. But, as the occurrence frequency of signals is kept constant throughout all of the experiments, the outgoing confusibility in our case is reduced to the representation of only the dispersion of correspondence. Therefore the increase or decrease in outgoing confusibility can be considerd as reflecting simply the degree of quality destruction due to distortion. Although the incoming confusibility takes into account both the dispersion and frequency of correspondence, it can be also conceived that the confusibility in this direction truly represents the degree of quality construction. The large value of the incoming confusibility means that to a considerable extent all signals tend to have a particular quality. For the exact evaluation of quality effect of each condition of distortion, however, it is necessary to compare the value of the outgoing confusibility with that of the incoming one. When, for instance, quality judgment becomes sufficiently ambiguous as a whole by certain distortion, it is quite conceivable that the outgoing confusibility as well as the imcoming confusibility increases. If, for certain distortion, the relation:

$$C^i_{\mathrm{out}} > C^i_{\mathrm{in}}$$

is obtained, this distortion is considered to have a destructive action of a quality x_i with regard to the signal group; and if the relation

$$C^i_{\mathrm{in}} > C^i_{\mathrm{out}}$$

is obtained, the distortion is considered to have a constructive action of the same quality regarding the same signal group.

3.2.4. Representation of Experimental Results by Confusibility

Making use of the data of measurement in BED of experiment No. 2 as an example, the confusibilities defined above are calculated from the confusion matrix for each condition of distortion. The explanation of the experimental results based upon this manipulation of data will now be described. The confusion matrices are shown in Tables 6 and 7 for phonemic quality and voice quality respectively.

(1) Phonemic confusion

Individual confusibilities for five vowel phonemes are calculated in each cutoff condition and shown in Fig. 14. The results for LC and HC distortions are presented in Figs. 14(B) and (C) respectively. In Fig. 14(B) is shown five vowel patterns, each of which is averaged for four voices. It will be noticed from the general form of confusion curves that confusibilities in both directions are very different from each other in the particular cutting points, and also the confusibility curves take very characteristic shapes according to the kinds of vowel sound. In the succeeding paragraphs, we shall explain the shapes of curves for each combination of vowel sounds and quality.

"I"—"i"

The characteristic curve in HC distortion is more remarked than that in LC distortion. Outgoing confusion has rather simple characteristics in both distortion directions. This means that diminuition in phonemic quality is not remarkable in spite of the deformation of patterns within the distortion range. Incoming confusion in LC distortion becomes gradually conspicuous from LC 1.0 kc and reaches about 1.7 bits at LC 2.5 kc. As the conceivable maximum value of individual confusibility is 2.3 bits, it can be said that about 83 % of vowels in signal ensemble have the quality "i" at this cutting point. The formant components between 2–3 kc found in each pattern of the Fig. (B) have undergone a sort of emphasis influence, as the result of sudden cutting of the components in the lower band and level recovering of the remaining part at the same time. Thus, the band-cutting distortions from 1.5 to 2.5 kc are said to bring quality-constructive action of "i" with regard to vowel ensemble. With regard to HC distortion, incoming confusion does not surpass outgoing confusion within the range of distorting conditions used. As it seems too hasty to conclude from this figure that neither sudden cutting off in the higher region nor emphasis in the lower region contributes to forming "i" quality, it is necessary to prepare more finely and sharply cutting-off steps

Table 6

PHENOME-QUALITY CONFUSION MATRIX IN BED (EXPERIMENT NO. 2)

LC : 1. 0 kc

	i	e	a	o	u	Σ
I	223	17	0	0	0	240
E	1	236	3	0	0	240
A	0	0	232	6	2	240
O	0	1	71	101	67	240
U	0	0	88	5	147	240
Σ	224	254	394	112	216	1200

LC : 2. 1 kc

	i	e	a	o	u	Σ
I	224	4	0	0	12	240
E	0	237	1	0	2	240
A	0	0	232	8	0	240
O	0	1	4	222	13	240
U	0	0	5	0	285	240
Σ	224	242	242	230	262	1200

LC : 1. 5 kc

	i	e	a	o	u	Σ
I	212	28	0	0	0	240
E	25	201	10	1	3	240
A	41	102	56	8	33	240
O	43	64	3	27	103	240
U	14	31	10	8	177	240
Σ	335	426	79	44	316	1200

HC : 1. 0 kc

	i	e	a	o	u	Σ
I	66	3	2	7	162	240
E	0	41	41	139	19	240
A	0	0	232	8	0	240
O	0	8	19	197	16	240
U	2	1	4	6	227	240
Σ	68	53	298	354	424	1200

LC : 2. 5 kc

	i	e	a	o	u	Σ
I	169	56	4	3	8	240
E	128	83	12	4	13	240
A	200	22	0	2	16	240
O	201	12	0	0	27	240
U	201	14	8	9	8	240
Σ	899	187	24	18	72	1200

HC : 0. 5 kc

	i	e	a	o	u	Σ
I	75	1	2	6	155	240
E	5	68	25	128	14	240
A	9	69	30	100	32	240
O	0	29	23	173	15	240
U	30	13	7	34	156	240
Σ	120	87	180	441	372	1201

Table 7

Voice-Quality Confusion Matrix in BED (Experiment No. 2)

all-pass

	y	k	n	f	Σ
Y	258	33	7	2	300
K	18	271	9	2	300
N	12	18	250	20	300
F	1	1	13	285	300
Σ	289	323	279	309	1200

LC : 1. 5 kc

	y	k	n	f	Σ
Y	162	65	41	2	300
K	85	172	36	7	300
N	40	16	210	34	300
F	0	6	33	261	300
Σ	317	259	320	304	1200

LC : 0. 4 kc

	y	k	n	f	Σ
Y	223	48	29	0	300
K	64	227	9	0	300
N	10	8	272	10	300
F	0	2	28	270	300
Σ	297	285	338	280	1200

HC : 2. 1 kc

	y	k	n	f	Σ
Y	196	72	36	6	300
K	43	221	30	6	300
N	17	29	224	30	300
F	9	7	12	272	300
Σ	265	329	292	314	1200

LC : 0. 6 kc

	y	k	n	f	Σ
Y	232	39	27	2	300
K	72	205	20	3	300
N	24	14	248	14	300
F	1	2	29	268	300
Σ	329	260	324	287	1200

HC : 1. 0 kc

	y	k	n	f	Σ
Y	190	59	44	7	300
K	52	162	70	16	300
N	22	43	204	31	300
F	7	10	23	260	300
Σ	271	274	341	314	1200

Voice: All male voices.

Table 7

HC : 0. 5 kc

	y	y	n	f	Σ
Y	153	71	62	14	300
K	52	111	103	34	300
N	51	66	160	23	300
F	8	23	28	241	300
Σ	264	271	353	312	1200

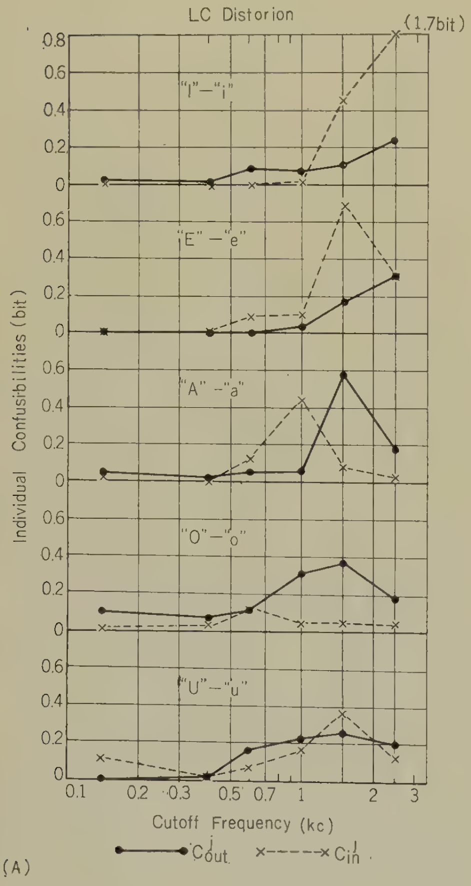

(A)

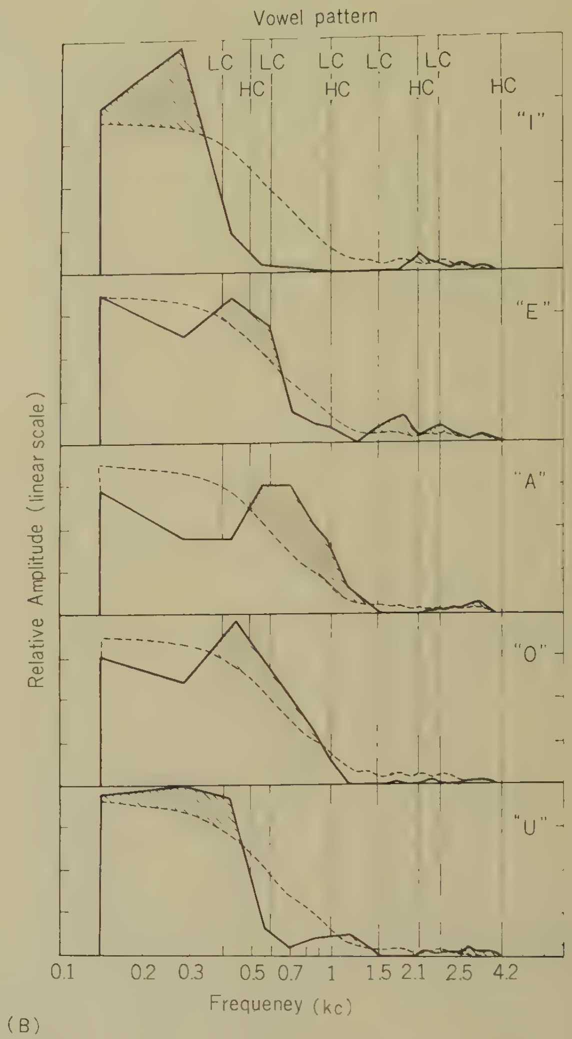

(B)

Fig. 14—Representation of phonemic confusion in BED and display of vowel patterns (Experiment No. 2).

covering the frequency region lower than 0.5 kc. The phonemic quality of "I" is duly represented by the pattern differences between the vowel pattern (in full line) and mean vocal pattern (in dotted line) as shown in the figure (B), and the differences are observed a little concentrated in the frequency regions of the neighborhood of 2 kc and 0.2–0.3 kc. The components near 2 kc, which may well be considered as the main formant of phoneme "I" are sharply emphasized as

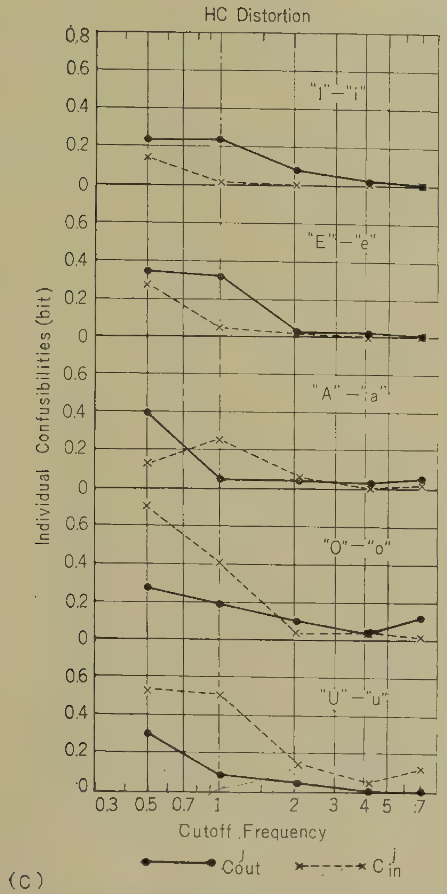

Fig. 14—Representation of phonemic confusion in BED and display of vowel patterns (Experiment No. 2).

the last residuals of band components in LC distortion, while in HC distortion, many lower components remain uncut and critical emphasis of particular components can not be expected.

"E"—"e"

The confusion characteristics of this vowel is similar to those of "I". The strong trend in quality construction is recognized from LC 1.5 kc, and this means, as in the case of "i", that the quality transition to "e", i.e., quality formation, takes place by emphasizing the pattern components of each vowel near this cutting-off point (Confusion toward "i" from "E" increases at LC 2.5 kc, but incoming towards "e" decreases there, and thus the quality effect of distortion becomes ambiguous). In HC distortion, the outgoing confusion is generally stronger than the incoming one, and particularly, distortion of HC 1.0 kc seems only to have a destructive action of quality "e". The components near 1 kc as shown by the pattern of "E" in the Fig. (B) seems to have what we call "negative importance" of phoneme "E". To put it concretely, the second formant necessary in quality formation of "e" is cut off and the timbre of residual patterns comes to resemble "o", "u", "a", etc.

The note regarding "i" will also apply to "e" for HC distortion.

"A"—"a"

The confusion characteristic of this vowel is that the trend of quality formation becomes maximum at 1 kc in distortions of both directions. This means that the partial emphasis of components in this region of vowel signals is most powerfully contributing to quality formation of "a". Concretely speaking, incoming confusion from "E", "O", "U", etc. towards "a" is increased in this frequency region.

Marked trend in outgoing confusion at LC 1.5 kc is mainly due to confusions going toward "e", "i" and "u", but at this cutting-off point the distortion is absolutely destructive for phoneme "A", being reflected by outgoing confusion which tends toward "e", "i", "u", etc. Thus, the components in this region of vowel "A" are considered to be contributing to quality "a" only in the "negative" sense. Outgoing confusion is strengthened at 0.5 kc in HC distortion. As seen in the pattern of "A" in the figure (B), this corresponds to the fact that the negative importance of phoneme "A" exists in two parts just above and below the frequency band 1 kc.

"O"—"o"

Generally speaking, LC distortion is quality destructive and HC distortion is constructive for this phonemic quality. Neither the deterioration in phonemic quality of this vowel, nor the quality transition from other vowels towards "o" will take place until LC 0.6 kc. Confusion outgoing from this vowel is a little conspicuous at the cutting points of LC 1.0 kc and up. The pattern components in these regions 1.0–1.5 kc, having the action of forming other phonemic qualities, clearly have negative importance for the phonemic quality "o". LC 1.0 kc and under are the regions where imcoming confusion is dominant – a fact due to the conspicuous confusion incoming from "I" and "E" towards "o". Probably the center of phonemic quality of "o" may exist at some points lower than 1 kc.

"U"–"u"

The characteristics of this vowel are a little more complicated than those of others. The characteristics seem to be particularly well reflected in LC distortion. It has, in both directions of LC and HC distortions, cutting points yielding the quality formation, yet those cutting frequencies do not necessarily conform in both directions. Speaking in more detail, emphasis of components by LC 1.5 kc and the elimination of components by HC 2.1 kc and under are all quality constructive for phoneme quality "u". The former corresponds to emphasis of components near 1.5 kc of "A" and "O" patterns, and the latter to the elimination of the second formant of "I" and "E", respectively. After all, both the second formant and the first one found in 0.3–0.4 kc are contributing to quality formation of "u". This mechanism of quality formation is more complicated than that observed in other vowels.

In the above, the trend in phonemic confusion in the BED with level recovering process has been considered by the aid of individual confusibility for each vowel. The important fact as found therein is as follows. Vowel patterns are, after all, of gradually diminishing type of amplitude with increase of frequency domain, component emphasis in the neighborhood of the cutting point of a filter is more effective in lower-cut than higher-cut, and in many cases it is better to consider that the main function of higher cut-off consists in the elimination of components in the attenuation region of a filter and not in the emphasis of the remaining band. Therefore, a sharp cutoff filter acts on quality "destructively" in some regions and "constructively", in other regions, and so it is possible to distinguish two kinds of frequency bands, namely, the part of "positive importance" and the part of "negative importance".

Fig. 15 was obtained by plotting the values of ensemble confusibility at each cutting point as the total sum of individual confusibilities of all phonemes.

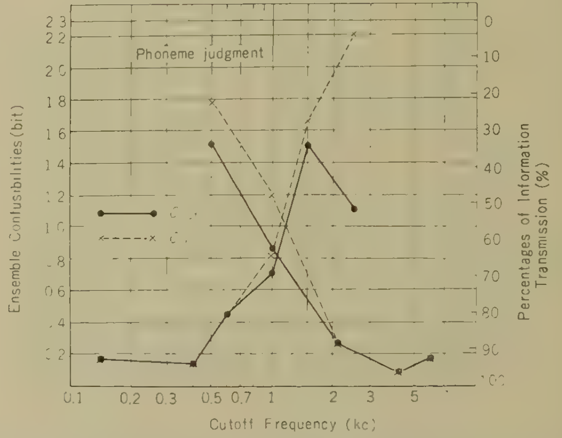

Fig. 15—Ensemble phonemic confusibility characteristics in BED (Experiment No. 2).

The reason C_{in} is generally not smaller than C_{out} is because of the experimental scheme as already stated. Except the LC 2.5 kc, HC distortion shows the more conspicuous confusion trend than LC. The equality of outgoing and incoming confusibilities means that no directivity is found in the confusion trend in an average sense.* (* If a pair of signals is considered, confusion between signals may have reciprocity. But when a group consisting more than two signals are considered, regressive confusion trend, such as "I"→"E"→"A"→"I", may be conceivable. In these examples, however, there is found no such particular confusion trend). In such a case confusion occuring may be considered as being at random. The difference between both confusibilities is the result of the facts that the outgoing confusion from a particular phoneme decreases, or that the incoming confusion to a particular quality increases.

In these cases, where the difference between confusibilities in observed, the confusion may be regarded to have a certain trend instead of being at random. In short, confusion trend reflects in inequality ($C_{\text{in}} > C_{\text{out}}$) in these experiments. The figure showing the trend just mentioned can be a clue to interpret the frequency construction of phonemic quality. Conspicuous difference between confusibilities at LC 2.5 kc results from the fact that confusion towards phoneme quality "i" at this cutting point becomes definitive throughout the vocal ensemble. LC distortion at this cutting point can be interpreted to be remarkably quality-constructive.

With the exception of this cutting point, greater difference between both confusibilities is more generally found in HC distortion than in LC. This means that HC distortion happens more frequently to behave as quality-constructive, and furthermore, that there is more negative importance in the lower part of the vowel pattern than in the upper part. This seems to be caused by the greater contribution of the second formant to phonemic quality, especially in the case of vowels "I" and "E". As has already been stated, the difference between the information amount of input signals and ensemble incoming confusibility, $R = H(X) - C_{\text{in}}$, shows amount of information transmitted. In the figure these values at each cutting point are shown in percentage for the maximum values in the vertical axis on the right side. It is of interest to note that about 50 % of information amounts are transmitted at the crossing point of C_{in} curves.

2) Vocal confusion

Contents of confusion matrix obtained from voice judgment will be treated by the introduction of individual confusibility as in the case of phonemic confusion. In this case, however, some confusions are noticed even in the distortionless condition, and furthermore the confusion occurs in a different way according to each voice. In Fig. 16 individual confusibility in the reference condition is shown for each combination of voice signal and voice quality.

The outcome of such characteristics can not be clarified immediately, but one fact is that the contents of voice quality impressed upon listeners depends to a certain extent upon the kinds of vowels, as will be later explained. It may be said that in the case of the voices which are classified by the listener in a stable manner regardless of vowel kinds, the outgoing confusion is less than the incoming one, while on the contrary, in the cases of voices the qualities of which are impressed on listener only by a particular vowel, incoming confusion is less than the outgoing confusion. As an illustration, the values of difference $C_{\text{in}} - C_{\text{out}}$ of individual confusibilities in two directions are calculated and shown in Fig. 17 for each vowel sound.

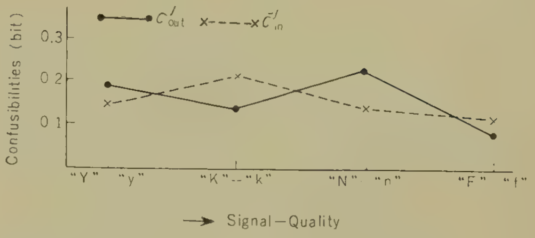

Fig. 16—Comparison of individual outgoing and incoming confusibilities for each combination of voice signal and voice quality in the distortionless condition (Experiment No. 2).

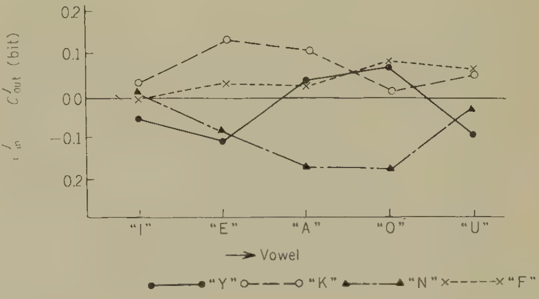

Fig. 17—Comparison of dependency of outgoing and incoming confusibility upon kinds of vowel in voice judgment in the distortionless condition.

These confusibilities are obtained from the confusion matrix which are tabulated for each vowel. As will readily be understood from the figure, voices "K" and "F" which generally show more confusion in the incoming direction give little deviation in confusibility difference by vowel kinds, on the other hand, voices "N" and "Y" which show more confusion in the outgoing direction give considerable deviation. From the detailed inspection of the confusion matrix, it can be said that "N", the quality of which appears most clearly only in the vowels "I" and "U", is very liable to be confused with other voices when other vowels than "I" and "U" come up for judgment. And "Y", with the voice quality especially appearing in "A" and "O", has greater outgoing confusion in other vowels than these two. Anyhow, it should be kept in mind that the individual confusion due to BED start from such a stage in the reference condition. In Figs. 18 (A) and (C) are shown individual confusibility in each cutoff condition of LC and HC distortions with regard to each combination of voice signal and voice quality. Figs. 18 (B) shows the vocal pattern of four voices, and to each pattern an averaged mean pattern is superimposed in dotted line.

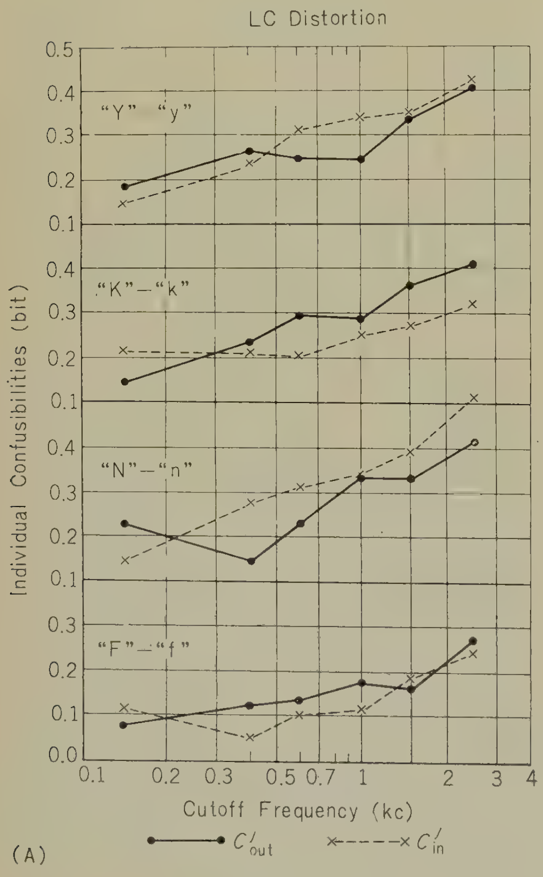

(A)

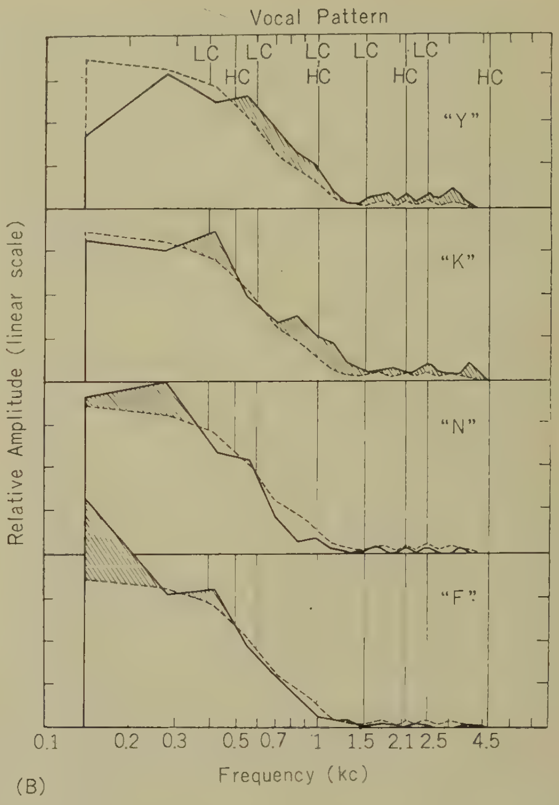

(B)

Fig. 18—Individual representation of confusibility of vocal confusion in BED and display of vocal patterns of four voices (Experiment No. 2).

The general trend of vocal confusion curves is such that the shape of the curve is simpler than that of phonemic confusion and no cutting step is recognized which shows so remarkable a trend toward quality destruction or quality construction as in phonemic quality. However, it is true that by using the curves in two directions, more abundant information

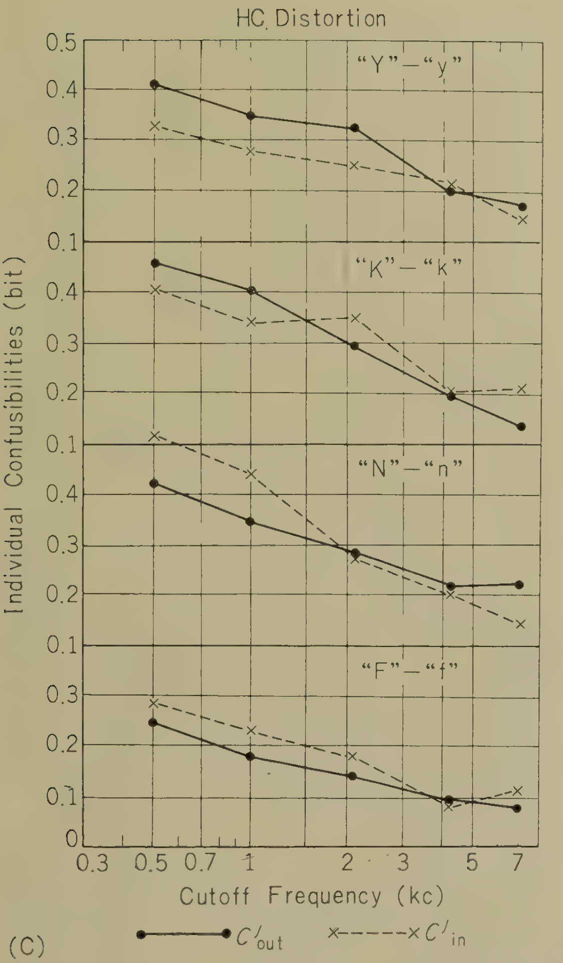

Fig. 18—Individual representation of confusibility of vocal confusion in BED and display of vocal patterns of four voices (Experiment No. 2).

regarding the mechanism of quality establishment is obtainable than that in the ordinary judgment curves already stated.

"Y"—"y"

For this voice, generally speaking, HC distortion is almost always quality-destructive, and LC distortion is nearly always quality-constructive in frequency band between 0.6–1.0 kc. With this voice, together with "K," we can observe the abundance of harmonic components as characteristics of their pattern. It is therefore conceivable that the elimination of these components due to HC distortion has caused similarity to the patterns "N" and "F" which are originally of attenuating type of higher components; this seems to correspond to quality destruction of this voice in HC destortion. In LC distortion, partial enhancement of the pattern parts in the band between 0.6–1.0 kc corresponds to the trend of quality construction of this voice in this band region. Then the positive shape of "Y" pattern (in a sence of relativeness to a mean pattern) in this band region is taken up as one of the quality factors of this voice, but this localized factor of voice quality cannot be detected by HC distortion, because of its general nature of quality destruction. It means probably that this quality factor of voice is not able to construct voice quality independently and solely, but dependently call upon other factors in other band regions. Meanwhile its outgoing confusion remarkably increases in 2–3 kc in HC distortion, thereby revealing the existance of voice quality element in this band, but this localized factor can never be detected in LC distortion.

"K"—"k"

LC distortion is nearly always quality-destructive, and HC distortion constructive in one part and destructive in another. Increase in outgoing confusion at LC 0.4 kc is mainly caused by the increase of the confusion towards "y." It is conceivable that the dominant part of pattern in the narrow region up to about 0.4 kc of vocal pattern of "K" is a constructive factor of voice quality "k." After all, with reference to the preceding section, it can be said that the voices "K" and "Y" are similar with respect to the abundance of harmonics in their pattern spectrum, and this causes the relatively fixed stable grouping of "K"–"Y." For the discrimination of voice qualities of the voices in the same group, the small difference in vocal pattern, in other words, the quality factor localized in a particular band as just noticed above, seems to be a clue. More confusion maintains throughout the LC distortion in the outgoing direction than in the incoming, and in HC distortion, also the same tendency is kept at HC 1 kc and lower cutting points.

These confusion characteristics can be explained by considering certain facts. First, notice the dispersed mode of energy distribution in this voice spectrum. This distribution mode appears in the peculiar shape of the vocal pattern for it has the strong fundamental component, and yet at the same time the higher components extend up to the highest region of any of the four voices. This is probably not the pattern characteristic due to vocal force in emission intensity. On the other hand, observing the confusion relatively increases at HC 4.2 kc. This leads to the statement that the quality factors of this voice exist near this cutting point or in the higher band as well as in the extreme lower band as mentioned first in this section. Thus two distortions HC and LC, in spite of their reversed directions, both bring much outgoing confusion.

The increase incoming confusion in HC 2.1 kc is mainly caused by confusion from voice "Y." This is seen in the preceding section as increase of outgoing confusion of "Y" at this cutting point. Thus some of voice-quality factors of "K" may be expected to also exist near this cutting point as well.

"N"—"n"

From the general trend of the curves it is seen that LC and HC distortions are equally quality-constructive for this voice quality. It should be remembered that this voice has vocal pattern most similar to the averaged one and the outgoing confusibility in reference condition has the greatest value among the four voices. Thus it can be expected that the mode of discrimination for this voice quality may not be the same kind of differential type as observed in the voice group "K—Y," but may be a different and rough type. At LC 0.4 kc the incoming confusion exceeds the outgoing. This can be explained as follows. If one eliminates, on the figures, the parts under this cutting point from the patterns of each voice, he will immediately notice that "Y" and "F" lose their characteristics of pattern shape. "K" neither loses its characteristics of pattern, nor is confused with "n" at this cutting point. With regard to "N" itself, it is noticed that it loses similarity to averaged pattern. These deformations of patterns can be considered to correspond to the decrease of outgoing confusion and increase ot incoming confusion of this voice at this cutting point. Concerning the HC distortion, the increase in incoming confusion at HC 4.2 kc is mainly caused by increase of incoming from "K" and "Y." This seems to relate to the fact that the vocal patterns of those voices, by this distortion, loss their quality factors localized in higher frequency region, and begin to resemble the mean pattern. The larger incoming confusion in HC 1 kc and 0.5 kc is mainly caused by increase of confusion which comes from "K," and this simply corresponds to the similarity in both shapes in the lower part of pattern.

In short, this voice whose vocal pattern is most similar to the mean pattern has no voice-quality factor localized in a particular frequency band. The increase in incoming confusion due to BED comes from the elimination of localized quality factors of other voices. For this voice itself, ambiguity disappears from the pattern shape in BED, and in some cases, the outgoing confusion decreases.

"F"—"f"

Generally speaking, LC distortion is quality-destructive and HC distortion, on the contrary, is quality-constructive. The confusion, the trend of which follows the distortion direction, may be said to be systematic, and the correspondence between the trend and pattern characteristics can be comparatively easily obtained. The characteristics of vocal pattern of this voice is the strongest fundamental component and the most remarkable diminuition of harmonics among the four voices. This is the general characteristic of vocal pattern brought about by vocal-intensity of pianissimo, and it is readily conceivable that low cut or higher emphasis of such vocal pattern is to destroy its voice quality. On the other hand, higher cut or lower emphasis is not a cause to make it lose these pattern shape characteristics, but is one to give the pattern characteristics of this voice to the patterns of other voices. This seems a reasonable explanation of confusion trend in this case, that is, LC distortion is quality-destructive and HC distortion quality-constructive.

From the analysis of voice quality confusion for four voices as above, it is safe to make the following conclusions. The discrimination or classification of voice quality generally dapends upon outlined shapes of envelope of vocal pattern. Concerning each individual, however, it can be said that among voices forming a particular subgroup by voice quality depends on the pattern part localized in a particular band. When the voice having such localized quality factors subjects to BED, the outgoing confusion generally exceeds the incoming confusion as the result of disappearance of quality factors. On the other hand, the voice having no localized quality factors does not show critical increase in outgoing confusion at any cutting step, but on the contrary, conspicuous increase of incoming confusion is observed as the result of the quality destruction of other voices having the localized quality factors. Attention should be paid, however, to the fact that localized voice-quality factors recognized by analysis of such confusion trend are not simultaneously detected in the two distortions of LC and HC, and further that their mutual independency is not so difinite as in phonemic quality factors.

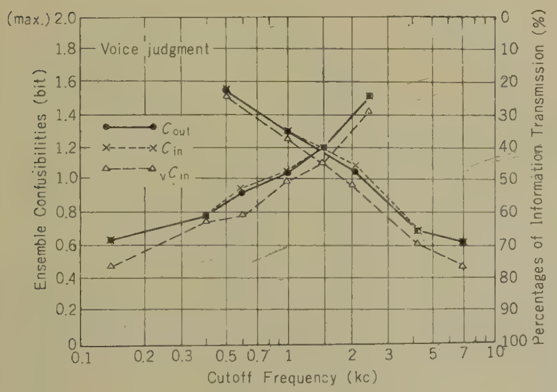

Fig. 16—Characteristics of ensemble confusibility of voice quality in BED (Experiment No. 2).

Finally, the ensemble confusion characteristics calculated as the sum of all individual confusibilities are shown in Fig. 19.

Compared with the case of phonemic quality, it is noticed that the slopes of the curves are not so irregular. The same trend was also observed before in the judgment curves. The difference between outgoing and incoming curves is much less than in phonemic quality. Some differences are observed only in LC 0.6 kc and HC 2.1 kc. This means that the confusion occurring in voice ensemble is random or not systematic, and it can be said that BED as a whole is neither quality-constructive nor quality-destructive for voice quality. The difference between curves at LC 0.6 kc means that the incoming confusion towards the voice quality "y" becomes systematic to some extent at this cutting point. Another difference between curves at HC 2.1 kc shows that this cutting point is likely to cause comparatively conspicuous confusion trend of "Y"→"k." These characteristics of curves both reflect the localized quality factors of voice "Y," and mean that, with this voice, the voice quality is concentrated on the frequency band to somewhat higher degree than with the other voices. In this figure, the amount of information transmitted is shown in percentage in the vertical line on the right side. The crossing point of curves presents 40%; about 0.6 times the value in the reference condition.

(to be continued to "Review of E.C.L. Vol. 9, Nos. 1-2 issue")

* * * *

REVIEW OF THE ELECTRICAL COMMUNICATION LABORATROY
VOLUME 8, NUMBERS 11-12, NOVEMBER-DECEMBER, 1960

U.D.C. 541.64

Theory of Solution of Chain Molecules*

Hirosi OKAMOTO†

By using the first order Bethe approximation, a theory of the solution of chain molecules is developed. Though it is a well-known fact that the first order Bethe approximation and the method of the quasi-chemical equilibrium coincide with each other in the case of a lattice gas or of the solution of short chain molecules, the author found that this coincidence does not always hold for the solution of long chain molecules. His theory can better explain the experimental observations on the mixing energy and the phase separation than the previous theories do.

1. Introduction

Many years have passed since the pioneering work of Flory's(1) quasi-crystalline model of chain polymer solutions was developed. Miller,(2) Orr,(3) Guggenheim,(4) and other investigators also studied a similar problem and succeeded in explaining the general features of chain polymer solutions.

Dispite the apparent success of these theories, they are not able to predict accurately, the detailed behavior observed experimentally. For example, the experimental values of the concentration at the critical mixing point are almost twice as high as those the theories predict and the concentration dependency of the mixing energy is more complicated than the theories predict.(6)

To improve these theories, the concentration dependency of the interaction parameter was proposed by Tompa(7) and Huggins.(8) Huggins also introduced additional concentration dependent terms in the entropy part. But the author considers that these methods are very artificial and undesirable.

In this paper, the detailed configurations of the polymer will be considered and it will be shown that the results can explain the experimental data which the previous theories could not. Though it is a well-known fact that the first order Bethe approximation and the quasi-chemical equilibrium coincide with each other in the case of a lattice gas or in the case of a solution of short-chain molecules, it was found that this coincidence is not always true in the case of a solution of long-chain molecules.

2. The First Order Bethe Approximation

A lattice space whose coordination number is z is considered. The system consists of n_α α-type chain molecules and n_β β-type solvent molecules. The α-type chain molecule consists of n elements which occupy n contiguous lattice sites, while the β-type solvent molecule is a point molecule occupying one site. The first neighboring pairs of two elements $(\alpha\sim\alpha)$, $(\beta\sim\beta)$, and $(\alpha\sim\beta)$ contribute the potential energy of $\varepsilon_{\alpha\alpha}$, $\varepsilon_{\beta\beta}$ and $\varepsilon_{\alpha\beta}$ respectively.

For the case of the first order Bethe approximation, all the possible configurations that can be illustrated on a set of $z+1$ sites consisting of a central sete and its first coordination shell, provided that the first shell sites are not themselves the closest neighbors, are considered in detail. The group of these $z+1$ sites is hereafter called a "local system." The outer part of the local system affects

---

* Ms received by the Electrical Communication Laboratory on 14, September, 1960. Originally published in the *Journal of the Physical Society of Japan*, Vol. 15, No. 4, April, pp. 650–657, 1960,

† High Polymers Research Section.

the detailed configurations of the system in the following way. (Fig. 1)

When three consecutive elements of a chain occupy the central site and two of the first shell sites, and the other elements of the same chain chain occupy none of the first shell sites, then the outer part of the local system weights the configuration with a factor $\lambda_{\alpha,1}$.

When the chain takes a configuration in which the chain passes through the central site and occupies $l-1$ sites out of the $z-2$ first shell sites, then its weight is $\lambda_{\alpha,l}$; in particular, if the end element of the chain occupies the central site, the weight is $\varepsilon_e\lambda_{\alpha,l}$.

When the chain occupies one or two of the first shell sites (without occupying the central site), the weights are $\varphi\lambda_\alpha$ and $\psi\lambda_\alpha^2$ respectively.

For simplicity, the configurations in which the elements of the same chain occupy three or more of the first shell sites, without occupying the central site, are not considered.

When a solvent molecule occupies one of the $z+1$ sites, the weight is λ_β.

The two functions A and B are defined by

$$A=\varphi\lambda_\alpha x_{\alpha\alpha}+\lambda_\beta\chi_{\alpha\beta}$$

$$B=\varphi\lambda_\alpha x_{\alpha\beta}+\lambda_\beta x_{\beta\beta}$$

where

$$x_{\alpha\alpha}=\exp\left(\frac{-\varepsilon_{\alpha\alpha}}{KT}\right),$$

$$x_{\beta\beta}=\exp\left(\frac{-\varepsilon_{\beta\beta}}{KT}\right),$$

$$x_{\alpha\beta}=\exp\left(\frac{-\varepsilon_{\alpha\beta}}{KT}\right).$$

The local partition function G is written as follows;

$$G=\sum_l G_{\alpha,l}+G_\beta, \qquad (2.1)$$

where

$$G_{\alpha,l}=\binom{z}{2}\lambda_{\alpha,l}\sum_r\left(\binom{z-l-1}{r}\right)(\psi\lambda_\alpha x_{\alpha\alpha}{}^2)^r A^{z-l-1-2r}$$
$$+z\varepsilon_l\lambda_{\alpha,l}\sum_r\left(\binom{z-l}{r}\right)(\psi\lambda_\alpha{}^2 x_{\alpha\alpha}{}^2)^r A^{z-l-2r} \qquad (2.2)$$

$$G_{\alpha,z-1}=\binom{z}{2}\lambda_{\alpha,z-1}+\varepsilon_{z-1}\lambda_{\alpha,z-1}A+z\varepsilon_z\lambda_{\alpha,z} \qquad (2.3)$$

$$G_\beta=\lambda_\beta\sum_r\left(\binom{z}{r}\right)(\psi\lambda_\alpha{}^2 x_{\alpha\beta}{}^2)^r B^{z-2r}. \qquad (2.4)$$

The symbol $\left(\binom{z-l-1}{r}\right)$ represents the number of ways to select r site pairs from among $z-l-1$ sites.

Three cases; (I), (II), and (III); will be considered in the following.

(I) Suppose
$\lambda_{\alpha,l}=0,\ l\geqslant 2$ and $\psi=0$.

This is the cass in which a chain never passes through the local system two or more times.

Orr's work$^{(3)}$ corresponds to this case. According to his results, the average number of $(\alpha\sim\beta)$ contacts, $z\overline{X}$, is given by

$$\overline{X}=\frac{q_\alpha n_\alpha n_\beta}{q_\alpha n_\alpha+n_\beta}\,\frac{2}{1+\beta} \qquad (2.5)$$

$$zq_\alpha=nz-2n+2 \qquad (2.6)$$

$$\beta^2=1+4\xi(1-\xi)(e^{2w/KT}-1) \qquad (2.7)$$

$$\xi=\frac{q_\alpha n_\alpha}{q_\alpha n_\alpha+n_\beta} \qquad (2.8)$$

$$2w=2\varepsilon_{\alpha\beta}-(\varepsilon_{\alpha\alpha}+\varepsilon_{\beta\beta}). \qquad (2.9)$$

This is the well-known case in which the first order Bethe approximation leads to the same formula for $\overline{X}$ as that given by the quasi-chemical equilibrium.

Miller$^{(2)}$ and Guggenheim$^{(4)}$ obtained the same result as Orr.

(II) Next assume that
$\lambda_{\alpha,l}\neq 0,\ l\geqslant 1$ and $\psi=0$.

The procedure of the first order Bethe approximation makes the probability of occupation of the central site and the first shell site by α and β molecules respectively equal to the probability of occupation in the reverse manner. This equivalence is expressed, in a formal way, by the relation

$$\lambda_\alpha\frac{\partial G_\beta}{\partial\lambda_\alpha}=\lambda_\beta\frac{\partial G_\alpha}{\partial\lambda_\beta}. \qquad (2.10)$$

Hereafter, in the equilidrinm state, the relative probability of the occurrence of the configuration of α molecules in the (α,l) form (see Fig. 1) will be described by $p(l)$.

$$\frac{G_{\alpha,l}}{G_{\alpha,1}}=p(l). \qquad (2.11)$$

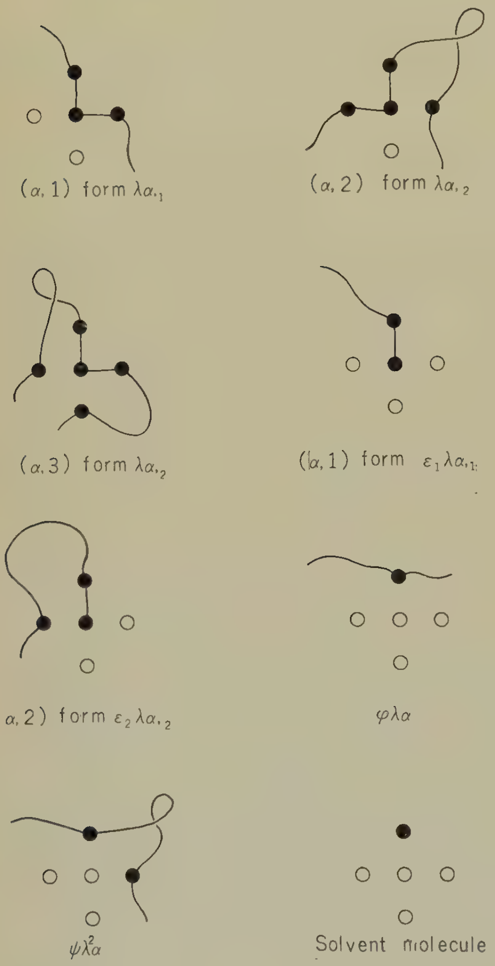

$(\alpha, 1)$ form $\lambda_{\alpha,1}$

$(\alpha, 2)$ form $\lambda_{\alpha,2}$

$(\alpha, 3)$ form $\lambda_{\alpha,2}$

$(\alpha, 1)$ form $\varepsilon_1\lambda_{\alpha,1}$

$\alpha, 2)$ form $\varepsilon_2\lambda_{\alpha,2}$

$\varphi\lambda_\alpha$

$\psi\lambda^2_\alpha$

Solvent molecule λ_β

Fig. 1—Various configurations and their weight factors in the local system.

The probability function $p(l)$ depends on the state of the whole system, including the concentration and the temperature, and it may be considered to have a close relation with the equilibrium extension of the chain molecule.

Furthermore, the ratio of the probability of occupation of the central site by the end elements to that of the other elements is represented by $q(l)$ as

$$\frac{z\varepsilon_l\lambda_{\alpha,l}A^{z-l}}{\binom{z}{2}\lambda_{\alpha,l}A^{z-l-1}}=q(l). \qquad (2.12)$$

From Eq. (2.10), the following relation is obtained by the use of Eqs. (2.2), (2.3), (2.11) and (2.12).

$$z\varphi\lambda_\alpha\lambda_\beta x_{\alpha\beta}B^{z-1}=\binom{z}{2}\lambda_{\alpha,1}\lambda_\beta x_{\alpha\beta}A^{z-3}$$

$$\times\sum_l\frac{1+q(1)}{1+q(l)}p(l)\{(z-l-1)+(z-l)q(l)\}. \qquad (2.13)$$

The equilibrium properties of the whole system are also given by

$$\frac{v_\alpha}{v_\beta}=\frac{\sum G_{\alpha,l}}{G_\beta} \qquad (2.14)$$

where v_α and v_β are the volume concentrations of the α and the β molecules respectively.

In this paper, the following abbreviations are used:

$$q_\alpha'=\frac{\sum\frac{p(l)}{1+q(l)}\{(z-l-1)+(z-l)q(l)\}}{\frac{z}{n}\sum p(l)}$$

$$=\frac{nz-2n+2-\rho}{z} \qquad (2.15)$$

$$\rho=\sum_{l}(l-1)\sum_{j}Q_{j,l},$$

$$q(l)=\frac{2Q_{1,l}}{\sum\limits_{i=2}^{n-1}Q_{j,l}},$$

where $Q_{j,l}$ is the probability with which $l-1$ elements of the same chain, other than the two elements adjacent to the elements at the central site, also occupy the first shell sites, when the jth element of the chain passes through the central site.

$\overline{X}$ is given by

$$\frac{\overline{X}}{nn_\alpha+n_\beta}=\frac{\partial G/\partial x_{\alpha\beta}}{2zG}. \qquad (2.16)$$

From Eq. (2.16) the following equation is obtained

$$\overline{X}=\frac{q_\alpha' n_\alpha n_\beta}{q_\alpha' n_\alpha+n_\beta}\cdot\frac{2}{1+\beta'} \qquad (2.17)$$

$$\beta'^2=1+4\xi'(1-\xi')(e^{2w/KT}-1) \qquad (2.18)$$

$$\xi'=\frac{q_\alpha' n_\alpha}{q_\alpha' n_\alpha+n_\beta} \qquad (2.19)$$

zq_α' may be considered to be the effective number of possible contacting first neighbors of the chain molecule. Therefore, it is seen from Eq. (2.17) that in case II, the first order Bethe approximation and the quasi-chemical equilibrium are equivalent in some sense. But it is important that q_α' should be determined so as to minimize the free energy of the whole system. q_α' is never constant but depends on the concentration and the temperature of the system.

(III) In the most general case, the following relations hold:

$$\lambda_{\alpha,l}\neq 0,\quad l\geqslant 1 \quad\text{and}\quad \psi\neq 0.$$

The relations shown by Eqs. (2.10), (2.11), (2.14) and (2.16) should also hold in this, case but instead of Eq. (2.12), the following equation is used:

$$\frac{z\varepsilon_l\lambda_{\alpha,l}\sum\left(\binom{z-l}{r}\right)(\psi\lambda_\alpha{}^2x_{\alpha\alpha}{}^2)^r A^{z-l-2r}}{\binom{z}{2}\lambda_{\alpha,l}\sum\left(\binom{z-l-1}{r}\right)(\psi\lambda_\alpha{}^2x_{\alpha\alpha}{}^2)^r A^{z-l-1-2r}}=q(l). \qquad (2.19)'$$

In addition to the above relations, the following relation is also necessary

$$\varphi\frac{\partial G}{\partial\varphi}=R\psi\frac{\partial G}{\partial\psi}. \qquad (2.20)$$

The above relation Eq. (2.20) show that a proportionality exists between the number of the chains which occupy only one of the first shell sites and that of the chains which occupy two of the first shell sites. Obviously R has a close relation with the equilibrium extension of the chain. If the chain spreads, R becomes larger; and if the chain contracts R becomes smaller. R, as well as ρ, should be determined so as to minimize the free energy of the whole system.

With the help of Eqs. (2.10), (2.11), (2.12′), and (2.14); Eq. (2.16) gives the expression for $\overline{X}$ as,

$$\overline{X}=\overline{X}'+\overline{X}''$$

$$\overline{X}'=\frac{\left(q_\alpha''n_\alpha-\frac{2r_\beta}{z}n\right)n_\beta}{q_\alpha''n_\alpha+q_\beta'n_\beta}\cdot\frac{2}{1-\frac{4r_\beta n_\beta/z}{q_\alpha''n_\alpha+q_\beta'n_\beta}+\sqrt{\frac{4q_\alpha''n_\alpha n_\beta}{(q_\alpha''n_\alpha+q_\beta'n_\beta)^2}(e^{2w/KT}-1)}}$$

$$\overline{X}''=\frac{\frac{2r_\beta}{z}n_\beta{}^2e^{2w/KT}}{q_\alpha''n_\alpha+q_\beta'n_\beta}\cdot\frac{2}{1+\frac{2n_\beta}{q_\alpha''n_\alpha+q_\beta'n_\beta}(e^{2w/KT}-1)+\sqrt{1+\frac{4q_\alpha''n_\alpha n_\beta}{(q_\alpha''n_\alpha+q_\beta'n_\beta)^2}(e^{2w/KT}-1)}}$$

$$q_\alpha''=q_\alpha'-\frac{2r_\alpha}{z},\qquad q_\beta'=1-\frac{2r_\beta}{z}e^{2w/KT}$$

where, r_α and r_β represent the numbers of chains which occupy two of the first shell sites when α and β molecules occupy the central site respectively.

$$r_\alpha=\frac{1}{\sum\limits_l p(l)}\sum_l r_{\alpha,l}p(l)$$

$$r_{\alpha,l}=\frac{\sum\limits_r\binom{z}{2}\lambda_{\alpha,l}\left(\binom{z-l-1}{r}\right)r(\psi\lambda_\alpha{}^2x_{\alpha\alpha}{}^2)^rA^{z-l-1-2r}}{G_{\alpha,l}}$$

$$r_\beta=\frac{\sum\limits_r\lambda_\beta\left(\binom{z}{r}\right)r(\psi\lambda_\alpha{}^2x_{\alpha\beta}{}^2)^rB^{z-2r}}{G_\beta}.$$

To obtain r_α and r_β, we must make use of (2.20). Unfortunately, this prpcedure is so complicated that it seems to be difficult to obtain the results in a closed form.

For example, for a two dimensional hexagonal lattice, if the chain is sufficiently long, so that

$$\frac{1}{n}\ll 1$$

we obtain

$$r_\alpha=0$$

$$r_\beta=\frac{1-\frac{\rho}{n}}{R+2}v_\alpha+\frac{1-\frac{\rho}{n}}{R+2}v_\alpha{}^2\ldots\ldots.$$

This problem will not be considered further for this case, but it is noteworthy that in case (III), the equivalence of the first order Bethe approximation and the quasi-chemical equilibrium are no longer correct.

In the following, we confine ourselves to case (II), because the formulas obtained in this case are relatively simple and yet seem to retain the desirable characteristics.

3. Thermodynamical Quantities

The partition function of the whole system, Ω, is written as follows:

$$\Omega=\sum_\rho\Omega(\rho).\tag{3.1}$$

The partition function for fixed ρ, $\Omega(\rho)$, can be written as

$$\Omega(\rho)=\Omega_0\exp\left[\frac{-z\bar{\bar{X}}(\rho)w}{KT}\right]\sum_X w(n_\alpha,n_\beta,\rho,X)\tag{3.2}$$

$$\Omega_0=\zeta_\alpha{}^{n_\alpha}\zeta_\beta{}^{n_\beta}\exp\left(\frac{-1}{KT}\left\{\frac{z}{2}q_\alpha n_\alpha\varepsilon_{\alpha\alpha}+\frac{z}{2}n_\beta\varepsilon_{\beta\beta}\right\}\right)\tag{3.3}$$

$$\bar{\bar{X}}(\rho)=T\int_0^{1/T}\bar{X}(\rho)d\left(\frac{1}{T}\right)\tag{3.4}$$

where, ζ_α and ζ_β are the kinetic energy terms, $\sum\limits_X\omega(\rho,X)$ is the number of configurations for constant ρ, $z\bar{X}(\rho)$ is the statistical mean of zX for the constant ρ, and

$$z\bar{X}(\rho)=-KT\frac{\partial\log\Omega(\rho)}{\partial w}.$$

We can generally follow Orr's method[3] in deriving the terms $\bar{\bar{X}}$ and $\sum\omega(\rho,\bar{X})$. Orr used $z(z-1)^{n-2}$ for the number of configurations of the isolated chain. This factor is replaced by $f(\rho)$ in our case. $f(\rho)$ is the total number of configurations which the isolated chain of constant ρ takes.

The derivation of $f(\rho)$ will be deferred until the next paragraph.

The free energy of the whole system, $F=-kT\log\Omega$ can be approximated well by the maximum $\Omega(\rho)$ in the summation of Eq. (3.1).

$$F=-kT\log\Omega(\rho).$$

The following formula of F is obtained by the formal extension of the Orr's formula to our case.

$$F=F_0+\frac{zkT}{2}\left\{q_\alpha'n_\alpha\log\frac{\beta'-1+2\xi'}{\xi'(\beta'+1)}\right.$$

$$+n_\beta \log \frac{\beta'+1-2\xi'}{(1-\xi')(\beta'1+)}\Bigg\}$$

$$+\frac{N}{n}kT\left\{\frac{n(n-1)}{n-q_\alpha'}\log\frac{n}{n-q_\alpha'}\right.$$

$$+v_\alpha \log\frac{2}{f(\rho)z(z-1)}\cdot\frac{1}{n}\cdot\left(\frac{n}{n-q_\alpha'}\right)^{n-1}$$

$$-(n-1)\left(\frac{n}{n-q_\alpha'}-v_\alpha\right)\log\left(\frac{n}{n-q_\alpha'}\right.$$

$$\left.\left.-v_\alpha\right)+v_\alpha\log v_\alpha+n(1-v_\alpha)\log(1-v_\alpha)\right\},\tag{3.5}$$

The free energy F must satisfy the relation

$$\frac{\partial F}{\partial\rho}=0$$

or

$$\frac{1}{2}kTn_\alpha\log\frac{\beta'-1+2\xi'}{\xi'(\beta'+1)}+\frac{N}{n}kT$$

$$\times\left[-\frac{n-1}{nz}\left(\frac{n}{n-q_\alpha'}\right)^2\log\frac{n}{n-q_\alpha'}\right.$$

$$+v_\alpha\left\{-\frac{d\log f(\rho)}{d\rho}+\frac{n-1}{z}\frac{1}{n-q_\alpha'}\right\}$$

$$\left.+\frac{n-1}{nz}\left(\frac{n}{n-q_\alpha'}\right)^2\log\left(\frac{n}{n-q_\alpha'}-v_\alpha\right)\right]=0.\tag{3.6}$$

ρ is determined from the above equation. The mixing energy ΔH is shown by

$$\Delta H=z\overline{X}w=\frac{q_\alpha' n_\alpha n_\beta}{q_\alpha' n_\alpha+n_\beta}\cdot\frac{2zw}{1+\beta'}.\tag{3.7}$$

The mixing entropy ΔS is derived from

$$T\Delta S=\Delta H-\Delta F.\tag{3.8}$$

The chemical potentials of the α and β components are

$$\frac{1}{kT}\mu_\alpha=\frac{1}{kT}\left(\frac{\partial F}{\partial n_\alpha}\right)_{\rho,n_\beta}+\frac{1}{kT}\left(\frac{\partial F}{\partial\rho}\right)_{n_\alpha,n_\beta}\frac{\partial\rho}{\partial n}$$

$$=\frac{1}{kT}\left(\frac{\partial F}{\partial n_\alpha}\right)_{\rho,n_\beta}$$

$$\frac{\mu_\alpha}{kT}=-\zeta_\alpha+\frac{zq_\alpha}{2kT}\varepsilon_{\alpha\alpha}+\frac{zq_\alpha'}{2}\log\frac{\beta'-1+2\xi'}{\xi'(\beta'+1)}$$

$$-\log\binom{z}{2}nf(\rho)+\frac{(n-1)q_\alpha'}{n-q_\alpha'}\log\frac{n}{n-q_\alpha'}$$

$$-\frac{(n-1)q_\alpha'}{n-q_\alpha'}\log\left\{\frac{n}{n-q_\alpha'}-v_\alpha\right\}+\log v_\alpha\tag{3.9}$$

$$\frac{\mu_\beta}{kT}=-\zeta_\beta+\frac{z}{2kT}\varepsilon_{\beta\beta}+\frac{z}{2}\log\frac{\beta'+1-2\xi'}{(1-\xi')(1+\beta')}$$

$$-\frac{n-1}{n-q_\alpha'}\log\left(1-\frac{n-q_\alpha'}{n}v_\alpha\right)+\log(1-v_\alpha).\tag{3.10}$$

The critical mixing point is determined by the following simultaneous equations.

$$\frac{\partial\mu_\alpha}{\partial v_\alpha}=0,\quad \frac{\partial^2\mu_\alpha}{\partial v_\alpha^2}=0.$$

The resultant formulas which give the critical point are very complicated, but if the chain is sufficiently long, it is found that the critical concentration is proportional to $1/\sqrt{n}$, and ρ is approximated well by linear form of v_α at that concentration.

$$\rho(v_\alpha)=\rho_0+\rho_1 v_\alpha.$$

The approximate solutions of the critical point are

$$v_{\alpha,c}=\frac{1}{\sqrt{n}}\sqrt{\frac{z^2}{(z-2-\rho_0/n)(z-1-2\rho_0/n)+1.5\rho_1/nz}}\tag{3.11}$$

$$\exp\frac{2w}{kT_c}=1+\frac{1}{z-2-\rho_0/n}+\frac{2}{\sqrt{n}}\frac{1}{(z-2-\rho_0/n)}$$

$$\times\sqrt{\frac{z-1-2\rho_0/n}{z-2-\rho_0/n}+\frac{1.5z}{(z-2-\rho_0/n)^2}\cdot\frac{\rho_1}{n}}.\tag{3.12}$$

4. The Derivation of $f(\rho)$

Perhaps the most orthodox method to obtain $f(\rho)$ is a matrix method. The method presented is a matrix method modified slightly to obtain the partition function of an isolated chain molecule. By a step-by-step process on the lattice space the configurations of a chain are constructed from one of its ends. When the rth step is finished, an allowed configuration of m segments from the $(r-m)$th to the step is called $\varphi_i(r)$. The interactions between the segments more than m steps apart are neglected. The number of all possible configurations of m segments is ν. These configurations are designated by $\varphi_1(r)$, $\varphi_2(r)$, ……$\varphi_\nu(r)$. When one step is added, any configuration of m segments from the $(r-m+1)$th to the $(r+1)$th correspond to one of these φ_i; these are designated by $\varphi_1(r+1)$, $\varphi_2(r+1)$, ……$\varphi_\nu(r+1)$. The factor η^μ is weighted to each process, if the segment of the $(r+1)$th step has μ nearest neighbor contacts with some segments from $(r+1)$th to $(r-m+1)$th. The weight is 0 when overlapping occurs, and 1 when there is no interaction.

In matrix form, this is described as

$$\begin{pmatrix}\varphi_1(r+1)\\ \varphi_2(r+1)\\ \cdots\cdots\\ \cdots\cdots\\ \varphi_\nu(r+1)\end{pmatrix}=(\gamma_{ij})\begin{pmatrix}\varphi_1(r)\\ \varphi_2(r)\\ \cdots\cdots\\ \cdots\cdots\\ \varphi_\nu(r)\end{pmatrix} \tag{4.1}$$

$$\gamma_{ij}=0,\ 1,\ \eta,\ \cdots\cdots\eta^{z-1}.$$

The largest eigenvalue of (γ_{ij}) is $\lambda_m(\eta)$, and then, for sufficiently large n,

$$\varphi(n)=\lambda^{n-m}_{m}\varphi(m). \tag{4.2}$$

On the assumption $\eta=e^{2w/kT}$, λ^{n-m}_{m} is the partition function of an isolated chain.

When λ^{n-m}_{m} is expanded into a power series of η, $f(\rho)$ is the coefficient of $\eta^{\rho/2}$. If $f(\rho)\eta^{\rho/2}$ is sufficiently large for some value of η and $n\gg m$,

$$\log f(\rho)=n\cdot\log\lambda_m-\left(\frac{\rho}{2}\right)\log\eta. \tag{4.3}$$

We consider that this ρ is equal to its mean value

$$\frac{\rho}{2}=\eta n\frac{d\log\lambda_m}{d\eta}. \tag{4.4}$$

Differentiating Eq. (4.3) with respect to ρ, we obtain

$$\frac{d}{d\rho}\log f=-\frac{1}{2}\log\eta. \tag{4.5}$$

The above relation must be substituted into Eq. (3 6). Particularly, if the concentration of the chain molecules is sufficiently dilute, Eq. (3.6) is reduced to

$$\frac{w}{kT}+\frac{d}{d\rho}\log f=0$$

or

$$\eta=e^{2w/kT}.$$

This is a satisfactory result, because in this case λ^{n-m}_{m} must be the partition function of the chain.

5. Numerical Calculations

5.1. The Mixing Energy is Expressed as

$$\Delta H=z\overline{X}w. \tag{5.1}$$

In case (I) (Orr, Miller, and Guggenheim), $\overline{X}$ is given by Eq. (2.5). According to this equation, the curve of ΔH versus $\xi(1-\xi)$ is expected to be a single curve. Contrary to this expectation, however, the measured curve of the mixing energy of polymethylmethacrylate and trichloroethylene against $\xi(1-\xi)$ is found to be not a single but a closed curve.(5) (See Fig. 2.)

This is explained by Eq. (2. 17) in case (II). Because q_α' is not constant but changes in value as the concentration increases, the curve ΔH versus $\xi(1-\xi)$ is never a single curve, it is a closed curve.

5.2. Critical mixing Point

In case (II), the critical point is given by

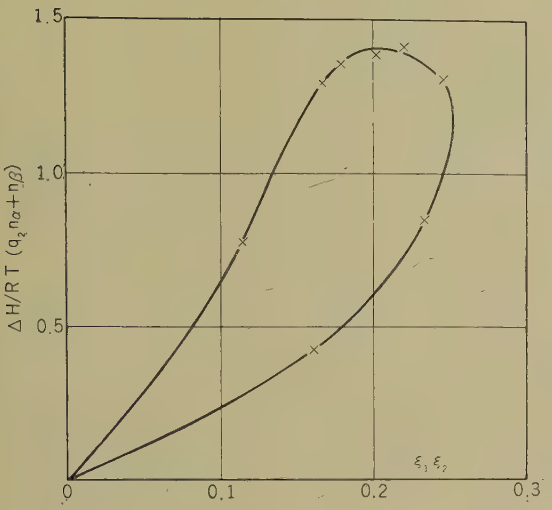

Fig. 2—Value of $\Delta H/RT(q_\alpha n_\alpha+n_\beta)$ plotted versus $\xi_1\ \xi_2(z=6)$ for solutions of polymethylmethacrylate in trichloroethylene; X: experimental points. Data from Staverman and Dekking.[5]

Eq. (3.11) and Eq. (3.12). These formulas are reduced to those of Guggenheim when $\rho_0=\rho_1=0$. So, in case (II), a larger value of $v_{\alpha,c}$ can be predicted than in case (I).

ρ_0 and ρ_1 in case (II) are given by

$$\rho_0=2\eta\left(\frac{d\log Q}{d\eta}\right)_{v_\alpha=0}$$

$$\rho_1=2\eta\left\{\left(\frac{d\log Q}{d\eta}\right)_{v_\alpha=0}+\eta\left(\frac{d^2\log Q}{d\eta^2}\right)_{v_\alpha=0}\right\}$$

$$\times\left\{\frac{n-1}{nz}-\frac{2(z-2-\rho_0/n)(\eta-1)}{z}\right\}. \tag{5.3}$$

The following are numerical calculations for simplified cases.

5.2.1. Two Dimensional Square Lattice

In deriving $Q(\eta)$, the "fundamental configurations" or "vectors" are

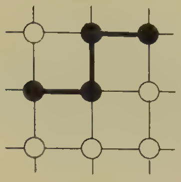

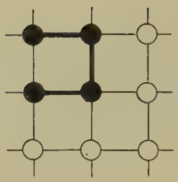

Q is given by

$$Q(\eta)=\lambda^n,$$

where λ is the maximum eigenvalue of the following matrix:

$$\begin{pmatrix} 1 & 1 \\ \eta & 0 \end{pmatrix}$$

$$\lambda=\frac{1+\sqrt{1+4\eta}}{2}$$

$$\eta_c=1.74$$

$$\frac{\rho_0}{n}=0.646$$

$$\frac{\rho_1}{n}=-0.091$$

$$v_{\alpha,c}=\frac{2.67}{\sqrt{n}};$$

whereas Guggenheim's formula gives

$$v_{\alpha,c,G}=\frac{1.63}{\sqrt{n}},$$

and Flory's theory gives

$$v_{\alpha,c,F}=1/\sqrt{n}.$$

5.2.2. Three Dimensional Cubic Lattice

The "fundamental vectors" are

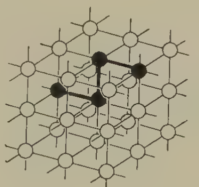

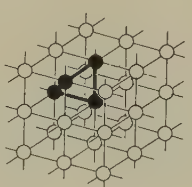

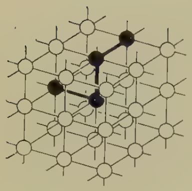

; φ_3

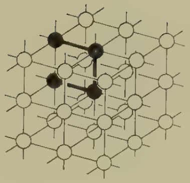

; φ_4

λ is maximum eigenvalue of the following matrix:

$$\begin{pmatrix} 1 & 1 & 1 & 1 \\ 1 & 1 & 1 & 1 \\ 1 & 1 & 1 & 1 \\ \eta & \eta & \eta & 0 \end{pmatrix}$$

$$\lambda=\frac{3+\sqrt{9+12\eta}}{2}$$

$$\eta_c=1.28$$

$$\frac{\rho_0}{n}=0.391$$

$$\frac{\rho_1}{n}=-0.032$$

$$v_{\alpha,c}=\frac{1.54}{\sqrt{n}};$$

whereas Guggenheim's formula gives

$$v_{\alpha,c\cdot G}=\frac{1.34}{\sqrt{n}},$$

and Flory's theory gives

$$v_{\alpha,c\cdot F}=\frac{1}{\sqrt{n}}.$$

The experimental results(7) show that

$$v_{\alpha,c\cdot\exp}\cong 2/\sqrt{n}.$$

Therefore, our formulae Eqs. (3.10) and (3.11) predict a better value for $v_{\alpha,c}$ that the previous formulas. But the agreement is not yet satisfactory.

7. Discussion

It is already known that the binodial curve of the phase diagram of the polymer∼solvent system predicted by Flory's theory is too narrow to explain the experimental results. The author has not yet calculated such a binodial in the present paper; however, he considers that a broader binodial will result from his theory than from Flory's.

This is reasonable because, in our theory, the concentration dependency of the extension of the molecule is considered.

It has been found that our theory can explain the experimental facts better than the previous theories, but the numerical calculations given in the preceding paragraph show that there still remain some differences between our theory and experiment. The reason is partly because of the fact that the number of the "fundamental configurations" or "vectors" φ_ν used in calculating $Q(\eta)$ is too small. In the calculation for the cubic lattice, only φ_4 has an intrachain interaction. This means that in the summation $\rho=\sum_l(l-1)\sum_j Q_{j,l}$, the terms for $l\geqslant 3$ are all neglected. If all of these terms are included, ρ becomes larger, which makes $v_{\alpha,c}$ larger.

Even if the factor ρ is correctly taken into the calculation, some unsatisfactory points will still remain. For example, the curve of ΔH versus $\xi(1-\xi)$ may not be expected to be such a large loop as the experiments show. However, if the theory can be constructed from case (III), further improvements can be expected. Unfortunately this seems to be very complicated.

In addition to the above discussion, the concentration dependency of ρ will yield valuable information concerning the concentration dependency of the equilibrium extension of the molecular chain.

7. Conclusion

By using the first order Bethe approximation, the author tried to include the effects of the extension of chain molecules in the theory of the solution of chain molecules, and calculated the various thermodynamical quantities. It was found that the effects of the extension of chain molecules are important to the problems of the mixing energy and the concentration at the critical mixing point. Our theory applied to those problems gave better agreement with experimental results than did Flory's theory.

Further, it was shown that the well-known theorem of the coincidence of the result of the first order Bethe approximation with that of the quasi-chemical method does not always hold in the solution of long-chain molecules.

The author considers that further efforts to include the complete effects of the extension of chain molecules in the theory will yield more satisfactory results.

References

(1) P. J. Flory; "*Principles of Polymer Chemistry*" p. 495 (1953), Cornell Univ. Press.
(2) A. R. Miller; "*The Theory of Solutions of High Polymers*" (1948), The Clarendon Press, Oxford.
(3) W. J. C. Orr; "The Free Energies of Solutions of Single and Multiple Molecules" *Trans, Farad. Soc.* 40, p. 320 (1944).
(4) E. A Guggenheim; "Statistical Thermodynamics of Mixtures with Non-zero Energies of Mixing" *Proc. Roy. Soc. London* A. 183 p. 213 (1944).
(5) H. Tompa; "*Polymer Solutions*" p. 144 (1956), Butterworths Scientific Publications, London.
(6) H. Tompa; Ibid. p. 207.
(7) H. Tompa; "Ibid." p. 174.
(8) M. L. Huggins; "The Thermodynamic Properties of Solutions" *J. Polymer Sci*, 16, p. 205 (1955).

* * * *

REVIEW OF THE ELECTRICAL COMMUNICATION LABORATORY
VOLUME 8, NUMBERS 11-12, NOVEMBER-DECEMBER, 1960

U.D.C. 621. 318. 57 : 621. 318. 1 : 621. 374. 3

A Channel Selector Applying Error-Correcting Codes*

Shoji YOSHIDA† and ***Keisuke TOMARU***†

This paper describes a channel selector, which makes use of error-correcting codes. Parametrons are used as the source of selection signals. The operation of the selector is stable, and its time for selection is short. It can be constructed simply and economically. Causes of variations of the selecting ratio for a partially equipped selector are clarified, and some countermeasures are suggested.

1. Introduction

There are many types of channel selecting circuits, such as diode matrices and a tree circuits, that are used in exchanges and computers. The function of these circuits is to select one specific circuit or element out of many.

New type of selecting circuit is presented. Nature of error-correcting codes is applied to the selective principle of the selecting circuit. This method enables a simple and economical construction of the selecting circuit. Moreover, the time needed for its selective action is usually shorter than that of a tree circuit. Parametron signals are used as input signals in this selecting circuit. Oscillation phases of parametrons (0-phase and π-phase) are made to correspond to the "1" and the "0" respectively of binary selecting codes. Small ferrite troidal cores with a linear characteristic are used as circuit elements. This kind of selecting circuit can be widely used.

2. Selective Principle

For any two codes with the same code-length n (the number of bits in the code) and with mutual destance d, the selecting ratio R_s is defined as follows:

$$R_s = \frac{n}{n-2d}. \tag{1}$$

Now let us consider the following two codes:

$$\left.\begin{array}{l} X=(x_1, x_2, \cdots\cdots\cdots, x_n) \\ \\ Y=(y_1, y_2, \cdots\cdots\cdots, y_n). \end{array}\right\} \tag{2}$$

d is given by the following equation:

$$d=\mathrm{dis}(X\ Y)=\sum_{\nu=i}^{n}(x_\nu-y_\nu)^2. \tag{3}$$

For example, if the codes X and Y are:

$$\left.\begin{array}{l} X=1\ \ 0\ \ 0\ \ 0\ \ 0\ \ 1 \\ \\ Y=0\ \ 1\ \ 0\ \ 0\ \ 0\ \ 1. \end{array}\right\} \tag{4}$$

d is 2. ($n=6$ in this case.)

If all the code-lengths are the same and the mutual distance between any two codes is not smaller than d_0, the following equation can be obtained:

$$R_s \geq \frac{n}{n-2d_0}. \tag{5}$$

---

* MS in Japanese received by the Electrical Communication Laboratory, June 8, 1960. Originally published in the *Kenkyû Zituyoka Hôkoku* (*Electrical Communication Laboratory Technical Journal*), N.T.T., Vol. 9, No. 6, pp. 585-620, 1960.

† Switching Research Section.

By making R_s larger, higher selection stability and higher selection reliability can be expected.

Table 1

SELECTING CODES
($N=16$, $n=6$, $R_s=3$)

T \ C	1	2	3	4	5	6
0	0	0	0	0	0	0
1	1	0	0	0	0	1
2	0	1	0	0	0	1
3	1	1	0	0	0	0
4	0	0	1	0	1	0
5	1	0	1	0	1	1
6	0	1	1	0	1	1
7	1	1	1	0	1	0
8	0	0	0	1	1	0
9	1	0	0	1	1	1
10	0	1	0	1	1	1
11	1	1	0	1	1	0
12	0	0	1	1	0	0
13	1	0	1	1	0	1
14	0	1	1	1	0	1
15	1	1	1	1	0	0

Table 1 indicates the selecting codes for $n=6$, $R_s=3$ and $N=16$. (N is the number of the channels to be selected.) Correspondingly to this table, six input windings are wound on each core, as illustrated in Fig. 1. Each core has an output winding with a tuned circuit. The output voltage vs. input ampere-turn characteristic of each coil is linear as shown in Fig. 2.

When six input currents are applied simultaneously to the windings in the directions indicated in Fig. 1, magnetic flux is induced in each core in the direction shown by the arrow. If the value of the magnetic flux induced by each input current is equal to J, a total magnetic flux of $6J$ is induced in core #1 in the same direction and an output voltage V_0 is induced in the output winding. As the value of the magnetic flux in core #0 or in core #15 is only $4J-2J=2J$, the consequent output voltage is only $V_0/3$, which is smaller than that of core #1. In this case, the selecting output voltage appears across the output winding of the core #1, for the code pattern of input current and that of input windings of core #1 coincide with each

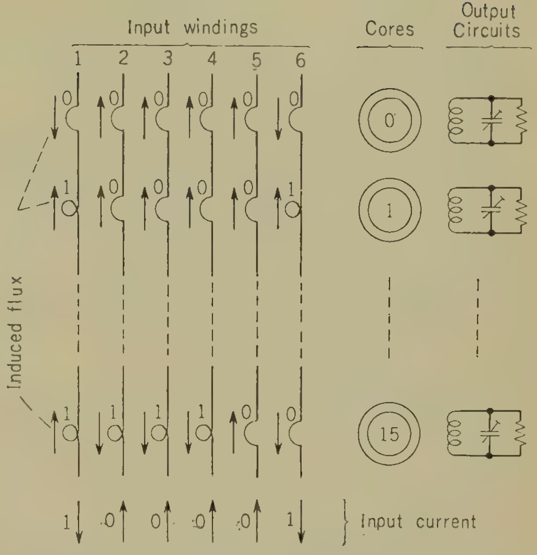

Fig. 1—Construction of selecting circuit.

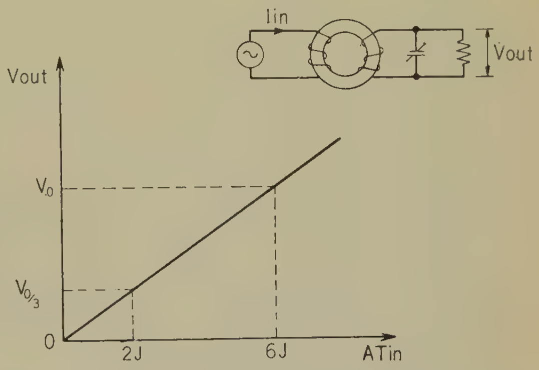

Fig. 2—Characteristics of the selecting-circuit core.

other. If the load circuit operates for the voltage V_0 while it does not operate for $V_0/3$, the selective operation is performed satisfactorily.

Since the oscillation phase of a parametron is either in phase or opposite phase to the stanpard phase, patametrons can be used as the input power source of selecting signals. For reference, the relation between the code-length (n) and the number of the channels to be selected (N) is shown below, when the selection ratio is 3.

n	3	6	12	18
N	4	16	64	256

3. Design of the Selecting Circuit

3.1. Characteristics of the Ferrite Cores to be Used

In the design of the selecting circuit, the values for the following items are given previously:

1) Output power. (Output voltage, load impedance, etc.)

2) The minimum selecting ratio.

3) The number of channels to be selected.

In order to obtain the required output, it is necessary first to select a code which satisfies the above conditions, to determine the input current value, to determine the turns ratio of windings, etc. Special attention should be paid to the selection of the cores to be used, because saturation of the core will reduce the selecting ratio. Input vs. output characteristics of some ferrite cores are illustrated in Fig. 3.

In the subsequent experiments, L_1D_{14} double cores, made of Cu-Zn ferrite for high frequency use, are used to avoid the reduction of the selecting ratio caused by saturation, and to obtain a large output voltage.

3.2. Selection of the Core

Variations in the output voltage between cores cause a reduction of the selecting ratio. Therefore, variation must be kept to a minimum.

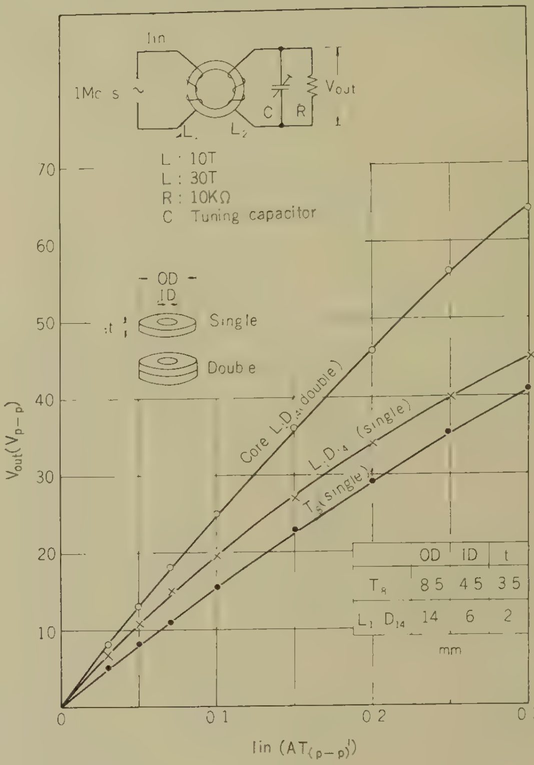

Fig. 3—Input vs. output characteristics of ferrite troidal cores.

In the secondary tuned circuit which is illustrated in Fig. 3, the variation of the output voltage depends mainly on the variation of Q of the core used. Therefore, Q was measured to provide a criterion for selecting the cores. The correlation factor between Q and output voltage was 0.85. An allowable output voltage variation of ±5% was assumed, and cores which had a $Q=26\sim36$ at 1 Mc/s were selected. This measurement was carried out after winding a ten-turn coil around the L_1D_{14} double cores.

3.3. Design of the Input Coupling Circuit

As illustrated in Fig. 1, the input windings of the cores are connected in series. If the output circuits are complete, the mutual couplings between the input windings are negligible, because of the nature of the code. Consequently, the input impedance is given by

$$Z_{in}=nR. \tag{6}$$

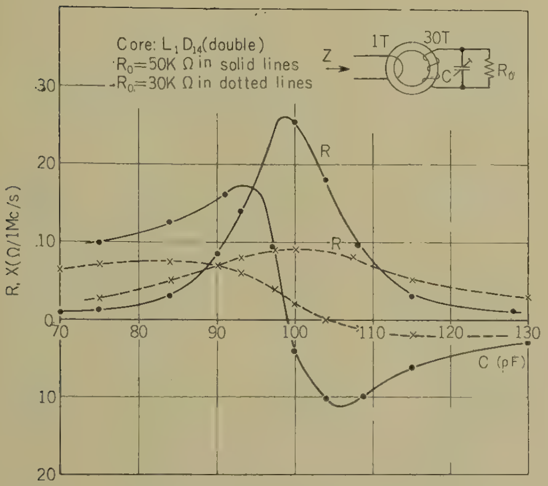

Fig. 4—Input impedance of the selecting circuit.

R is load resistance seen from one input winding of a core. The value for R is given in Fig. 4 as a function of the tuning capacitor. The power (P) consumed in the load is given by,

$$P=nI^2R. \tag{7}$$

I is the input current required to obtain the required output power. Input signals must satisfy all these conditions. And then in practice it is not desired that the input current is varied by the load effect, for the variation reduces the selecting ratio. Under a partially equipped condition, the input windings couple among themselves and reduce the selecting ratio. For these reasons, it is desirable for each input circuit to be a constant current source. On the other hand, the operation of parametrons becomes unstable with a increase in the value of the load impedance. This instability makes the use of parametrons as input signal sources undesirable.

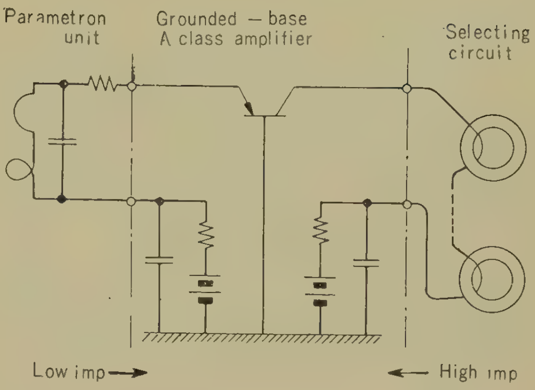

Fig. 5—Transistor coupling circuit. (Impedance converter.)

Because of the above reasons, an impedance converter is required which has a low input impedance to ensure stable parametron operation and a high output impedance to operate as a constant current sourse. Such an impedance-converting input-coupling circuit is shown in Fig. 5. A common-base amplifier using a Germanium transistor with an alpha cutoff frequency of 10 Mc/s is used. The input impedance of this circuit is approximately 25 Ω and the output impedance is approximately 3 kΩ at 1 Mc/s. Therefore, the constant-current-source requirement is satisfied. Besides, the operation of parametrons is not disturbed by load effects. The main reasons that the transistor is employed in the common base configuration are as follows:

1) The largest output impedance may be obtained.

2) The influence of the variation in the current amplification factor of the transistor is less than that in other configurations.

4. Experimental Results

Experimental results are tabulated in Table 2 and in Table 3. The cores used in these experiments were selected according to the principle explained in the preceding section. The experimental result shown in Table 2 corresponds to the error-correcting selecting codes presented in Table 1. The operation of the selecting circuit was examined in both fully and partially loaded conditions. The selected ontput voltage was approximately 13 volts.

In the experiment whose results are given in Table 3, another code ($N=256$, $n=18$, $R_s=3$ or 9) was used, and 48 loads were partially loaded. In this experiment the selected output voltage was approximately 18 volts across a 50 kΩ load resistor.

In Table 2 and Table 3, the term "direct coupled" means that input windings of the selecting circuit were connected directly to the output terminals of the parametron units, and the term "TR coupled" signifies that common-base transistor amplifiers were inserted as illustrated in Fig. 5.

Table 2

MEASURED SELECTING RATIO
($N=16$, $R_s=3$)

No. of equipped circuits	Input connection	Selecting ratio		
		mean	max.	min.
16 (full)	Direct coupled	2.7	2.8	2.6
12 (part)	Direct coupled	2.8	5.5	2.1
12 (part)	TR coupled	2.9	3.0	2.7

In Table 3, the symbols "+" and "−" are used as follows: When a code pattern of the input current is compared with the pattern of any input winding, and when corresponding digits are the same, this condition is represented by "−"; whereas when corresponding digits are opposite, this condition is represented by "+." After all the digits are compared, the number of "+" and the number of "−" are added, and when the former is larger than the latter, this condition is indicated by "+" in Table 3, and the opposite by "−."

For example, in Fig. 1, the code patten of the input windings on core ♯1 and the pattern of the input currents are the same. But at core ♯0, they are not all the same: 4 same digits and 2 opposite digits are seen. Therefore, this situation is represented by "−." In the same manner, the symbol "+" is given to core ♯15. The difference between "+" and "−" will be explained in the following section.

Oscillation phases "0" and "π" of the parametron are made to correspond to "1" and "0" respectively of the binary number.

Table 3

MEASURED SELECTING RATIO $N=256$ (Number of equipped circuits: 48) $R_s=3$ or 9

Selecting ratio / Input connection		3			9		
		mean	max.	min.	mean	max.	min.
Direct coupled	mean	3.2	5.4	2.4	12.8	50	4.4
	+	3.5	5.4	2.9	24	50	9.3
	−	2.2	2.4	2.1	5.5	7.8	4.4
TR coupled	mean	2.8	3.3	2.3	7.5	10.2	4.5
	+	2.9	3.3	2.7	8.7	10.2	7.5
	−	2.3	2.4	2.3	5.6	6.2	4.5

The variation of the input current due to the variation of the oscillation voltage of the parametrons and to α of the transistors was smaller than ±5%.

5. Variation of the Selecting Ratio

5.1. Causes of Variation

The following terms are considered as the causes of variations:

1) Variation between cores.
2) Variation in the input current.
3) Phase shift between input cutrents.
4) Asymmetry and distortion of the input current wave form.
5) Change of the input current due to the effect of coupling between input windings.

The effects of 1) and 2) have deen described. Term 3) is negligible when parametrons mounted on the same wiring board are used. Term 4) is also negligible when parametrons are used as input signal sources. Therefore, only the effect of 5) is thought to be large. The coupling between input windings takes place mainly through the core as an intermediary. The effect of the winding stray capacitance may be neglected.

When all the cores and the load circuits are mounted, the coupled current flowing in each input winding is completely cancelled by the characteristic of the code. (It is assumed that coupling factors on every core are the same.) However, when the selecting cores are partially equipped, the values of the input currents will be changed because of the incomplete cancellation of the coupling currents. Therefore the variation in the input currents may become large.

In order to prove the above assumptions and to explain the causes of the variation of the selecting ratio indicated in Table 2 and in Table 3, some basic experiments, as described below, were carried out.

5.2. Basic Experiments and Considerations

A selecting circuit, illustrated in Fig. 6, was constructed using the code indicated in

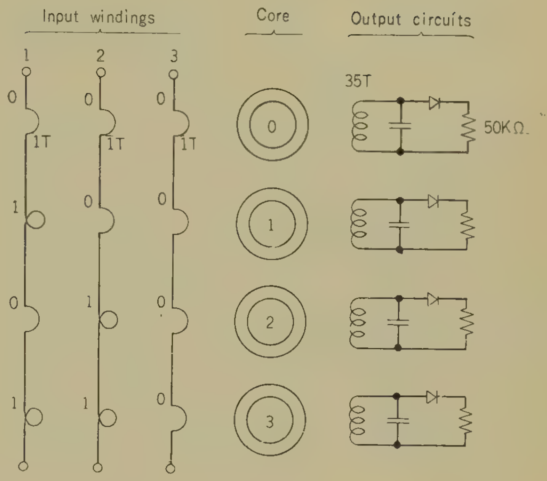

Fig. 6—Configuration of selecting circuits.

Table 4

SELECTING CODES ($N=4$, $n=3$, $R_s=3$)

T \ C	1	2	3
0	0	0	0
1	1	0	0
2	0	1	0
3	1	1	0

Table 4. ($N=4$, $n=3$, & $Rs=3$.) The coupling between the input windings 1 and 2 through core #0 is indicated by α_{120}, and the other coupling constants are indicated in the same manner. Input currents without coupling are presented as I_1, I_2, and I_3, and those with coupling are presented as I_1', I_2', and I_3'. By taking into consideration only the coupling current of the primary term, and neglecting those of other terms, the following equation is obtained:

$$\begin{vmatrix} I_1' \\ I_2' \\ I_3' \end{vmatrix} = \begin{vmatrix} 1 & \sum\alpha_{12i} & \sum\alpha_{13i} \\ \sum\alpha_{21i} & 1 & \sum\alpha_{21i} \\ \sum\alpha_{31i} & \sum\alpha_{32i} & 1 \end{vmatrix} \begin{vmatrix} I_1 \\ I_2 \\ I_3 \end{vmatrix} \qquad (8)$$

$$i=0, 1, 2, 3.$$

Now the following conditions are assumed:

1) $|I_1|=|I_2|=|I_3|=I,$ (9)

2) The absolute value of α is constant.

3) The sign for α is "−" when any pair of the windings have the same directions, and "+" when they have oposite directions.

4) The output voltage is proportional to the total sum of the input currents applied to that core.

These assumptions are appropriate for practical purposes.

(A) Fully loaded condition (See Fig. 6)

Equation (10) is obtained from Eq. (8).

$$\begin{vmatrix} I_1' \\ I_2' \\ I_3' \end{vmatrix} = \begin{vmatrix} 1 & 0 & 0 \\ 0 & 1 & 0 \\ 0 & 0 & 1 \end{vmatrix} \begin{vmatrix} I_1 \\ I_2 \\ I_3 \end{vmatrix} = \begin{vmatrix} I_1 \\ I_2 \\ I_3 \end{vmatrix}. \qquad (10)$$

The values of the output voltage of each core are indicated in Table 5. Input currents are shown above the oblique lines. Their values are proportional to the values of the output voltage, as explained above. Measured values of output voltages are shown below the oblique lines. In this experiment as well as in the following ones in this section, input windings of the selecting circuit were coupled directly to output terminals of the parametrons. The variation in output voltage shown in Table 5 was mainly because of variation between cores.

Table 5

CALCULATED & MEASURED OUTPUT VOLTAGE (VOLT)
(Under the fully equipped condition)

Input code / Core number	0	1	2	3
0	$3I$ 8.0	I 2.7	I 2.8	I 2.7
1	I 2.7	$3I$ 7.5	I 2.8	I 2.8
2	I 2.8	I 2.9	$3I$ 8.0	I 2.8
3	I 2.8	I 2.8	I 2.7	$3I$ 7.8

(B) The case in which core #0 is omitted

Equation (11) is obtained from Eq. (8).

$$\begin{matrix} I_1' \\ I_2' \\ I_3' \end{matrix} = \begin{matrix} 1 & \alpha & \alpha \\ \alpha & 1 & \alpha \\ \alpha & \alpha & 1 \end{matrix} \begin{matrix} I_1 \\ I_2 \\ I_3 \end{matrix}. \qquad (11)$$

Two digits of the binary code, "0" and "1," were made to correspond to "+" and "−" respectively. For example, if the input current pattern is (1 0 0),

$$I_1=-I, \quad \text{and} \quad I_2=I_3=I.$$

Therefore, from Eq. (11),

$$I_1'=-I+2\alpha I, \quad \text{and} \quad I_2'=I_3'=I.$$

Since the input winding pattern of core #1 is (1 0 0), the total input current given to this core is

$$-I_1'+I_2'+I_3'=I-2\alpha I+I+I=3I-2\alpha I.$$

On the other hand, as the input winding pattern of core #2 is (0 1 0), the total input current is

$$I_1'-I_2'+I_3'=-I+2\alpha I-I+I=-I+2\alpha I$$

$$=-(I-2\alpha I).$$

In Table 6, only the absolute value is taken into consideration as the output voltage, and both calculated and measured values are tabulated.

Table 6

CALCULATED & MEASURED OUTPUT VOLTAGE (VOLT)
(Under a partially equipped condition I)

Input code / Core number	0	1	2	3
1	$I+2\alpha I$ 3.0	$3I-2\alpha I$ 8.0	$I-2\alpha I$ 2.6	$I-2\alpha I$ 2.6
2	$I+2\alpha I$ 3.0	$I-2\alpha I$ 2.6	$3I-2\alpha I$ 8.0	$I-2\alpha I$ 2.6
3	$I+2\alpha I$ 3.0	$I-2\alpha I$ 2.6	$I-2\alpha I$ 2.6	$3I-2\alpha I$ 8.0

Table 7

CALCULATED & MEASURED OUTPUT VOLTAGE (VOLT)
(Under a partially equipped condition II)

Input code / Core number	0	1	2	3
2	I 2.8	I 2.8	$3I-4\alpha I$ 8.0	$I-4\alpha I$ 2.5
3	I 2.8	I 2.8	$I-4\alpha I$ 2.5	$3I-4\alpha I$ 8.0

(C) The case in which both cores ♯0 and ♯1 are omitted

Both calculated and measured values of the output voltage for this condition are tabulated in Table 7.

Since the measurements for cases (A), (B), and (C) was done independently, it is meaningless to compare the selected output voltages of each case with one another.

(D) Coupling factor α

In the above experiments, the coupling between any two of the windings is considered a result of the effect of the output winding. In other words, if some of the output windings are opened, the same results are obtained as those when the corresponding cores were not equipped from the beginning.

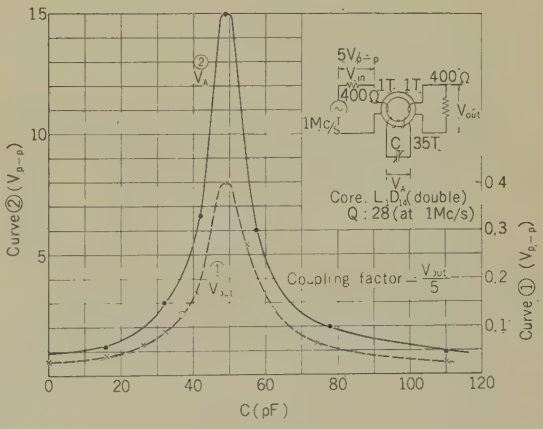

Fig. 7—Change of the coupling constant due to the effect of a tertiary winding with a tuning capacitance.

Fig. 7 illustrates the measured values of the coupling which occurred between two windings due to the effect of a tertiary winding with a tuned circuit. The core was a L_1D_{14} double core ($Q=28$ at 1 Mc/s). When the tertiary winding was opened, namely when $C=0$, the coupling constant between two coils with a one turn winding each was approximately 0.006 (44 dB). This coupling constant is given as the ratio of V_{out} to V_{in} in Fig. 7. With an increase of tuning capacitance, however, the coupling constant changed, as is illustrated by curve 1. Curve 2 represents the induced voltage in the tertiary winding. In an actual circuit, a resistance is added in parallel with the tuning capacitance. This causes a change in the coupling constant. Besides, the coupling constant is changed by detuning or the variation in the element.

From Table 6 and Table 7, α was calculated to be approximately 0.025, under the assumption that the output voltage is proportional to the input current. In the above experiments, the tuned circuit voltage was observed with an oscilloscope while the tuned circuit was being adjusted. When the oscilloscope probe is disconnected, the resonant frequency shifts because of the removal of the approximately 12 pF of prove capacitance. This point is indicated in Fig. 7 by the small circle P. At this point V_{out}/V_{in} is nearly equal to 0.025. This value corresponds to the value obtained above by calculation.

5.3. Other Experiments

Finally, the calculated results of input current and measured values of output current under the conditions indicated in Table 3 are tabulated in Table 8: $N=256$, 48 cores, and output circuits were partially equipped. In this experiment, transistor coupling circuits were used.

Table 8

CALCULATED & MEASURED OUTPUT VOLTAGE
($N=256$, Number of equipped circuits: 48)

Core	Input Signal	Output voltage (volt)	Input current
Selected	+18	18.5	$18I-352\alpha I$
Non-selected	+6	6.6	$6I-352\alpha I$
	−6	8.0	$6I+224\alpha I$
	+2	2.0	$2I-288\alpha I$
	−2	3.0	$2I+288\alpha I$

6. Some Hints to Improve the Selecting Ratio

1) Use cores which have a large saturation flux density and good linearity. (In general these requirements are opposite to those for miniaturization.)

2) Make the input signal source impedance high, avoiding variation in the input current due to the coupling.

3) Clip the output voltage at a proper level. For example if the selected output voltage is 20 volts and the non-selected output voltage is 10 volts, the selecting ratio is 2; whereas by clipping each output voltage at 5 volts, the selecting ratio becomes 3.

4) Reduce variations between circuit elements and between input currents.

7. Conclusion

By applyjng error-correcting codes to a selecting circuit in which small ferrite cores with linear characteristics were used, a good selecting circuit with high speed operation was obtained.

The causes which lower the selecting ratio and make the selection unstable were explained, and some methods of improving the ratio were suggested.

The partially equipped (48 out of 256) selecting circuit has been employed in an experimental all-electronic telephone exchange, and has been operating stably for more than one year.

* * * *

REVIEW OF THE ELECTRICAL COMMUNICATION LABORATORY
VOLUME 8, NUMBERS 11-12, NOVEMBER-DECEMBER, 1960

U.D.C. 621.372.814

Reflections and Mode Conversions in Imperfect Junctions of TE$_{01}$ Wave Transmission Line*

Ken-ichi NODA†

Imperfect junctions cause attenuation increase and delay distortion in the TE$_{01}$ wave transmission line. It is known, that the magnitudes of reflections at a slight tilt and at a offset do not have a first order term of tilt angle or distance between two waveguide axes respectively. Reflections at a tilt and at a offset have been calculated from the continuity condition of the electric and magnetic fields at the junctions. Mode conversion at the junction of true circular with elliptically distorted waveguides has also been calculated by a similar method. The results of these calculations provide fundamental data to determine the dimension tolerances and installation tolerances for this kind of waveguide.

Introduction

Imperfect junctions in a TE$_{01}$ wave transmission line cause reflection and mode conversion. Imperfect junctions are classified into the following types: tilt, offset, diameter discontinuity, elliptically deformed discontinuity, etc. Several of these types may occur simultaneously in a practical case. First order solutions were obtained for the cases of the slight tilt and the slight offset in terms of the tilt angle and the offset between the two waveguide axes respectively.(1) It was also shown that in both cases the reflection coefficient does not have a first order term.

In the case of diameter discontinuity, reflection and mode conversion were calculated in the first order term of the diameter difference.(2)

Mode conversions due to imperfect junctions cause serious degradation of the characteristics of transmission lines. However, as the reflection coefficient does not have a first order term except in the case of diameter discontinuity, its value is usually quite small. However, when a helix waveguide is completely developed and used, the mode conversion may become little serious and the reflection remains as a important problem to determine the characteristics of this kind of the waveguide.

In this paper; first, the reflection at a slight tilt, and second, the reflection at a slight offset are calculated from the continuity condition at the junction plane. The results are formulated in the form of a summation of the series of functions with regard to the eigenvalues of the modes converted at these junctions.

The mode conversion at an elliptically deformed discontinuity is an important value useful for determining the dimensional tolerances of the waveguide. In a manner similar to that used for calculating reflections due to slight tilt and offset, the mode conversion can be obtained from the continuity condition of the electric and magnetic fields. The wave function in the elliptic waveguide has been obtained by the superposition of those of the circular cylindrical wave.(3)

If the dissipation loss of the waveguide is disregarded in the analysis, the mode conversion factor increases infinitely when the frequency approaches the cutoff frequency of

---

* MS in Japanese received by the Electrical Communication Laboratory, on 19, July, 1960. Originally published in the *Kenkyû Zituyôka Hôkoku* (*Electrical Communication Technical Journal*), N.T.T., Vol. 10, No. 1, pp. 85–94, 1961.

† Hyper-frequency Research Section.

some converted mode. Detailed analysis must be made in such a case to know the exact conversion factor. Taking into consideration the attenuation of the waveguide which has thus far been disregarded in the calculation of the mode conversion, it is found that the mode conversion at the cutoff frequency of a converted mode does not attain a very large value.

1. Reflection due to a Slight Tilt

Both ends of a waveguide are usually finished by attaching a flange or cutting a thread to connect to another waveguide. The end plane of the waveguide must be finished exactly perpendicular to the guide axis. A waveguide having a perfectly finished end plane and a waveguide having an obliquely finished end plane are assumed to be connetted as shown in Fig. 1. Most of the power of the incident wave goes to the right hand waveguide, a small part is reflected back in the same mode as the incident wave, and the remaining part is converted into many unwanted modes, which propagate both forward and backward. In Fig. 1, the letters in brackets are the mode voltages and currents, which will be defined later.

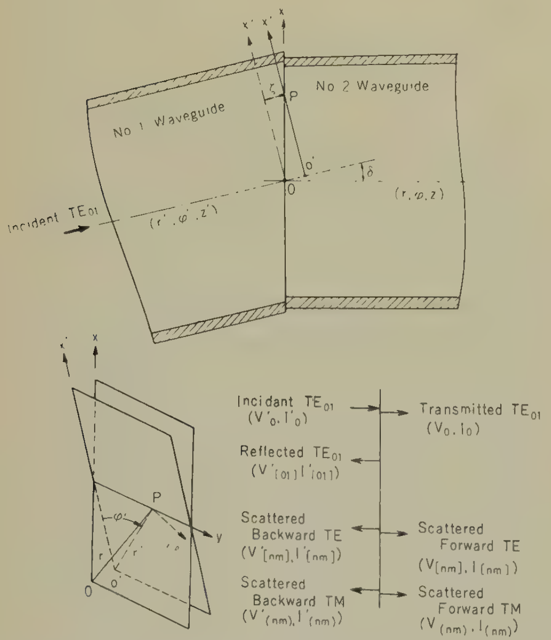

Fig. 1—Junction between a waveguide having a perfect flange and a waveguide having an oblique flange.

The electric and magnetic fields are expanded into a series by the mode functions,(4) namely:

$$\left.\begin{aligned} \boldsymbol{E}_t &= \sum_i V_{(i)}(z)\boldsymbol{e}_{t(i)} + \sum_i V_{[i]}(z)\boldsymbol{e}_{t[i]}, \\ \boldsymbol{H}_t &= \sum_i I_{(i)}(z)\boldsymbol{h}_{t(i)} + \sum_i I_{[i]}(z)\boldsymbol{h}_{t[i]}, \\ E_z &= \sum_i I_{(i)}(z)e_{z(i)}, \\ H_z &= \sum_i V_{[i]}(z)h_{z[i]}, \end{aligned}\right\} \quad (1)$$

where $\boldsymbol{E}_t$ and $\boldsymbol{H}_t$ are the transverse components of the electric and the magnetic fieilds respectively; E_z and H_z are the longitudinal components of the electric and the magnetic fields respectively; V_i and I_i are the voltage and the current of the mode respectively, and are designated as $V_{[i]}$ and $I_{[i]}$ for the case of the TE mode, and as $V_{(i)}$ and $I_{(i)}$ for the case of the TM mode. For the present, circular cylindrical coordinates (r, φ, z) are used. $\boldsymbol{e}_{ti}$ and $\boldsymbol{h}_{ti}$ are mode vectors which satisfy the normalized orthogonality conditions and are given in the following expressions for the TM and TE modes respectively,

$$\left.\begin{aligned} \boldsymbol{e}_{t(i)} &= \boldsymbol{h}_{t(i)} \times \boldsymbol{i}_z = \nabla_t T_{(i)}(r, \varphi), \\ \boldsymbol{e}_{t[i]} &= \boldsymbol{h}_{t[i]} \times \boldsymbol{i}_z = \nabla_t T_{[i]}(r, \varphi) \times \boldsymbol{i}_z, \end{aligned}\right\} \quad (2)$$

where $\boldsymbol{i}_z$ is the unit vector in the z direction. $e_{z(i)}$ and $h_{z[i]}$ in equation (1) are given as

$$\left.\begin{aligned} e_{z(i)} &= -\frac{\chi^2_{(i)}}{i\omega\varepsilon_0} T_{(i)}, \\ h_{z[i]} &= -\frac{\chi^2_{[i]}}{i\omega\mu_0} T_{[i]}, \end{aligned}\right\} \quad (3)$$

where the scalar functions $T_{(i)}$ and $T_{[i]}$ are

$$\left.\begin{aligned} T_{(i)} &= p_{(i)} J_n(\chi_{(i)} r) \begin{smallmatrix}\sin\\ \cos\end{smallmatrix}\, n\varphi, \\ T_{[i]} &= q_{[i]} J_n(\chi_{[i]} r) \begin{smallmatrix}\cos\\ \sin\end{smallmatrix}\, n\varphi, \end{aligned}\right\} \qquad (4)$$

which satisfy the equation $\nabla_t^2 T_i + \chi_i T_i = 0$, and $p_{(i)}$ and $q_{[i]}$ are normalizing factors.

The components of the electric field of a mode are writen with Cartesian coordinates as (e_x', e_y', e_z'), and with circular cylindrical coordinates as (e_r', e_φ', e_z'). Then, the transverse electric field $\boldsymbol{E}_{t1}'$ on the junction plane caused by the wave of a mode (V', I') is

$$\boldsymbol{E}'_{t1} = \{-(V'e'_x \cos\delta \pm I'e'_z \sin\delta)\sin\varphi$$
$$+ V'e'_y \cos\varphi\} e^{\mp ih\zeta} \boldsymbol{i}_\varphi + A\,\boldsymbol{i}_r, \qquad (5)$$

in which the primes are put on the quantities in the No. 1 waveguide (see Fig. 1), h is the propagation constant divided by the complex number i, and $\boldsymbol{i}_\varphi$ and $\boldsymbol{i}_r$ are the unit vectors in the φ and r directions respectively. In equation (5), the mode number i is omitted. If desired, the quantity A can easily be obtained, but since it is of no value in succeeding calculations, it is not necessary to find A explicitly. For a wave propagating in the $+z$ direction, the upper part of the double sign in equation (5) is used and for a wave propagating in the $-z$ direction, the lower part is used.

The functions of δ in equation (5) are expanded in power series of δ, and the terms of order δ^0, δ^1 and δ^2 are collected giving:

$$\boldsymbol{E}'_{t1} = \Big[V'e'_r \frac{\delta^2}{2} \sin 2\varphi + V'e'_\varphi \Big\{ 1 \mp \delta\, ihr\cos\varphi$$
$$- \frac{\delta^2}{2}(\sin^2\varphi + h^2 r^2 \cos^2\varphi) \Big\}$$
$$- I'e'_z(\pm\delta - \delta^2\, ihr\cos\varphi)\sin\varphi \Big] \boldsymbol{i}_\varphi + A\,\boldsymbol{i}_r. \qquad (6)$$

In the similar way, the transverse magnetic field on the junction plane caused by the wave of the mode becomes

$$\boldsymbol{H}'_{t1} \times \boldsymbol{i}_z =$$
$$-\Big[I'h'_r \Big\{ \pm 1 - \delta\, ihr\cos\varphi \mp \frac{\delta^2}{2}(1 + h^2 r^2)\cos^2\varphi \Big\}$$
$$+ V'h'_z(\delta \mp \delta^2\, ihr\cos\varphi)\cos\varphi \Big] \boldsymbol{i}_\varphi + B\,\boldsymbol{i}_r, \qquad (7)$$

where B also need not be found explicitly.

The electric and magnetic field components of each mode which is necessary in the succeeding calculations are derived using equations (6) and (7). At first, for the TE_{01} mode

$$\left.\begin{aligned}
\boldsymbol{E}'_{t1,0} &= V_0' q_{[01]} \chi_{[01]} \Big(J_1(\chi_{[01]} r) \\
&\quad - \delta\, ih_{[01]} r \cos\varphi J_1(\chi_{[01]} r) \\
&\quad - \frac{\delta^2}{2} \{ (\sin^2\varphi + h^2_{[01]} r^2 \cos^2\varphi) J_1(\chi_{[01]} r) \\
&\quad + \chi_{[01]} r \cos^2\varphi J_1'(\chi_{[01]} r) \} \Big) \boldsymbol{i}_\varphi, \\
\boldsymbol{H}'_{t1,0} \times \boldsymbol{i}_z &= -V_0' q_{[01]} \chi_{[01]} \Big(-Y_{[01]} J_1(\chi_{[01]} r) \\
&\quad + \delta \Big\{ Y_{[01]} ih_{[01]} r J_1(\chi_{[01]} r) \\
&\quad - \frac{\chi_{[01]}}{i\omega\mu_0} J_0(\chi_{[01]} r) \Big\} \cos\varphi + \frac{\delta^2}{2} Y_{[01]} \chi_{[01]} r \\
&\quad \times J_1'(\chi_{[01]} r) + Y_{[01]} (1 + h^2_{[01]} r^2) J_1(\chi_{[01]} r) \\
&\quad + \frac{2\chi_{[01]} r h_{[01]}}{\omega\mu_0} J_0(\chi_{[01]} r) \Big\} \cos^2\varphi \Big) \boldsymbol{i}_\varphi + C\boldsymbol{i}_r,
\end{aligned}\right\}$$
$$(8)$$

where C also need not be found explicitly. The normalizing factor q in equation (4) is

$$q_{[nm]} = \sqrt{\frac{\varepsilon_n}{\pi}} \frac{1}{\sqrt{k^2_{[nm]} - n^2} J_n(k_{[mn]})}, \qquad (9)$$

where $k_{[nm]}$ is the mth root of $J_n'(x) = 0$ for all values of m except zero, $k_{[nm]}=\chi_{[nm]}a$, and a is the inner radius of the waveguide. The admittance $Y_{[i]}$ for the TE mode in equation (8) is given as

$$Y_{[i]}=\frac{I_{[i]}}{V_{[i]}}=\frac{h_{[i]}}{\omega\mu_0}. \tag{10}$$

Secondly, the electric and magnetic fields on the junction plane caused by the reflected TE_{01} wave are

$$\left.\begin{aligned} \boldsymbol{E}'_{t1,[01]}&=V'_{[01]}q_{[01]}\chi_{[01]}J_1(\chi_{[01]}r)\boldsymbol{i}_\varphi,\\ \boldsymbol{H}'_{t1,[10]}\times\boldsymbol{i}_z&=-V'_{[01]}q_{[01]}\chi_{[01]}Y_{[01]}J_1(\chi_{[01]}r)\boldsymbol{i}_\varphi. \end{aligned}\right\} \tag{11}$$

In the same way, for the scattered backward TE_{1m} waves

$$\left.\begin{aligned} \boldsymbol{E}'_{t1,[1m]}=&-V'_{[1m]}q_{[1m]}\Big\{\chi_{[1m]}J_1'(\chi_{[1m]}r)(\cos\varphi\\ &+\delta ih_{[1m]}r\cos^2\varphi)+\delta Y_{[1m]}\frac{\chi^2_{[1m]}}{2i\omega\varepsilon_0}\\ &\times J_1(\chi_{[1m]}r)\sin 2\varphi\Big\}\boldsymbol{i}_\varphi+D\boldsymbol{i}_r,\\ \boldsymbol{H}'_{t1,[1m]}\times\boldsymbol{i}_z=&V'_{[1m]}q_{[1m]}\Big\{\chi_{[1m]}Y_{[1m]}\\ &\times J_1'(\chi_{[1m]}r)(\cos\varphi+\delta ih_{[1m]}r\cos^2\varphi)\\ &+\delta\frac{\chi^2_{[1m]}}{i\omega\mu_0}J_1(\chi_{[1m]}r)\cos^2\varphi\Big\}\boldsymbol{i}_\varphi+E\boldsymbol{i}_r, \end{aligned}\right\} \tag{12}$$

where D and E need not be found explicitly. In equation (11) and (12), it is taken into consideration that $V'_{[01]}$ is at most, the square of δ, and $V'_{[1m]}$ is first order of δ.$^{(1)}$ Moreover, the amplitudes of the scattered backward TM_{11} wave and the scattered waves other than TE_{1m} are zero,$^{(1)}$ therefore these waves need not be taken into consideration.

The continuity conditions of the electric and magnetic field at the junction plane are

$$\left.\begin{aligned} &\boldsymbol{E}'_{t1,0}+\boldsymbol{E}'_{t1,[01]}+\sum_m\boldsymbol{E}'_{t1,[1m]}+\sum_i\boldsymbol{E}'_{t1,i}\\ &\qquad=V_0\boldsymbol{e}_{t[01]}+\sum_j V_j\boldsymbol{e}_{tj},\\ &(\boldsymbol{H}'_{t1,0}+\boldsymbol{H}'_{t1,[01]}+\sum_m\boldsymbol{H}'_{t1,[1m]}+\sum_i\boldsymbol{H}'_{t1,i})\times\boldsymbol{i}_z\\ &\qquad=(I_0\boldsymbol{h}_{t[01]}+\sum_j I_j\boldsymbol{h}_{tj})\times\boldsymbol{i}_z, \end{aligned}\right\} \tag{13}$$

where i represents any mode other than [01] and [$1m$], and j represents any mode other than [01]. The scalar product of equations (13) and $q_{[01]}\chi_{[01]}J_1(\chi_{[01]}r)\boldsymbol{i}_\varphi$ are integrated on the junction plane, giving

$$\left.\begin{aligned} &V_0'(1-F\delta^2)+V'_{[01]}+\sum_m V'_{[1m]}\\ &\quad\times\frac{2\sqrt{2}\,ih_{[1m]}ak_{[01]}k^2_{[1m]}}{\sqrt{k^2_{[1m]}-1}\,(k^2_{[1m]}-k^2_{[01]})^2}\delta=V_0,\\ &V_0'Y_{[01]}(1-F\delta^2)-V'_{[01]}Y_{[01]}-\sum_m V'_{[1m]}\\ &\quad\times\Big\{\frac{2\sqrt{2}\,ih_{[1m]}ak_{[01]}k^2_{[1m]}}{\sqrt{k^2_{[1m]}-1}(k^2_{[1m]}-k^2_{[01]})^2}\delta Y_{[1m]}\\ &\quad+\frac{\sqrt{2}\,ik_{[01]}k^2_{[1m]}}{h_{[1m]}a\sqrt{k^2_{[1m]}-1}(k^2_{[1m]}-k^2_{[01]})}\\ &\quad\times\delta Y_{[1m]}\Big\}=V_0Y_{[01]}, \end{aligned}\right\} \tag{14}$$

where the F's in both equations are equal. Therefore, they vanish in succeeding calculations, and need not be calculated. Equations (14) are simultaneous algebraical equations, in which $V'_{[01]}$ and V_0 are the unknown quantities. By solving these equations, $V'_{[01]}$ can easily be obtained. The reflection coefficient R_t is the ratio of $V'_{[01]}$ to the voltage of the incident TE_{01} wave. Using the mode conversion factors $V'_{[1m]}$ from the incident TE_{01} wave to the TE_{1m} waves,$^{(1)}$ namely

$$V'_{[1m]}=-\frac{\sqrt{2}\,ik_{[01]}k^2_{[1m]}(h_{[01]}-h_{[1m]})^2a}{2\sqrt{k^2_{[1m]}-1}\,(k^2_{[1m]}-k^2_{[01]})^2h_{[1m]}}\delta V_0', \tag{15}$$

then the reflection coefficient becomes

$$R_t=\frac{V'_{[01]}}{V_0'}=-\frac{k^2_{[01]}\delta^2}{2h_{[01]}a^2}\times\sum_m\frac{k^4_{[1m]}}{(k^2_{[1m]}-1)(k^2_{[1m]}-k^2_{[01]})h_{[1m]}}. \qquad (16)$$

The reflection coefficient due to a slight tilt has been formulated as the summation of the functions of the eigenvalues of the modes generated at this slight tilt. In the calculations of equations (5), (6) and (7), the following relations concerning the coordinate transformation have been used.

$$\left.\begin{aligned}\zeta&=r(\cos\varphi)\delta,\\ r'&=r-\frac{\delta^2}{2}r\cos^2\varphi,\\ \varphi'&=\varphi+\frac{\delta^2}{4}\sin 2\varphi.\end{aligned}\right\} \qquad (17)$$

The cross section of the No. 1 waveguide with the junction plane is an ellipse and its area is a slightly larger than that of the No. 2 waveguide. But the area of the part of the No. 1 waveguide, not contained in the cross section of the No. 2 waveguide is only the order of δ^2, and moreover the value $q_{[01]}\chi_{[01]}J_1(\chi_{[01]}r)$ which is used to multiply the equation (13) to obtain the equation (14), is the order of δ at least in the vicinity of the waveguide wall. Therefore, this area does not contribute of the order of δ^2 to the integral.

We now show a numerical calculation for the reflection due to a slight tilt at the junction of the circular electric wave transmission line. For the case where the waveguide diameter is 51 mm and the frequency is 50 Gc/s, the terms following the sign $\sum\limits_m$ in equation (16) are divided into three parts and they are calculated separately as follows:

$$\sum_m=\sum_{m=1}^{8}+\sum_{m=9}^{16}+\sum_{m=17}^{\infty}. \qquad (18)$$

The first term concerns the modes which can propagate, and is a real number. The second and third terms concern modes which are below the cutoff frequency, and are imaginary numbers. The value m which is the boundary between the second and the third terms does not have any special mathematical meaning, but the larger m we choose, the higher the accuracy of the calculation becomes. We calculate the third term roughly as follows:

$$\sum_{m=17}^{\infty}\fallingdotseq -i\frac{a}{\pi^3}\sum_{m=17}^{\infty}\frac{1}{m^3}=-i\frac{a}{\pi^3}\left(\sum_{m=1}^{\infty}\frac{1}{m^3}-\sum_{m=1}^{16}\frac{1}{m^3}\right)=-i\,1.505\times10^{-6}, \qquad (19)$$

in which the relation

$$\sum_{m=1}^{\infty}\frac{1}{m^3}=1.20206, \qquad (20)$$

is used. After the calculation, the reflection coefficient is

$$R_t=(-0.0259+i\,0.000268)\delta^2. \qquad (21)$$

When the angle of the tilt is 10′, we obtain, using equation (21), a reflection coefficient of −133 dB.

2. The Reflection due to a Slight Offset

Reflection and mode conversion occur at the junction of a circular electric wave transmission line if the axes of the two waveguides do not coincide. For this mode conversion, the first order solution had been obtained, moreover, it had been shown that the first order reflection is zero.(1) Therefore, the reflection is much smaller than the mode conversion factor if the offset value is not large. But, in case of the helix waveguide, the reflection coefficient is an important value when we intend to investigate the delay characteristics of the waveguide, as explained above.

The electric and magnetic fields in the circular waveguide can be derived from two scalar functions $T_{[nm]}$ and $T_{(nm)}$. We will now transform the coordinates of the function

T in the No. 1 waveguide as shown in Fig. 2 into the coordinates of the No. 2 waveguide.

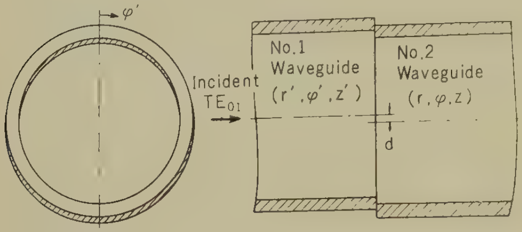

Fig. 2—Slight offset at a waveguide junction.

Namely, from an additional theorem concerning the circular cylindrical wave,(5)

$$T_{[nm]}=q_{[nm]}J_n(\chi_{[nm]}r')\begin{matrix}\cos\\ -\sin\end{matrix}n\varphi'$$

$$=q_{[nm]}\sum_{i=-\infty}^{\infty}J_i(\chi_{[nm]}d)J_{n+i}(\chi_{[nm]}r)\begin{matrix}\cos\\ -\sin\end{matrix}(n+i)\varphi, \tag{22}$$

where the primes are put on the quantities in the No. 1 waveguide.

The fields in both waveguides are considered as the superposition of all modes as shown in the lower right-hand corner of Fig. 1. Using equation (22) and the series expansion of the circular cylindrical function concerning $\delta=\alpha/a$,

$$J_i(\chi_i d)=J_i(k_i\delta)=\left(\frac{k_i\delta}{2}\right)^i\left\{\frac{1}{i!}-\frac{1}{(i+1)!}\left(\frac{k_i\delta}{2}\right)^2+\cdots\cdots\right\},$$

$$i=0,1,2,\cdots\cdots, \tag{23}$$

the fields of each mode in the incident waveguide are expressed by the coordinates of the No. 2 waveguide, and are calculated up to the order of δ^2. Using the definitions

$$\left.\begin{aligned}\frac{k_{(nm)}\delta}{2}&=\delta_{(nm)},\\ \frac{k_{[nm]}\delta}{2}&=\delta_{[nm]},\end{aligned}\right\} \tag{24}$$

we calculate the transverse electric field $\boldsymbol{E}'_{t1}$. At first, for the incident TE_{01} mode,

$$\left.\begin{aligned}\boldsymbol{E}'_{t1,0}=V_0'q_{[01]}\{&\chi_{[01]}(1-\delta^2_{[01]})J_1(\chi_{[01]}r)\\ &-2\delta_{[01]}\chi_{[01]}J_1'(\chi_{[01]}r)\cos\varphi\\ &+\delta^2_{[01]}\chi_{[01]}J_2'(\chi_{[01]}r)\cos 2\varphi\}\boldsymbol{i}_\varphi\\ &+G\boldsymbol{i}_r,\\ \boldsymbol{H}'_{t1,0}\times\boldsymbol{i}_z=Y_{[01]}&\boldsymbol{E}'_{t1,0},\end{aligned}\right\} \tag{25}$$

where G can easily be calculated, but need not be, because it is of no use in the succeeding calculations. Secondly, for the reflected TE_{01} mode,

$$\left.\begin{aligned}\boldsymbol{E}'_{t1,[01]}&=V'_{[01]}q_{[01]}\chi_{[01]}J_1(\chi_{[01]}r)\boldsymbol{i}_\varphi,\\ \boldsymbol{H}'_{t1,[01]}\times\boldsymbol{i}_z&=-Y_{[01]}\boldsymbol{E}'_{t1,[01]}.\end{aligned}\right\} \tag{26}$$

Thirdly, for the scattered backward TE_{1m} modes,

$$\left.\begin{aligned}\boldsymbol{E}'_{t1,[1m]}=-V'_{[1m]}q_{[1m]}\chi_{[1m]}\{&J_1'(\chi_{[1m]}r)\cos\varphi\\ &+\delta_{[1m]}J_1(\chi_{[1m]}r)+\delta_{[1m]}J_2'(\chi_{[1m]}r)\\ &\times\cos 2\varphi\}\boldsymbol{i}_\varphi+H\boldsymbol{i}_r,\\ \boldsymbol{H}_{t1,[1m]}\times\boldsymbol{i}_z=-Y_{[1m]}&\boldsymbol{E}'_{t1,[1m]},\end{aligned}\right\} \tag{27}$$

where H need not be calculated also. The continuity conditions of the transverse electric and magnetic fields are

$$\left.\begin{aligned}&\boldsymbol{E}'_{t1,0}+\boldsymbol{E}'_{t1,[01]}+\sum_m\boldsymbol{E}'_{t1,[1m]}+\sum_i\boldsymbol{E}'_{t1,i}\\ &\qquad=V_0\boldsymbol{e}_{t[01]}+\sum_j V_j\boldsymbol{e}_{tj},\\ &(\boldsymbol{H}'_{t1,0}+\boldsymbol{H}'_{t1,[01]}+\sum_m\boldsymbol{H}'_{t1,[1m]}+\sum_i\boldsymbol{H}'_{t1,i})\times\boldsymbol{i}_z\\ &\qquad=(I_0\boldsymbol{h}_{t[01]}+\sum_j I_j\boldsymbol{h}_{tj})\times\boldsymbol{i}_z,\end{aligned}\right\} \tag{28}$$

where i represents any mode, except [01] and [$1m$], transmitted backward, and j represents any forward wave except [01].

Both sides of the two equations of (28) are multiplied by $q_{[01]}x_{[01]}J_1(x_{[01]}r)$ scalarly and integrated in the junction plane giving

$$\left.\begin{aligned} &V_0'+V'_{[01]}-\sum_m K_m V'_{[1m]}\doteqdot V_0,\\ &Y_{[01]}V_0'-Y_{[01]}V'_{[01]}\\ &\quad+\sum_m Y_{[1m]}K_m V'_{[1m]}=Y_{[01]}V_0, \end{aligned}\right\} \tag{29}$$

where

$$K_m=\frac{\sqrt{2}\,k_{[01]}k^2_{[1m]}\delta}{\sqrt{k^2_{[1m]}-1}\,(k^2_{[1m]}-k^2_{[01]})}. \tag{30}$$

Then the mode conversion factor from the incident TE_{01} mode to the TE_{1m} modes, namely

$$V'_{[1m]}=\left(\frac{Y_{[01]}}{Y_{[1m]}}-1\right)\times\frac{k_{[01]}k^2_{[1m]}\delta}{\sqrt{2}\,\sqrt{k^2_{[1m]}-1}\,(k^2_{[1m]}-k^2_{[01]})}V_0', \tag{31}$$

which is given in reference,⁽¹⁾ is substituted into equation (29), and equation (29) becomes two simultaneous equations having two unknowns, $V'_{[01]}$ and V_0'. We can easily obtain $V'_{[01]}$ by solving these two equations, and the reflection coefficient R_0 is the ratio of $V'_{[01]}$ to V_0', namely

$$R_0=\frac{V'_{[01]}}{V_0'}=\frac{k^2_{[01]}\delta^2}{2}\sum_m\left(\frac{h_{[01]}}{h_{[1m]}}-\frac{h_{[1m]}}{h_{[01]}}\right)\times\frac{k^4_{[1m]}}{(k^2_{[1m]}-1)(k^2_{[1m]}-k^2_{[01]})^2}. \tag{32}$$

The reflection coefficient has been obtained in the summation form of the functional terms of all eigenvalues of the modes which are generated by this offset in the first order.

We now proceed to calculate numerically using equation (32) for the case where the waveguide diameter is 51 mm and the frequency is 50 Gc/s. The term following the sign $\sum_m$ in the equation (32) is divided into three parts, and they are calculated separately as follows:

$$\sum_m=\sum_{m=1}^{8}+\sum_{m=9}^{16}+\sum_{m=17}^{\infty}. \tag{33}$$

The first term concerns the modes which can propagate and is a real number, while the second and the third terms concern the modes which are below the cutoff frequency and are therefore imaginary numbers. The value m which is the boundary between the second and the third terms does not have any special mathematical meaning, but the larger m we choose, the higher the accuracy of the calculation becomes. The third term does not converge if the following rough estimation is used. That is, for large m, using the relation $k_{[1m]}\doteqdot m\pi$, we have

$$\begin{aligned}\sum_{m=17}^{\infty}&\sim i\sum_{m=17}^{\infty}\frac{1}{h_{[01]}a}\,\frac{1}{k_{[1m]}}\\ &\doteqdot\frac{i}{h_{[01]}a\pi}\sum_{m=17}^{\infty}\frac{1}{m}\rightarrow\text{Divergent.}\end{aligned} \tag{34}$$

The divergence occurs because only the first term of the power series (23) is used at the time of the coordinate transformation, however large k_i is. To prevent this divergence, the third term is calculated from the original cylindrical functions as follows:

$$\sum_{m=17}^{\infty}\doteqdot -i\frac{2}{h_{[01]}a\pi^2}\sum_{m=17}^{\infty}{}'\frac{J_1(m\pi\delta)}{m^2\delta}. \tag{35}$$

Since $\delta\ll1$, the right-hand side of equation (35) can be obtained using the following integral relation:

$$\begin{aligned}\sum_{m=p}^{\infty}{}'\frac{J_1(m\pi\delta)}{m^2\delta}&\doteqdot\pi\int_{p\pi\delta}^{\infty}\frac{J_1(x)}{x^2}dx\\ &=\pi\left(\frac{J_1(p\pi\delta)}{2p\pi\delta}-\frac{\log(p\pi\delta)J_0(p\pi\delta)}{2}\right.\\ &\qquad\left.-\frac{1}{2}\int_{p\pi\delta}^{\infty}\log x J_1(x)dx\right).\end{aligned} \tag{36}$$

If $p\pi\delta\ll1$ is assumed, the integration of the last term of equation (36) can be performed changing the lower limit, $p\pi\delta$, to zero, without serious error, because the integrand is very small in the vicinity of $x=0$. The integration in such a case is

$$\int_0^{\infty} \log x J_1(x)dx = -\gamma + \log 2, \qquad (37)$$

where γ is Euler's constant, namely $\gamma = 0.557721$. Using the integration relation, equation (36) becomes

$$\sum_{m=p}^{\infty}{}' \frac{J_1(m\pi\delta)}{m^2\delta} \doteqdot 0.604 - 0.5\pi \log (p\pi\delta). \qquad (38)$$

When the frequency is 50 Gc/s and the waveguide diameter is 51 mm,

$$R_0 = [0.126 - i\{0.154 - 0.0888 \log (17\pi\delta)\}]\delta^2. \qquad (39)$$

If the offset is 0.1 mm, for example, the reflection coefficient is −108 dB.

When the mode conversion factor (31) is calculated,⁽¹⁾ only the first term of equation (23) is used. Therefore, for very high order modes, large errors occur.

3. Mode Conversion at the Junction between Circular and Elliptically Deformed Waveguides

Mode conversion occurs at the junction between a circular waveguide and an elliptically deformed waveguide having the same peripheral length as the circular waveguide, as shown in Fig. 3. There are many types of deformation of the cross section of the waveguide, but elliptical deformation is most liable to happen in practice and is easiest to analyze.

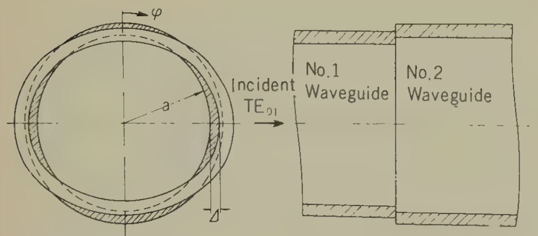

Fig. 3—Elliptic deformation discontinuity at a waveguide.

The T functions of each mode in the elliptic waveguide are given as⁽³⁾

$$\left.\begin{aligned}
T'_{[01]} &= q'_{[01]}\Big\{ J_0(\chi'_{[01]}r') \\
&\qquad + \frac{k'^2_{[01]}}{8} e^2 J_2(\chi'_{[01]}r') \cos 2\varphi \Big\}, \\
T'_{[nm]} &= q'_{[nm]} J_n(\chi'_{[nm]}r') \begin{matrix}\cos\\ -\sin\end{matrix}\, n\varphi', \\
T'_{(nm)} &= p'_{(nm)} J_n(\chi'_{(nm)}r') \begin{matrix}\sin\\ \cos\end{matrix}\, n\varphi',
\end{aligned}\right\} \qquad (40)$$

where the primes are put on the quantities of the No. 1 waveguide, and e is the ellipticity. In equation (40), the necessary terms to calculate the mode conversion factor up to the order of δ are used. The T functions in the No. 2 waveguide are

$$\left.\begin{aligned}
T_{[01]} &= q_{[01]} J_0(\chi_{[01]}r), \\
T_{[nm]} &= q_{[nm]} J_n(\chi_{[nm]}r) \begin{matrix}\cos\\ -\sin\end{matrix}\, n\varphi, \\
T_{(nm)} &= p_{(nm)} J_n(\chi_{(nm)}r) \begin{matrix}\sin\\ \cos\end{matrix}\, n\varphi.
\end{aligned}\right\} \qquad (41)$$

From equation (2), the continuity conditions of the electric and magnetic fields at the junction plane become

$$\left.\begin{aligned}
&V_0'\nabla_t T'_{[01]} \times \boldsymbol{i}_z + V'_{[01]}\nabla_t T' \times \boldsymbol{i}_z \\
&\quad + \sum V'_{[nm]}\nabla_t T'_{[nm]} \times \boldsymbol{i}_z + \sum V'_{(nm)}\nabla_t T'_{(nm)} \\
&\quad = V_0\nabla_t T_{[01]} \times \boldsymbol{i}_z + \sum V_{[nm]}\nabla_t T_{[nm]} \times \boldsymbol{i}_z \\
&\quad + \sum V_{(nm)}\nabla_t T_{(nm)}, \\
&Y'_{[01]}V_0'\nabla_t T'_{[01]} \times \boldsymbol{i}_z - Y'_{[01]}V'_{[01]}\nabla_t T'_{[01]} \times \boldsymbol{i}_z \\
&\quad - \sum Y'_{[nm]}V'_{[nm]}\nabla_t T'_{[nm]} \\
&\quad - \sum Y'_{(nm)}V'_{(nm)}\nabla_t T'_{(nm)} = Y_{[01]}V_0\nabla_t T_{[01]}
\end{aligned}\right\}$$

$$\left.\begin{array}{l}\times \boldsymbol{i}_z+\sum Y_{[nm]}V_{[nm]}\nabla_t T_{[nm]}\times \boldsymbol{i}_z \\ +\sum Y_{(nm)}V_{(nm)}\nabla_t T_{(nm)}.\end{array}\right\} \tag{42}$$

The electric and magnetic fields in both waveguides are represented as the superposition of all modes as shown in the lower right-hand corner of Fig. 1. The value Δ in Fig. 3 is related to the ellipticity in the equation $4\Delta/a=e^2$, and we define δ by $\delta=2\Delta/a$. At first, the first equation of (42) is multiplied by $q_{[2m]}\nabla_t\{J_2(\chi_{[2m]}r)\cos 2\varphi\}\times \boldsymbol{i}_z$ scalarly and is integrated in the junction plane. Neglecting the terms of order higher than δ^2, we get

$$\begin{aligned}V_0'q'_{[01]}\frac{k'^2_{[01]}}{8}e^2q_{[2m]}\iint\nabla_t\{J_2(\chi'_{[01]}r)\cos 2\varphi\}\times \boldsymbol{i}_z \\ \cdot\nabla_t\{J_2(\chi_{[2m]}r)\cos 2\varphi\}\times \boldsymbol{i}_z dS+V'_{[2m]}=V_{[2m]}.\end{aligned} \tag{43}$$

If the same operations are performed on the lower equation as on the upper one, we obtain equation (43) in which the first term of the left-hand side is multiplied by $Y'_{[01]}$, the second term is multiplied by $Y'_{[2m]}$, and the right-hand side is multiplied by $Y_{[2m]}$. By integration in the region which is not common to the circular and elliptical cross sections, we do not get the term $0(\delta)$, therefore the integration range of (43) may be set equal to the circular cross section. From equation (43) and the result calculated from the lower equation of (42), we get

$$\left.\begin{array}{l}V_{[2m]}-V'_{[2m]}=L_m V_0'e^2, \\ Y_{[2m]}V_{[2m]}+Y'_{[2m]}V'_{[2m]}=L_m Y'_{[01]}V_0'e^2,\end{array}\right\} \tag{44}$$

where

$$L_m=\frac{\sqrt{2}\ k_{[01]}k^2_{[2m]}}{4\sqrt{k^2_{[2m]}-4}\ (k^2_{[2m]}-k^2_{[01]})}. \tag{45}$$

Equations (44) are simultaneous algebraic equations having two unknowns, $V_{[2m]}$ and $V'_{[2m]}$, and the solutions of these equations are

$$\left.\begin{array}{l}V_{[2m]}=\dfrac{Y'_{[2m]}+Y'_{[01]}}{Y'_{[2m]}+Y_{[2m]}}L_m V_0'e^2, \\ V'_{[2m]}=\dfrac{Y'_{[01]}-Y_{[2m]}}{Y'_{[2m]}+Y_{[2m]}}L_m V_0'e^2.\end{array}\right\} \tag{46}$$

The mode conversion factor from the incident TE_{01} mode to the scattered forward TE_{2m} mode, $C^+_{[2m]}$; and the mode conversion factor to the scattered backward TE_{2m} mode, $C^-_{[2m]}$; are given in one equation

$$C^{\pm}_{[2m]}\fallingdotseq\frac{\lambda_{g[2m]}\pm\lambda_{g[01]}}{2\sqrt{\lambda_{g[01]}\lambda_{g[2m]}}}L_m e^2, \tag{47}$$

where L_m is a coefficient not dependent on frequency nor dimensions and is shown in Table 1. In the case where the frequency is 50 Gc/s and the waveguide diameter is 51 mm, and when there are discontinuities of $2\Delta=0.1$ mm at intervals of 5 m, and if the converted power is immediately transformed into heat loss due to the conductivity of the wall, then the mode conversion loss is 0.065 dB/km. As is easily calculated from equation (40), the mode conversion to other than the TE_{2m} mode does not occur in the first order of δ. And also, reflection does not occur in the first order of δ.

Table 1

L_m IN EQUATION (47)

Mode	TE_{21}	TE_{22}	TE_{23}	TE_{24}	TE_{25}	TE_{26}	TE_{27}	TE_{28}
L_m	−1.024	0.313	0.163	0.114	0.088	0.071	0.062	0.054

4. Mode Conversion in the Vicinity of the Cutoff Frequency

As the frequency approaches the cutoff frequency of some mode, the mode conversion factor increases infinitely for any case of mode conversion. This corresponds to the phenomenon in a cavity where the field strength increases infinitely as the frequency approaches the resonant frequency if the dissipation loss is neglected. It may be considered that a waveguide at the cutoff frequency is a resonant cavity in which the resonance is independent of cavity length. We will now calculate the exact mode conversion, taking the dissipation loss into consideration, when the frequency is near the cutoff of some mode, for the case of an elliptically deformed discontinuity.

The mode conversion factor has been shown in equation (47), with the assumption of zero dissipation, but when dissipation is taken into consideration, this factor becomes

$$C^{\pm}{}_{[2m]}=\frac{L_m e^2}{2\sqrt{h_{[01]}}}\,\frac{h_{[01]}\pm h_{[2m]}}{\sqrt{h_{[2m]}}}. \tag{48}$$

From equation (47), the mode conversion factor when the frequency is much higher than the cutoff frequency is

$$C^{+}{}_{[2m]\mathrm{far}}\doteqdot L_m e^2, \tag{49}$$

and from equation (48), when the frequency is near the cutoff frequency, it becomes

$$C^{+}{}_{[2m]}\doteqdot C^{-}{}_{[2m]}\doteqdot L_m e^2\frac{\sqrt{h_{[01]}}}{2}\,\frac{1}{\sqrt{h_{[2m]}}}. \tag{50}$$

The eigenvalues of L_m of the equation (45) become complex numbers if the dissipation loss is taken into consideration, but L_m for the case of no dissipation has been used because the imaginary parts are negligible compared with the real parts. The ratio of the mode conversion factor near the cutoff frequency to the value at frequencies much higher than the cutoff frequency is

$$T=\frac{|C^{+}{}_{[2m]}|}{C^{+}{}_{[2m]\mathrm{far}}}=\frac{|C^{-}{}_{[2m]}|}{C^{+}{}_{[2m]\mathrm{far}}}=\frac{\sqrt{h_{[01]}}}{2}\left(\alpha^2{}_{[2m]}+\beta^2{}_{[2m]}\right)^{-\frac{1}{4}} \tag{51}$$

where $\alpha_{[2m]}$ and $\beta_{[2m]}$ are the attenuation constant and the phase constant of the TE_{2m} mode respectively, and when the frequency is near the cutoff frequency, they become⁽⁶⁾

$$\left.\begin{aligned}\alpha_{[nm]}&=\sqrt{\frac{-(x+S)+\sqrt{(x+S)^2+S^2}}{2}},\\ \beta_{[nm]}&=\sqrt{\frac{(x+S)+\sqrt{(x+S)^2+S^2}}{2}},\end{aligned}\right\} \tag{52}$$

where x and S are

$$\left.\begin{aligned}x&=k_0{}^2\,\frac{2(f-f_c)}{f_c},\\ S&=\frac{2}{\delta\sigma}\,\frac{\omega\varepsilon_0}{a}\left\{\left(\frac{f}{f_c}\right)^2+\frac{n^2}{k^2{}_{[nm]}-n^2}\right\},\end{aligned}\right\} \tag{53}$$

and where f_c is the cutoff frequency; k_0 is the phase constant in free space; δ is the skin depth; σ is the conductivity; and a is the waveguide diameter. Then T in equation (51) becomes

$$T=\frac{\sqrt{\beta_{[01]}}}{2}\{(x+S)^2+S^2\}^{-1/8}. \tag{54}$$

This value becomes maximum when $x=-S$, and it is

$$T_{\max}=\frac{\sqrt{\beta_{[01]}}}{2}\,S^{-1/4}. \tag{55}$$

When the waveguide diameter is 51 mm, the cutoff frequency of the TE_{28} mode is slightly lower than 50 Gc/s. At a frequency a little lower than the cutoff of the TE_{28} mode, namely when the relation $x=-S$ is satisfied, T becomes maximum and is 8.5 for the case when the relative conductivity is 100 %. The mode conversion loss was 0.065 dB/km for the elliptically deformed discontinuity of 0.1 mm at intervals of 5 m as shown above. At the frequency at which T becomes its maximum value, the mode conversion to the forward and backward TE_{28} waves increases, therefore the mode conversion loss increases by 36 % and becomes 0.088 dB/km.

Here we studied the effects of the cutoff frequency only for the elliptically deformed discontinuity, but similar phenomena would occur for the case of other types of discontinuities, and similar analyses could be made.

Conclusion

A method to calculate the reflection and the mode conversion due to a slight discontinuity at the junction of circular waveguide has been derived, and the reflection due to a slight tilt and a slight offset, and the mode conversion due to a slight elliptically deformed discontinuity have been obtained. It has been proved that the reflection coefficients at the slight discontinuity are very small in the above two cases, but these must not be ignored when the delay distortion of the circular waveguide transmission line is analyzed, especially in the case of a helix waveguide.

The calculation of the mode conversion due to a slight elliptically deformed discontinuity would be useful to determine the necessary accuracy of the dimensions and installation of the waveguide transmission line. The mode conversion loss was 0.065 dB/km, due to the discontinuity of 0.1 mm successively located at an interval of 5 m, and at the frequency near the cutoff of the TE_{28} mode, it increased to 0.088 dB/km.

Acknowledgment

The author is grateful to Dr. I. Someya and Mr. S. Shimizu for their suggestions and discussions.

References

(1) S. Iiguchi: Mode Conversion in the Transmission of TE_{01} Waves through a Slight Tilt and a Slight Offset of Waveguide, International Conference on Ultra-High-Frequency Circuits and Antennas. Paris, 1957.
(2) H. Larsen: Delay Distortion and Equalization in H_{01} Waveguides for Long-Range Communication, *Proc. I.E.E.*, 106, Part B, Supplement 13, p. 188, 1959.
(3) B. Oguchi and M. Kato: On Elliptic Waveguides, International Conference on Ultra-High-Frequency Circuits and Antennas, Paris, 1957.
(4) N. Marcuvits: Waveguide Handbook, McGraw-Hill Book Co., New York. 1951.
(5) J. A. Stratton: Electromagnetic Theory, Mc Graw-Hill Book Co., New York, p. 373, 1941.
(6) Y. Shimizu: Theory of Transmitting Circular Electric Wave around Bends, International Conference on Ultra-High-Frequency Circuits and Antennas, Paris, 1957.

* * * *

REVIEW OF THE ELECTRICAL COMMUNICATION LABORATORY
VOLUME 8, NUMBERS 11-12, NOVEMBER-DECEMBER, 1960

U.D.C. 621.385.632

Matching between Traveling-wave Tube Helix and Waveguide*

Tomoyuki UNOTORO†

The method of orthogonal array layout of experiments was applied to the determination of dimensions of the three factors which can be chosen independently of the required performance of a traveling wave tube and affect the matching between the waveguide and the helix. As a result, these factors were found to affect the matching only independently. A broad band matching has resulted from the design thus made over the frequency range of up to 20 percent of 11 Gc/s. In addition, the contribution of each wide factor to the admittance components has definitely been determined.

1. Introduction

The helix type traveling-wave tube has broadband characteristics. The practical frequency band, however, is limited by the matching between the traveling-wave tube helix circuit and the input and output coupling circuits. The matching method may be divided into two main categories: one in which a coupling helix is used for connection to a coaxial circuit, and the other in which a short antenna is provided at the end of the helix and inserted in a waveguide. The matching method using a coupling helix, which results in an extremely broad bandwidth, i. e. a bandwidth of an octave or more, is widely used in measuring instruments and for other purposes. However, since some residual reflection due to mismatching occurs in the pass band, this matching method may not be used for multichannel communications systems with an extremely large number of channels, in which even slight phase distortion will cause cross-talk troubles. The second method, whereby connection is made to a waveguide, will provide a somewhat narrower bandwidth, but as it is possible to make the residual reflection in the pass band very small, this method has been adopted for the most part in the ultra multichannel microwave relay systems now in general use. The coupling structure connecting the helix and the waveguide has thus far been empirically designed. Therefore, it has not necessarily been possible to determine whether a design was optimum.

In this study, the factors controlling the matching characteristics, have been qualitatively ascertained as a result of systematic experiments on the coupling circuit between the helix and the traveling-wave tube as a part of 11 Gc band traveling-wave tube development researches. These results are applicable not only to 11 Gc tubes but also to tubes for other frequencies, as long as they have the same structure. The conclusions should also prove valuable in the design of coupling circuits.

In this coupling circuit, as described in detail later, a short antenna is connected to the end of the helix circuit and the other end of this antenna is connected to a small cylinder. The circuit is inserted into the center of the waveguide. That the conductance component of the coupling point ad-

---

* MS in Japanese received by the Electrical Communication Laboratory, April 18, 1960. Originally published in the *Kenkyû Zituyôka Hôkoku* (*Electrical Communication Laboratory Technical Journal*), N.T.T., Vol. 9. No. 6, pp. 639-648, 1960.

† Electronic Components Research Section.

mittance varies with antenna length, while the susceptance component of the coupling point admittance varies with cylinder length. Each component is independent, there is no interaction between them.

A coupling circuit was thus made with the best dimensions obtained by making use of this result, so that good ultra-broadband matching characteristics could be obtained in the 11 Gc band over a bandwidth of 2200 Mc. It could also be deduced by the investigation made based on the method of statistical analysis of an orthogonal array layout of experiments that matching giving a voltage standing wave ratio of less than 1.3 could be obtained without adjustment in mass produced tubes with less than 2 % loss.

2. Coupling Structure

Many methods have been used for coupling between a traveling wave tube helix and a waveguide. One of the structures much used is a tapered helix,(2) in which the end of the helix is straightened gradually into a straight wire which is inserted into the wave guide. Another is a straight antenna,(3) in which a short antenna is provided directly at the end of the helix and inserted into the waveguide. In the former type, it is difficult to determine the dimensions of the tapered part where end of the helix is to be straightened gradually, and furthermore, this part does not contribute to the gain of the tube, but instead has a harmful effect on the focusing of the electron beam. And, moreover, when tape is used for the helix, it is difficult to straighten. For this reason, the latter type was used in this Laboratory for all the tubes that were developed.

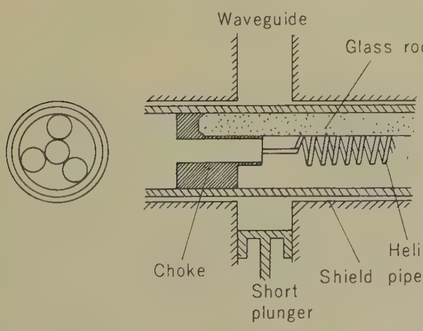

Fig. 1—Coupling structure between helix and waveguide.

The structure of the straight antenna type coupling has been designed, taking has been into account mechanical requirements, as shown in Fig. 1.

The helix circuit is supported by three quartz or ceramic rods, whose ends are inserted into three holes made in the choke. The helix end is connected directly to the antenna running parallel to the tube axis, and the antenna is connected to a hollow cylinder jutting out from the choke. This assembly is inserted in the center of the waveguide, as shown in the figure. One end of the waveguide is shorted with a short plunger, so that microwave power comes in or out through the other end.

The radius of helix is determined by the electronic design of the traveling-wave tube, the diameter of glass tube is determined by mechanical dimensions of supporting insulator rods, and the height of waveguide is limited by the focusing magnet. Therefore, there are only three coupling circuit dimensions which can be freely changed, without regard to these requirements, for the purpose of controlling the microwave matching characteristics. They are antenna length, cylinder length and position of the short waveguide plunger. In some cases, a tuning mechanism is provided at waveguide circuit outside the tube, thus making it possible to effect matching by adjusting the tuning. This method, however, is not desirable, since it will essentially deteriorate frequency characteristics. The consideration, therefore, should be to make out the design of the coupling circuit without reflection. Systematic study has been thus made as regards above mentioned three dimensions, which can be changed in the tube by itself, on the standpoint such as how they affect matching characteristics and, further whether complete matching can be obtained by merely adjusting these dimensions.

The samples measured are intended for 11

Table 1

Design of 11 Gc T.W.T. Circuit (mm)

Tape helix dimensions	0. 5× 0. 2
Mean helix radius	2. 3
Helix pitch	0. 9
Inner diameter of shield pipe	10. 0
Coupling waveguide dimension	5. 2×22. 9

Gc band high power tubes. The dimensions determined in designing traveling-wave tube are as shown in Table 1; while cylinder length *l*, antenna length *g*, and the distance from the glass wall of the tube to the short plunger *p* shown in Fig. 2 represent the dimensions that can be changed. Since the diameter of the glass tube is 8.5 mm, adding 4.25 mm to the value of *p* will give the distance from the center of the tube to the short plunger.

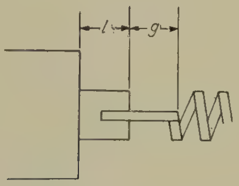

Fig. 2—Coupler dimensions to be changed.

In making this study, not only admittance was sought for, but also statistical analysis of the orthogonal array layout of experiments was made. The question, therefore, was how many levels should be chosen for the above-mentioned three dimensions. If only two levels were taken, only the first order tendency of effects could be obtained. In this case it would not be possible to determine the optimum level, although it would be possible to determine a good one. In order to obtain the optimum value, at least three levels are required, so that the second order approximation can be obtained. The increase in number of levels will raise the accuracy. However, if four levels are used, 64 sets of experiments will be required, so that a great deal of labor will be necessary.

It was, therefore, decided to make experiments with three levels. In choosing these three levels, it would be meaningless to take them far from the point which gives good matching. In our case, however, it was not known at first which point would give good matching, so that levels over a rather wide range were used. The values to be adopted for the analysis of variance of the orthogonal array layout of experiments were determined after the results of the measurements were examined.

The design values of samples and the values obtained by measuring the dimensions of samples are given in Table 2. In manufacturing the samples, an ordinary industrial production process was followed, without any special attention and the order of manufacturing was random.

Table 2

Design and Measured Dimensions of Samples (mm)

Sample	Design		Measured	
	l	*g*	*l*	*g*
A	0. 5	2. 5	0. 66	2. 44
B	0. 5	3. 5	0. 54	3. 56
C	0. 5	4. 5	0. 62	4. 62
D	1. 5	1. 5	1. 54	1. 92
E	1. 5	2. 5	1. 42	2. 89
F	1. 5	3. 5	1. 49	3. 36
G	1. 5	4. 5	1. 54	4. 68
H	2. 5	0. 5	2. 52	0. 67
I	2. 5	1. 5	2. 45	1. 68
J	2. 5	2. 5	2. 53	2. 77
K	2. 5	3. 5	2. 51	3. 58
L	2. 5	4. 5	2. 61	4. 59

The position of inserting this coupling into waveguide should be so arranged that, as seen from the waveguide, the upper face of the choke at the joint of the cylinder is on the same horizontal plane as the inner wall of the waveguide. Although errors are unavoidable in doing this, the statistical study is industrially very effective, as the randomness of the results due to such errors can thereby be deduced.

3. Measurements

In making the measurements, the position of the short plunger in each sample changed by 1 mm at a time, and the admittance measured from the waveguide side, with the frequency changed markedly in each case. Since the helix circuit is very heavily loaded it may be considered that a virtually reflectionless termination is connected to it.

The measurement assembly consists of a coupling waveguide with a height of 5.2 mm, which was, as shown in Fig. 3, connected through a tapered waveguide 40.5 mm long, to the 11 Gc band standard waveguide, i. e. 10.2 × 22.9 mm waveguide. No tuning mechanism was used so as not to cause any reflections. The measured admittance was transformed into the value at the coupling point on the waveguide, thereby making it possible to examine the effect of the change in dimensions. In making statistical analysis of the experiments, only the voltage standing wave ratio was examined.

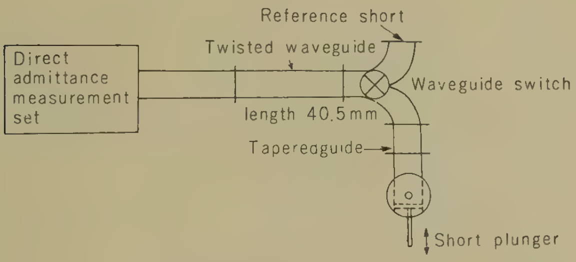

Fig. 3—Measurement assembly.

4. Analysis of Variance and Estimated Value by Orthogonal Array Layout of Experiments

The method of orthogonal array layout of experiments is a very effective means by which to obtain the combination of factors to give the optimum results by averaging the random errors of all factors, though there is anavoidable randomness in many factors that are considered to affect the final product in the production process.

In the case of this traveling wave tube coupling circuit, it is important not only to experimentally manufacture it carefully in the laboratory with an eye to obtaining good characteristics, but also to have it produced in the factory; where it will be necessary to cope with uncertain factors which might arise at any time and which are beyond the control of a mere gauge or jig. As the statistical estimation is considered quite effective in such a case, the following examination was conducted by making use of this method.

It is necessary, in making analysis, to express the matching quality numerically for each sample. Although it is indisputable that the quality of matching in each specific case may be indicated by the voltage standing wave ratio, opinion may be divided as to how the quality of matching of a certain sample for the whole frequency band should be expressed numerically. Here, however, the following tentative plan is proposed as a scale for expressing such quality. Namely, the standing wave ratio is taken at about 18 points, with the frequency changed within the band from 10.6 to 11.44 Gc., and the values of the standing wave ratio at the various points are averaged. If, in this case, a simple mathematical mean is taken, it will indicate a good value as a result of taking an average as a whole, even if there are considerably bad values at one or two points. Therefore, so the value thus obtained will not coincide with the quality determined by the observation of the measured points on an admittance chart. However, by taking a geometric mean, a reasonable value could be obtained which coincided well with the determination by an admittance chart. The geometric mean, therefore, was adopted. To state the calculation method concretely, a mathematical mean is taken of the values obtained by squaring the values of the standing wave ratio (>1) minus 1, and, with the square root of such mathematical mean extracted, 1 is added to the value thus obtained to make up a weighted geometric mean of the standing wave ratio. Needless to say, the smaller the value thus obtained, the better the matching will be.

Table 3

SQUARED MEANS OF STANDING WAVE RATIOS

Sample	l	g	Short plunger position (mm)					
			0	1	2	3	4	5
A	0.5	2.5			**1.662**	**1.598**	**1.918**	2.376
B	0.5	3.5		1.814	1.443	**1.319**	**1.273**	**1.818**
C	0.5	4.5				**2.055**	**1.566**	**1.602**
D	1.5	1.5	1.455	1.282	1.398			
E	1.5	2.5	1.334	**1.412**	**1.207**	**1.388**		
F	1.5	3.5		**1.349**	**1.159**	**1.265**		
G	1.5	4.5			1.946	**1.511**	**1.411**	**1.610**
H	2.5	0.5		2.690	3.450	4.118		
I	2.5	1.5		1.432	1.518	1.750		
J	2.5	2.5		**1.353**	**1.206**	**1.191**		
K	2.5	3.5		**1.238**	**1.135**	**1.222**		
L	2.5	4.5			**1.475**	**1.261**	**1.412**	

Table 3 shows the numerical values obtained by calculating the experimental results in this way, where the indicated position of the short plunger, as mentioned before, is the distance measured from the glass wall of the tube. As in the analysis of variance, only 3 levels were taken; 3 positions of the short plunger sufficed. Here, however, many positions were taken in some cases, in order to find out the best point for matching. As it is not necessary for analyzing variance to fix the level of each factor, such level may be selected at some point in close proximity to the best point. The values to be adopted for analysis may be determined by examining the results shown in this Table.

Table 4, which shows these numerical values layed out on the three level orthogonal array,[4)] comes next. Samples A, B, C...... have the dimensions given in Table 3, where the small suffixes indicate the positions of the short plunger p. As mentioned above, the values in Table 3 which are in close proximity to the best point, namely the bold-faced numerical values in the table have been adopted, whereas in Table 4 such numerical values minus 1 are used for the sake of convenience of calculations to be made later. Table 4 represents the 3 level 27 experiments type orthogonal array, where the experi-

Table 4

Layout of Experiments on the "$L_{24}(3^{13})$" Type Orthogonal Array and Measured Data

No. of experiment	l	g	$l \times g$		p	$l \times p$		$g \times p$		Sample	Measured mean value	Squared value
	1	2	3	4	5	6	7	8	……			
1	1	1	1		1	1		1		A_2	0.662	0.4380
2	1	1	1		2	2		2		A_3	0.598	0.3570
3	1	1	1		3	3		3		A_4	0.918	0.8440
4	1	2	2		1	1		2		B_3	0.319	0.1015
5	1	2	2		2	2		3		B_4	0.273	0.0745
6	1	2	2		3	3		1		B_5	0.818	0.6680
7	1	3	3		1	1		3		C_3	1.055	1.1120
8	1	3	3		2	2		1		C_4	0.566	0.3200
9	1	3	3		3	3		2		C_5	0.602	0.3620
10	2	1	2		1	2		1		E_1	0.412	0.1700
11	2	1	2		2	3		2		E_2	0.207	0.0428
12	2	1	2		3	1		3		E_3	0.388	0.1506
13	2	2	3		1	2		2		F_1	0.349	0.1220
14	2	2	3		2	3		3		F_2	0.159	0.0253
15	2	2	3		3	1		1		F_3	0.265	0.0700
16	2	3	1		1	2		3		G_3	0.511	0.2610
17	2	3	1		2	3		1		G_4	0.411	0.1688
18	2	3	1		3	1		2		G_5	0.610	0.3737
19	3	1	3		1	3		1		J_1	0.353	0.1249
20	3	1	3		2	1		2		J_2	0.206	0.0426
21	3	1	3		3	2		3		J_3	0.191	0.0366
22	3	2	1		1	3		2		K_1	0.238	0.0569
23	3	2	1		2	1		3		K_2	0.135	0.0183
24	3	2	1		3	2		1		K_3	0.222	0.0487
25	3	3	2		1	3		3		L_2	0.475	0.2252
26	3	3	2		2	1		1		L_3	0.261	0.0682
27	3	3	2		3	2		2		L_4	0.412	0.1698
										Total	11.616	6.4524

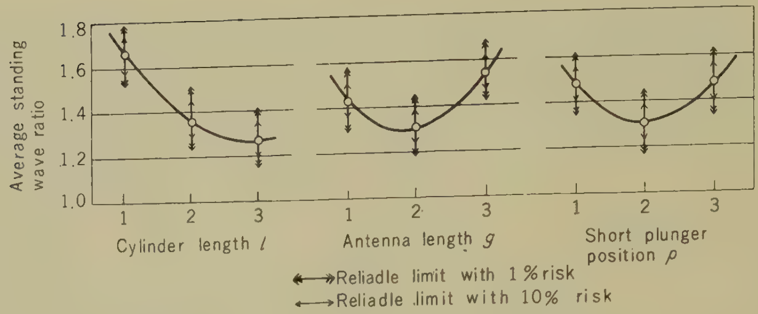

Fig. 4—Effects of each factor on the average standing wave ratio.

Table 5

ANALYSIS OF VARIANCE

Factor	Freedom	Sum of squares	Variance	F test
l	2	0. 66	0. 33	15. 4**
g	2	0. 25	0. 125	5. 83*
p	2	0. 18	0. 09	4. 20*
$l\times g$	2	0. 03	0. 015	0. 70
$l\times p$	2	0. 01	0. 005	0. 23
$g\times p$	2	0. 01	0. 005	0. 23
Error	14	0. 30	0. 021	
Total	26	1. 44		

* 1% level of significance.
** 5% //

ments are arranged so that in columns 1, 2, and 5, the main effect of l, g, and p; and in columns 3, 6, and 8, the interaction of l and g, l and p, and g and p respectively might be introduced.

The analysis of variance was made using this table, and the finally obtained is shown in Table 5, with the process of calculation omitted. The most important conclusion shown by this table may be derived from the results of F test, which mean that the effect of each independent factor is great, but no interaction is seen between any of the factors. In other words, it may be said that the effect of each factor is independent. It is, of deep significance that such a conclusion has been obtained on a statistical basis.

Fig 4 shows the effect of each factor graphically. The reliability limit determined separately, by making use of "Table t", at 0.145 with 99 % confidence and at 0.086 with 90 % confidence. It may also be seen from this graph that the difference in each dimension by 0.1 mm or so from the best point will have only a small effect on the standing wave ratio.

When sample K, which turned out to be the best as a result of the above-mentioned analysis, i. e. with $l=3$, $g=2$ and $p=2$, is adopted, the values with which the standing wave ratio is statistically expected to come out will be:

Central value	1.039
Upper limit with 99 % confidence	1.311
Upper limit with 98 % confidence	1.279

It was confirmed that from these numerical values, the weighted geometric mean of standing wave ratios of below 1.3 can be obtained with 98 % confidence, taking into account the randomness in the manufacturing. It may be seen also from Fig. 4 that the sample is quite promising for industrial production, as the effect of errors in each dimension does not seem to be so significant.

Since the above deduction is entirely based on the weighted geometric mean value, it should not be made a direct conclusion, but should rather be considered a statistical proof.

From this study, however, it has been made clear what combination of three dimensions will give the best matching statistically. By only such a method as described in the following section, whereby the admittance value is to be estimated, it would be difficult to determine the best combination mentioned above, since a distinct tendency of the effect of each factor as given in Fig. 4 may not be obtained. It may be said that this, together with the conclusion of non-interaction, is the significant result of the statistical analysis of the orthogonal array layout of experiments.

5. Analysis by Admittance Chart

In the preceding section has been described how the measured values of voltage standing wave ratio were dealt with statistically. Here, the effect of the dimensions of each part is investigated by entering in a Smith chart the admittance at the waveguide helix coupling. As for the admittance obtained by actual measurement, the positions of points on the chart are in disorder because of the effect of very small random reflection at the helix, in which case the better the matching, the greater such effect will be. Therefore, in finding the tendency of admittance variations due to changes in dimensions, it would be impossible to grasp the general effect of such variations, only by looking these charts. In order to see the tendencies clearly, the admittance at 3 points; i. e., at both ends and the center of the frequency band to be measured were examined.

First, admittance variations due to shift of the position of the short plunger were examined. On Fig. 5 are plotted the effect caused by the position of the short plunger as regards two samples A and H. Points with the numeral 1, 2, or 3 in the chart indicate the admittance at the coupling in the case of the frequencies of 11.4 Gc, 11.0 Gc and 10.6 Gc, respectively. Small suffixes given to sample symbols indicate, as heretofore, the positions of the short plunger *p*. A_2, for instance, means Sample A with dimensions of $g=2.5$ mm, $l=0.5$ mm, and short plunger position 2 mm from the glass wall of the tube.

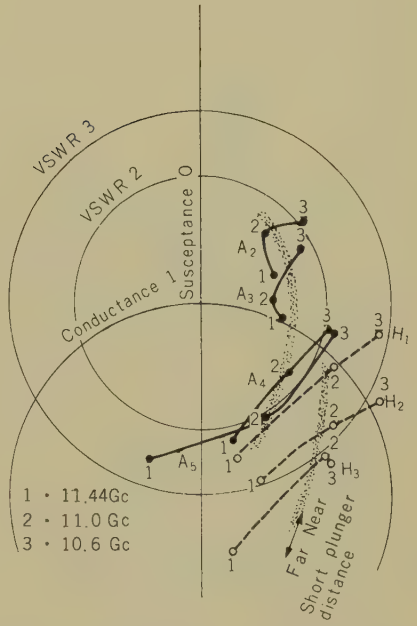

Fig. 5—Change in coupling point admittance depending on short plunger position.

As seen from Fig. 5, it has been confirmed that the admittance at the coupling is not only loaded in parallel with the susceptance produced at the short plunger, but that the two factors of conductance and susceptance are affected by the position of short plunger. Since the diameter of glass tube is, as mentioned before, 8.5 mm, the distance from the coupling point, in case the position of the short plunger is about 4.5 mm, will be 1/4 wave length, so that the parallel admittance produced on the side of the short plunger will be infinitely great. It should, however, be noted that the point to give good matching is, as seen from Fig. 4 as well as from many admittance charts, nearer than 1/4 wave length.

Then, investigations were made as to how the admittance produced at the coupling point varies when other factors, i. e. antenna length *g* and cylinder length *l* are changed. Fig. 6 shows, as in Fig. 5, a Smith chart on which the admittance measured at 3 points in frequency band for each sample is plotted.

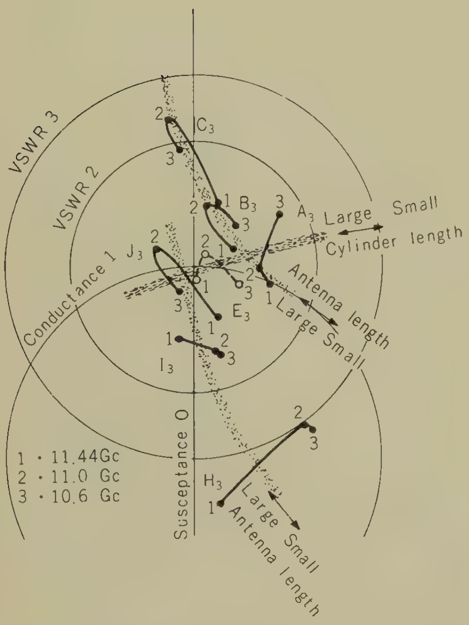

Fig. 6—Change in coupling point admittance due to change in antenna or cylinder length.

Table 6

LENGTH OF ANTENNA AND CYLINDER SAMPLES

Cylinder length / Antenna length	2.5	1.5	0.5
4.5	L	G	C
3.5	K	F	B
2.5	J	E	A
1.5	I	D	
0.5	H		

Here, however, having an eye only to the effect of antenna and cylinder length, the position of the short plunger is fixed at 3mm.

A very noteworthy characteristics is clarified from Fig. 6. Namely, as seen from this figure, the variations of admittance at the coupling point when antenna length g is changed and when cylinder length l is changed are orthogonal to each other on the Smith chart. For the convenience of comparison, the layout of g and l for each sample is shown in Table 6. It may be seen by comparing this table with Fig. 6 that the arrangement of sample dimensions completely coincides with that of the admittance points. This fact is also supported by the conclusion reached previously through the method of statistical analysis of the orthogonal layout that there is no interaction between the effects of dimensions.

Now that the change in antenna length mainly affects the conductance part, while the change in cylinder length mainly affects the susceptance part, the effects of the antenna and the cylinder at the coupling point may be understood as follows. Considering the coupling structure for the helix and the waveguide as an equivalent transformer, the change in antenna length will correspond to a change in the ratio of transformer, and thus the residual inductance due to leakage flux of the transformer will be neutralized through the capacitance introduced at the cylinder. In fact, it is well known that if a cylindrical post is provided inside the waveguide, it will introduce capacitance. Therefore, although the above-mentioned experiment made with respect only to one dimension of helix and waveguide, it may well be concluded that the obtained effect of antenna and cylinder length on the admittance may generally exist, regardless of the dimensions of helix and waveguide.

A similar conclusion has been reported[2)] with respect to a tapered helix type coupling circuit, in which case, however, the reason why such a characteristic comes out is not clear. Also, in the case of a tapered helix,

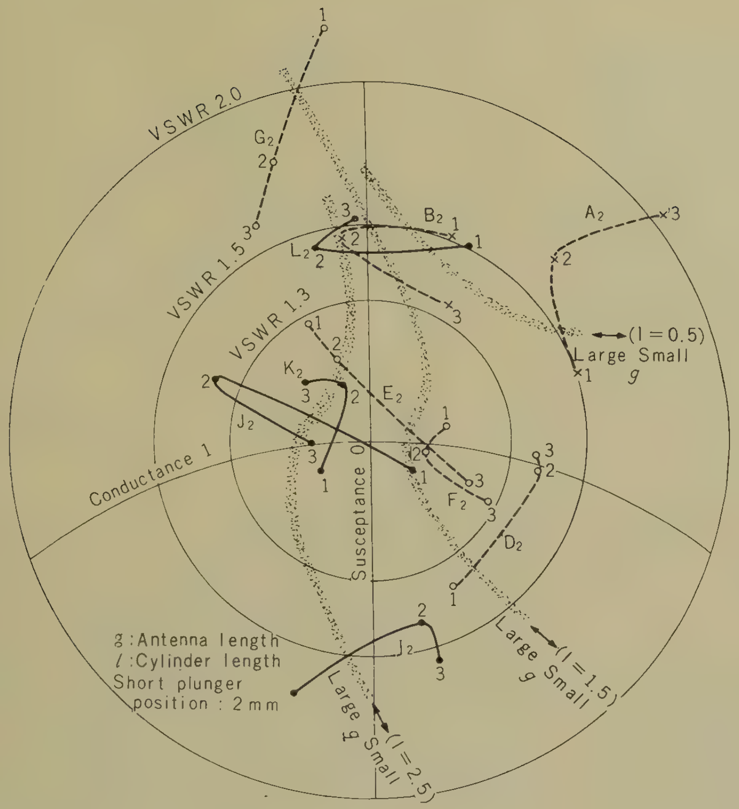

Fig. 7—Magnified chart of coupling point admittance.

it is difficult to control dimensions during manufacturing, and moreover, when tape is used for the helix, this method can not be used. For these reasons, the straight antenna type is much more practical; because its characteristics are plain and vivid, as described before.

Now that the characteristics have thus been clarified, it should be possible to obtain complete matching by selecting antenna and cylinder lengths, i. e. by bringing the admittance to the center of the Smith chart. With this object in view, closer examination was made by means of a magnified admittance chart, and then Fig. 7 was obtained. Now, since it has been made clear by the study described in the proceding section that in the best combination, the position of the short plunger is in the proximity of 2 mm, the admittance in the case of $p=2$ is sought. In the actual measurement result, the admittance points are, as already mentioned before, in disorder due to small random reflections, when matching is good. While, in this figure, the admittance at only 3 points in the frequency band are plotted in order to clarify the tendency. In this magnified Smith chart, the change in position of points at its central part as against the change in antenna length g shows, in some places, a retrogressive curve. The tendency in general, however, shows a change upwards and downwards. The best combination K_2 obtained in the preceding section by the method of statistical analysis shows, as expected, good matching. However, the curves for cylinder lengths of both 2.5 mm and 1.5 mm, as seen in the figure, do not pass through the center of the chart.

This shows the possibility of obtaining better matching by changing cylinder length. Then, as the second step, cylinder length of 2.0 mm was selected and studies were made in broadband matching.

6. Broadband Matching

As described above, by measuring with a direct-viewing device the admittance of many samples, general effect of each dimension has been made clear. And, possibility is found to obtain the best one with the cylinder length of 2.0 mm. The next consideration should be to measure the characteristics carefully to obtain a broader frequency band width and to determine the final design. For this purpose, the following two samples were prepared.

Sample	l	g
M	2.0 mm	3.5 mm
N	2.0	2.5

With regard to these samples, close measurement was made of the admittance for a wide frequency range by making use of a waveguide type standing wave detector. No mention is made here of the results one by one, but it was confirmed that Sample N was the best, and the admittance points, as shown in Fig. 8, pass through the center of the chart where the position of the short plunger was adjusted. In fact, the admittance chart of N is remarkably good as shown in Fig. 9.

The movable short plunger is liable to cause many troubles such as parasitic resonance or poor contact. Therefore, it would be desirable to use fixed short plungers for the finished tubes. The effect due to the position of short plunger was investigated. Fig. 10 shows the voltage standing wave ratios measured, with respect to Sample N, at intervals of 100 KC within the range from 10.2 Gc to 12.5 Gc. If the position of the short plunger is selected properly in such a way, very good matching of the standing wave ratio below 1.15 may be obtained for a band as broad as 2000 Mc. If a standing wave ratio of up to 1.3 is allowed, the band width will cover 2200 Mc, i. e. 20 % of the central frequency. It is also confirmed from this figure that, within the range of 10.7–11.7 Gc, used for 11 Gc radio relay, the position of the short plunger may be at any point between 1.4 mm and 1.85 mm. Therefore, even if the position of the plunger is fixed, satisfactory matching may be obtained.

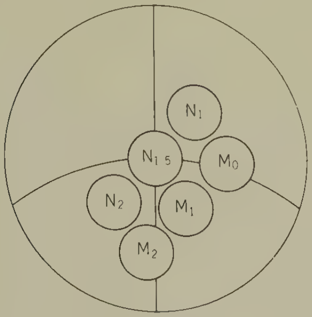

Fig. 8—Distribution of addmittance of sample M and N.

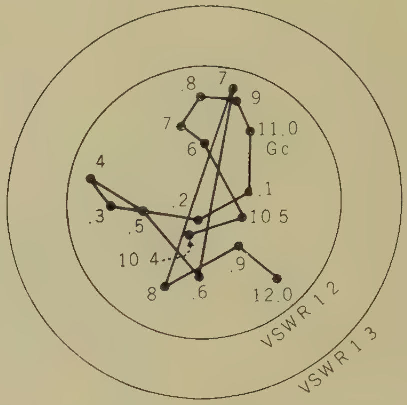

Fig. 9—Broadband admitance of sample $N_{1.5}$.

7. Conclusion

A systematic examination has been made with respect to the coupling circuit between the helix and the waveguide having the structure shown in Fig. 1. As a result, the effect on the matching characteristics due to the change of antenna length, cylinder length and position of short plunger, has been clarified distinctly.

First, by the method of statistical analysis

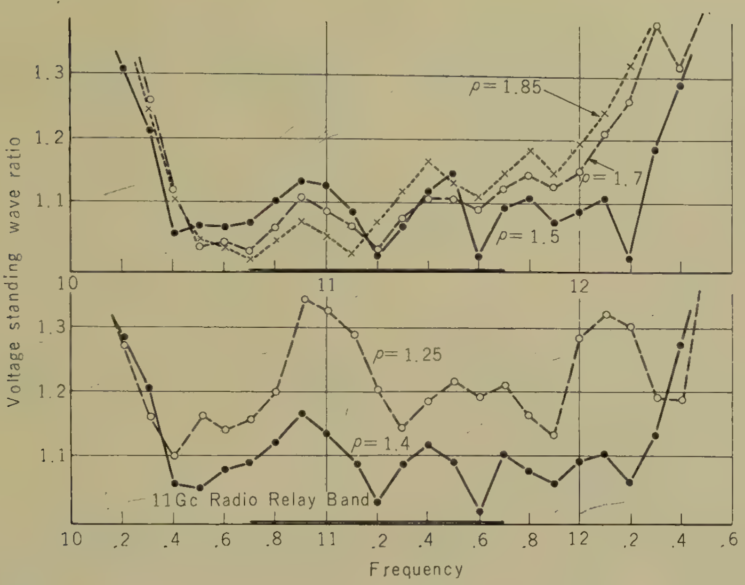

Fig. 10—Measured standing wave ratios of sample N at various short plunger positions.

of the orthogonal array layout of experiments, it could be deduced that no interaction occurred between the effects exerted by these three factors on the standing wave ratio over the entire bandwidth and that the matching of the standing wave ratio of below 1.3 without adjustment might be realized with statistical safety. It was also shown how the change in dimensions of each part affects the averaged standing wave ratio and what combination of such dimensions give the best matching. It may further be concluded that the accuracy of each dimension of ± 0.1mm or so will not be seen so significants and that it is promising for industrial production.

Also it was ascertained by examining on Smith chart the admittance at the coupling as seen from the waveguide that antenna length mainly affects the conductance factor and the cylinder length mainly affects the susceptance factor, while the position of short plunger affects both. Since such characteristics have been clarified, compensations can easily be taken by measuring the admittance, even if the matching condition is changed due to partial change in dimensions or raw materials or to thermal distortion and the like.

With the best design thus obtained by applying these results and with the position of the short plunger finely adjusted, very good matching characteristics for a bandwidth of 20 % of the center frequency could be obtained. Such matching characteristics are considered to be the best that have so far been reported. It was also confirmed that the fixed short plunger was available with enough safety. This, together with the statistical deduction made before, enables us to be fully convinced of a bright prospect for mass production of this coupling.

Such a successful result may not be obtained either by the statistical analysis of the orthogonal array layout of experiments or by the admittance chart method alone. If attention were paid only to admittance, there would be innumerable combinations of dimensions which would effect matching with respect to a certain frequency. In order, however, to determine the best combination, the method of statistical analysis should be applied.

At the same time, by this statistical method alone, the effect of each dimension on admittance chart could not be made clear. The best design was thus obtained by the simultaneous use of the two methods. Moreover, as already mentioned before, the cause of the above-described admittance characteristics can be reasoned quite clearly, so that these results may be applied to designs in future, since they are considered to exist also in the cases of other frequency or different dimensions of helix etc.

Acknowledgment

The experiments described in this paper were carried out in collaboration with Mr. Fumio Obata of Radio Section of this laboratory, to whom I wish to express my heartfelt thanks for his kind cooperation.

I wish also to thank Mr. Masatsugu Tsuchiya of the same Section who adjusted the direct viewing detector and allowed me to use it, Mr. Yukio Iwase, student of the Tokyo Telecommunications University, who assisted in making experiments and calculations, Mr. Shigetaka Hamada of the Electronic Components Research Section who gave me valuable instruction, Dr. Masanobu Kuwata, chief of the same section, who kindly guided me in carrying out this study, and all the other members of the Radio Section and the Electronic Component Parts Research Section.

I wish at the same time to express my sincere thanks to Messrs. Gen-ichi Taguchi and Shozo Konishi of the Nishibori Special Research Room who favored me with cordial guidance in the statistical analysis of the orthogonal array layout of experiments.

I also wish to express my appreciation to Messrs. Tadao Nemoto and Susumu Yasuda of the Electron Tube Engineering Department of the Nippon Denki K.K. for their ready compliance with my trouble-some requests to prepare and provide necessary samples.

References

(1) e. g. N. Rynn: Analysis of Coupled-Structure Traveling-wave Tubes, *IRE Trans. Electron Devices* ED-2, No. 3, p. 15, 1955.

(2) L. P. Laico et. al.: A medium Power Traveling-wave Tube for 6,000 Mc Radio Relay, *B.S.T. J.* **35,** 6, p. 1285, 1956.

(3) Shigetaka Hamada: Traveling-Wave Tube for 11,000 Mc Band, *Tech. Jour. of E.C.L* **.7,** 8, p. 609, 1958.

(4) Gen-ichi Taguchi: Statistical Analysis of Orthogonal Array Layout of Experiments, Maruzen Publishing Co., 1958.

* * * *

Papers Contributed to Scientific and Technical Journals by the Members of the Laboratory

Papers Published in Other Publications of the Electrical Communication Laboratory

U.D.C. 537.52 : 537.56
Theory of Electron Plasma Oscillations
Masao SUMI
Kenkyû Zituyôka Hôkoku (Electr. Comm. Labor. Techn. Journ.), NTT, **9**, 11, pp. 1223–1277, Nov. 1960

Electron plasma oscillations excited by the interaction of an electron beam and the plasma medium are theoretically investigated. Characteristics of excited waves are displayed for various conditions. Many experimental results are explained by this theory.

U.D.C. 534.53 : 546.12 : 546.28
Neutron Activation Analysis of Halogens in High-Purity Silicon
Tadashi NOZAKI
Kenkyû Zituyôka Hôkoku (Electr. Comm. Labor. Techn. Journ.), NTT, **9**, 9, pp. 1077–1084, Sept. 1960

A method of measuring quantitatively trace concentrations of halogens in high-purity silicon is described.

U.D.C. 546.28 : 548.55 : 621.923.7

The Effect of Abrasives on Crystals of Germanium and Silicon
Kazumasa ONO, Osamu MIKAMI, and *Joichi SUZUKI*
Kenkyû Zituyôka Hôkoku (Electr. Comm. Labor. Techn. Journ.), NTT, **9**, 10, pp. 1211–1219, Oct. 1960

Abrasive particles remaining on crystals of germanium and silicon are measured by an electron diffraction method. Silica powder is found to be preferable to other abrasives for polishing semiconductors.

U.D.C. 621.317.78.029.6 : 621.317.38.026.43 : 621.318.1.016.23

Power Measuring Equipment for Parametron
Sachinobu SHIMIZU
Kenkyû Zituyôka Hôkoku (Electr. Comm. Labor. Techn. Journ.), NTT, **9**, 10, pp. 1165–1174, Oct. 1960

This paper describes the circuit of power measuring equipment using the modulation product method for measuring the high-frequency low-power dissipation of a parametron or other ferrite core. Design problems encountered during the design of this equipment are also described.

Translations of many of these papers will appear in a future addition of the Review of Electrical communication Laboratory

Please address requests for copies of these papers, which are in Japanese, directly to the authors to whom credited at: The Electrical Commnnication Laboratory, 1551 Kitizyôzi, Musasino-1 Tokyo.

U.D.C. 621.318.1.001.2 : 538.2.2 : 538.2 : 534.321.9

Studies on Magnetic Cores by a Supersonic Magnetostriction Method

Katumi NISIGUTI and *Hirosi SAWABE*

Kenkyû Zituyôka Hôkoku (Electr. Comm. Labor. Techn. Journ.), NTT, **9**, 10, pp. 1149–1164, Oct. 1960

A supersonic magnetostiction method of measuring the characteristics of magnetic cores is described. Characteristics of some particular cores are described for variations of both H (magnetomotive force) and B (flux).

U.D.C. 621.318.1001.1.2 : 521.318.57 : 519.2

New Ferrite Materials for the Parametron

Kaxusi ONOSE and *Masaru ONO*

Kenkyû Zituyôka Hôkoku (Electr. Comm. Labor. Techn. Journ.), NTT, **9**, 11, pp. 1305–1327, Nov. 1960

A systematic investigation of ferrite materials for the purpose of developing new ferrite which will reduce the power consumption of parametrons is described.

U.D.C. 621.318.57 : 621.318.1 : 621.374.3

Channel Selector Circuit Applying an Error-Correcting-Code

Shozi YOSIDA and *Keisuke TOMARU*

Kenkyû Zituyôka Hôkoku (Electr. Comm. Labor. Techn. Journ.), NTT, **9**, 11, pp. 1329–1339, Nov. 1960

The circuit is constructed with 256 (=the number of channels to be selected) transformer. The connection of the transformer windings is based on an error-correcting theory.

U.D.C. 621.372.413 : 621.372.853.2

The Resonant Cavity Including a Semiconductor Sample

Naozo WATANABE

Kenkyû Zituyôka Hôkoku (Electr. Comm. Labor. Techn. Journ.), NTT, **9**, 10, pp. 1201–1210, Oct. 1960

The theory of a double mode cavity including a semiconductor sample and applications to the measurement of the Hall effect and to isolator action are described.

U.D.C. 621.372.823 : 621.372.85

Mode Exciters in Circular Waveguides

Ken-ichi NODA

Kenkyû Zituyôka Hôkoku (Electr. Comm. Labor. Techn. Journ.), NTT, **9**, 9, pp. 1065–1075, Sept. 1960

Experimental and theoretical aspects of new types of mode exciters for obtaining several kinds of circular waveguide modes from rectangular TE_{01} are described. Very pure modes are obtained from simple structures.

U.D.C. 621.372.832

Directivity of a Multi-Element Directional Coupler

Sin-ichi IIGUCHI

Kenkyû Zituyôka Hôkoku (Flectr. Comm. Labor. Techn. Journ.), NTT, **9**, 10, pp. 1175–1192, Oct. 1960

The properties of a multi-element directional coupler are analyzed by a matrix method which includes the backward wave of one coupling hole. The relations between the coupling, the forward, and the backward waves of the coupler are investigated.

U.D.C. 621.372.852.1

Faraday Rotation Isolator for Millimeter Waves
Ichiro NAKAGAWA
Kenkyû Zituyôka Hôkoku (Electr. Comm. Labor. Techn. Journ.), NTT, **9**, 10, pp. 1125–1147, Oct. 1960

This paper describes experimental and theoretical investigations on Faraday rotation isolators for the 35 Gc/s and 48 Gc/s regions. The desired broad-band characteristics were realized.

U.D.C. 621.375.9 : 621.375.121.1

Stagger Operation of Doubly Resonant Parametric Amplifiers
Sigetaka HAMADA and *Hisakazu MUKAI*
Kenkyû Zituyôka Hôkoku (Electr. Comm. Labor. Techn. Journ.), NTT, **9**, 10, pp. 1193–1200, Oct. 1960

The bandwidth of a microwave parametric amplifier is increased by stagger tuning several doubly resonant stages having a narrow bandwidth. The principles construction, and characteristics of this amplifier are described.

U.D.C. 621.375.9 : 538.561 : 621.318.12

Experiments on a Ferrite Parametric Amplifier
Takichi HASHIMOTO, Shigetaka HAMADA, Yasuhiro ISHII, Ken-ichi SATOMI,
and *Teruo YOKOYAMA*
Kenkyû Zituyôka Hôkoku (Electr. Comm. Labor. Techn. Journ.), NTT, **9**, 11, pp. 1279–1304, Nov. 1960

The results of experimental and theoretical investigations on a ferrite parametric amplifier and on the garnet from which it is made are reported.

U.D.C. 621.382.3.002 : 620.197.6 : 546.28

Oxidation Process in Silicon
Osamu MIKAMI and *Ryosaku KOMARU*
Kenkyû Zituyôka Hôkoku (Electr. Comm. Labor. Techn. Journ.), NTT, **9**, 11, pp. 1341–1353, Nov. 1960

A procedure for oxidizing silicon and the growth of the oxide is described. The oxide film is applied to mask or protect the silicon during the diffusion process.

U.D.C. 621.385.6.029.64

Research ou a Velocity-Jump Amplifier
Jun-ichiro IKEUCHI and *Masaaki KITAOKA*
Kenkyû Zituyôka Hôkoku (Electr. Comm. Labor. Techn. Journ.), NTT, **9**, 9, pp. 935–1000, Sept. 1960

Theoretical analysis of a velocity-jump amplifier and experimental measurements made on a 4 Gc, tube are described. This data is used to design and construct a high-gain tube for 24 Gc.

U.D.C. 621.394.441 : [621.394.6 : 621.382.3

Transistorization of Voice Frequency Carrier Telegraph System
Toshiaki KISHIGAMI, Nozomi EGASHIRA, and *Takeo MATSUZAKI*
Kenkyû Zituyôka Hôkoku (Electr. Comm. Labor. Techn. Journ.), NTT, **9**, 9, pp. 1043–1063, Sept. 1960

The purpose of this study is to determine whether frequency shift (F.S.) or amplitude modulation (A.M.) is preferable on a voice-frequency-carrier telegraph system.

U.D.C. 621.365.31.001.2(083.5)

Table of Erlang's Loss Formula
Terunobu SUZUKI and *Kenzo TAKAGI*
Kenkyô Zituyôka Hôkoku (Electr. Comm. Labor. Techn. Journ.), NTT, Special Issue 5, pp. 1–27, 1960

This table gives offerred traffic as a function of the number of outgoing channels for different fixed values of loss with higher accuracy and a more comprehensive range than previous tables.

U.D.C. 666.1.018 : 532.73 : 539

Fundamental Study on Infiltration in Power Metallurgy
Takashi KIMURA
Kenkyû Zituyôka Hôkoku (Electr. Comm. Labor. Techn. Journ.), NTT, **9**, 9, pp. 1001–1041, Sept. 1960

The effects of detergents and capillary blocking on infiltration, and the effects of various infiltrans and hard particle size on the mechanical properties are clarified as the fundamental problems of infiltration in powder metallurgy.

U.D.C. 678.602 658.562.6 : 620.193

Dimensional Accuracy and Stability of Molded Plastics
Tetsuo KUDO and *Takashi YAMANARI*
Kenkyû Zituyôka Hôkoku (Electr. Comm. Labor. Techn. Journ.), NTT, **9**, 9, pp. 1085–1116, Sept. 1960

Dimensional accuracy of molded plastic parts, especially gears, and relations between dimensional stability and crystallinity are described.

* * * *

REVIEW
of
THE ELECTRICAL COMMUNICATION LABORATORY,
NIPPON TELEGRAPH AND TELEPHONE PUBLIC CORPORATION

Published Bimonthy by
The Electrical Communication Laboratory, 1551, Kitizyôzi, Musasino-si, Tôkyô, Japan
Satoshi Kojima, *Director*

Annual Index

Volume 8—1960

page

NOS. 1-2, JANUARY-FEBRUARY

Coloring of Ionic Crystals by Electron Bombardment 1
Yoshitake IGARASHI

Oscillation Caused by Electron Sheath Breakdown 7
Seiji OHARA and *Kazuo TAKAYAMA*

Magnetic Properties and Ferrimagnetic Resonance in Polycrystalline $3Ye_2O_3 \cdot (5-x)Fe_2O_3 \cdot xIn_2O_3$ 12
Yuzo SHICHIJO and *Tomonao MIYADAI*

Deterioration of Contacts of a Polar Relay with a Rigid Tongue 18
Sanae AMADA, *Kosaku MUKAI*, and
Yukichi KANEKO

Harmonic Distortion Factor of Transistors 34
Seiichi KAWAGUCHI and *Minoru HIRAI*

GCR Discharge Tube (A new grid control cold cathode discharge tube) 39
Kiyo-ichi TAKATSU, *Hideo SHIMURA*,
Tomizo ITO, *Toshiharu TODA*, and
Takeshi HAYASHI

Design Requirements of a New Telephone Set from the Standpoint of Transmission Quality 48
Zenji YAMAGUCHI

On Dilatometric Measurements and Crystallization Phenomena in Various Polyethylenes 57
Ryuichi NAKANE

A Study of Colors for Molded Telephone Handsets 73
Yumio SUGIHARA

Papers Contributed to Scientific and Technical Journals by the Members of the Laboratory 85

page

NOS. 3-4, MARCH-APRIL

A Computer Program to Find Boolean Functions Representable by a Single Logical Elements Based on a Majority Decision Principle 89
Saburo MUROGA

Measurement of Thermal Conductivity in Semiconductors 99
Riro NII

Semiconductor Speech-Path Switches Suitable for Direct-Coupled Connection 105
Ichiro IDA and *Shoji YOSHIDA*

The Nonlinear Barrier Capacitance of Silver Bonded Diodes 112
Shoichi KITA and *Ryoichi SUGIHARA*

VHF Crystal Polishing and the Nature of Polished Quartz Surfaces 119
Ichiro IDA and *Yuzo ARAI*

High Speed Adding System 175
Noriyosi KUROYANAGI

On the Generation of Prime Numbers using the Eratosthenes' Sieve by the MUSASINO-1 189
Katuhiko ARAI

Papers Contributed to Scientific and Technical Journals by the Members of the Laboratory 194

NOS. 5-6, MAY-JUNE

Development of Paper for Laminates 199
Masaaki KATAGIRI

Non-Stationary Parametrons 204
Kazushi ONOSE

Properties of Compound Transistors for Speech-Path Switches 211
Ichiro ENDO, *Kingo YAMAGISHI*, *Shozi YOSHIDA*, and *Kazuhiko GOTO*

Characteristics of Beyond-Horizon Propagation Over Sea (I) 222
Tadasu FUKAMI, *Seiji IEIRI*, *Fumio IKEGAMI*, and *Hirofumi FUJIMURA*

The Cylindrical TE_{11} mode Cavity Including a Semiconductor Sample with Tensorial Electric Conductivity 256
Naozo WATANABE

Energy Build-up in Magnetrons 266
Daijiro KOBAYASHI

On Stochastic Representations for Incoming Telephone Calls 270
Gisaku NAKAMURA

page
Design of the Terminal Equipments for the 12 Mc/s System on Coaxial Pairs 280
Hideo IIJIMA

Thermal Degradation of Polytrifluorochloroethylene 288
Nobuo YAMADA

Papers Contributed to Scientific and Technical Journals by the Members of the Laboratory 292

NOS. 7-8, JULY-AUGUST

Analysis of Polar Relay 297
Yasuo TOMITA

Dielectric-Coated Waveguide Construction and Characteristics 309
Ken'ichi NODA and *Kazuo YAMAGUCHI*

Mode Conversion in the Excitation of TE_{01} Waves in a TE_{01} Mode Transducer (Rectangular→Sector Portion→Circular) 324
Shin'ichi IIGUCHI

Magnetic Gate Circuits Controlled by High Frequency Signals 335
Ichiro ENDO and *Kikunobu KUSUNOKI*

Distributed Amplifier Tube 343
Takuya KOJIMA

The Magnetic Circuit of Telephone Receiver 369
Ryozo ARAKI and *Tatsuo SHIMAMURA*

Refining of Castor Oil for Capacitor Dielectrics 376
Masaaki KATAGIRI and *Katunari KODATI*

Degradation of Polyethylene by Mastication 385
Hiroshi NOMURA and *Yuji YAMASHITA*

Papers Contributed to Scientific and Technical Journals by the Members of the Laboratory 392

NOS. 9-10, SEPTEMBER-OCTOBER

The Analysis of Frame Vibrating Systems 397
Motonobu YONEKAWA

On Fundamental Qualities of Vowel Sounds in Speech Communication (I) 410
Yoshiyuki OCHIAI and *Teruo FUKUMURA*

Circular Electric Wave Transmission through Hybrid-Mode Waveguide 426
Ken'ichi NODA

Mode Exciters in Circular Waveguides 465
Ken'ichi NODA

page

The Design of a New Telephone Receiver **477**
Kenrô MASUZAWA and *Kiyoshi TAJIMA*

Papers Contributed to Scientific and Technical Journals by the Members of the Laboratory **487**

NOS. 11-12, NOVEMBER-DECEMBER

Stress and Deformation in Conical Vibrating Plate **491**
Kazuo IKEGAYA

Some Investigations on the Conical Vibrating Plates for Telephone **498**
Kazuo IKEGAYA and *Masayuki MURAKAMI*

On Fundamental Qualities of Vowel Sounds in Speech Communication (II) **509**
Yoshiyuki OCHIAI and *Teruo FUKUMURA*

Theory of Solution of Chain Molecules **530**
Hirosi OKAMOTO

A Channel Selector Applying Error-Correcting Codes **540**
Shoji YOSHIDA and *Keisuke TOMARU*

Reflections and Mode Conversions in Imperfect Junctions of TE_{01} Wave Transmission Line **549**
Ken-ichi NODA

Matching between Traveling-wave Tube Helix and Waveguide **560**
Tomoyuki UNOTORO

Papers Contributed to Scientific and Technical Journals by the Members of the Laboratory **573**

* * * *

Vol. 8 Nos. 11-12 NOVEMBER-DECEMBER

CONTENTS

Stress and Deformation in Conical Vibrating Plate 491
Kazuo IKEGAYA

Some Investigations on the Conical Vibrating Plates for Telephone 498
Kazuo IKEGAYA and *Masayuki MURAKAMI*

On Fundamental Qualities of Vowel Sounds in Speech Communication (II) 509
Toshiyuki OCHIAI and *Teruo FUKUMURA*

Theory of Solution of Chain Molecules 530
Hirosi OKAMOTO

A Channel Selector Applying Error-Correcting Codes 540
Shoji YOSHIDA and *Keisuke TOMARU*

Reflections and Mode Conversions in Imperfect Junctions of TE_{01} Wave Transmission Line 549
Ken-ichi NODA

Matching between Traveling-Wave Tube Helix and Waveguide 560
Tomoyuki UNOTORO

Papers Contributed to Scientific and Technical Journals by the Members of the Laboratory 573

Copyright 1960 by the Electrical Communication Laboratory, NTT